Variable C:N Ratios of Particulate Organic Matter and Their Influence on the Marine Carbon Cycle

Variable C:N-Verhältnisse von partikulärem organischen Material und deren Einfluß auf den marinen Kohlenstoffhaushalt

Birgit Schneider

Birgit Schneider

Alfred-Wegener-Institut für Polar- und Meeresforschung
Postfach 120161, D-27515 Bremerhaven

Die vorliegende Arbeit ist die inhaltlich unveränderte Fassung einer Dissertation, die 2002 im Fachbereich Geowissenschaften der Universität Bremen vorgelegt wurde.

Eine elektronische Version der vorliegenden Arbeit ist erhältlich unter:
`http://www.awi-bremerhaven.de/GEO/Publ/PhDs/BSchneider`

Kurztitel: Variable C:N Ratios of POM and the Marine Carbon Cycle

Contents

Zusammenfassung

Das Thema der vorliegenden Arbeit sind systematische Variabilitäten in den Elementverhältnissen von partikulärem organischem Material (POM) im Ozean und deren Einfluß auf den marinen Kohlenstoffhaushalt. An der Grenzfläche Ozean/ Atmosphäre findet CO_2 Gasaustausch statt, dessen Stärke von den dort vorhandenen physikalischen und biologischen Prozessen bestimmt wird. Da der Ozean eine Senke für anthropogenes CO_2 ist, deren genaue Wirkungsweise und Größe bisher unbekannt sind, ist dies von besonderem Forschungsinteresse. Im Wesentlichen sind zwei Prozesse für den CO_2 Austausch verantwortlich: die Physikalische Pumpe, deren Stärke von der CO_2 Partialdruckdifferenz zwischen Ozean und Atmosphäre sowie der Tiefenwasserbildung abhängt und zweitens die Biologische Pumpe, die die Umwandlung von gelöstem anorganischem Kohlenstoff (DIC) und Nährstoffen in partikuläres Material umfaßt. Partikel werden durch Absinken in die Tiefe exportiert und dabei ganz oder teilweise remineralisiert, was zu vertikalen Gradienten in den Verteilungen von anorganischem Kohlenstoff und Nährstoffen führt. Die C:N:P Elementverhältnisse der sinkenden Partikel bestimmen dabei die relativen Anteile von Kohlenstoff bzw. Nährstoffen am Vertikaltransport. Biogeochemische Modelle benutzen bekannte physikalische und biologische Prozesse, um die Stärke der jeweiligen Pumpe zu simulieren, wobei gewöhnlich die konstanten Redfield Verhältnisse für C:N:P (106:16:1) zur Berechnung der Partikelflüsse verwendet werden.

Diese Arbeit stellt eine enge Verknüpfung zwischen Datenanalyse und Modellanwendung dar und sie liefert neue Erkenntnisse über die Zusammensetzung von partikulärem Material und dabei auftretende räumlich/zeitliche Variationen. Daten über die C:N Verhältnisse von POM wurden aus verschiedenen Quellen in eine Datensammlung zusammengefügt und analysiert, wobei 10200 einzelne C:N Werte aus Untersuchungen mit Sinkstofffallen, sowie aus groß- und kleinvolumigen Filterproben erhalten wurden. Die Datensammlung umfaßt alle großen Ozeane und geographische Breiten, hochproduktive sowie oligotrophe Regionen und Gebiete mit saisonaler Eisbedeckung. Aus der Analyse ergibt sich, daß die C:N Verhältnisse von POM sehr variabel sind, mit Werten unterhalb des Redfield Verhältnisses (C:N=6.6) bis zu einem Vielfachen dessen. Darüberhinaus wurden regionale, tiefenabhängige und saisonale Unterschiede in den C:N Verhältnissen des exportierten Materials gefunden. Im globalen Mittel betragen die C:N Verhältnisse von sinkenden Partikeln im Oberflächenwasser 7.1 mit einer Zunahme von 0.2 Einheiten pro 1000 m Wassertiefe. Diese Ergebnisse zeigen, daß in biogeochemischen Modellen höhere Werte als der Redfield Faktor und tiefenabhängige C:N Verhältnisse benutzt werden sollten, um die relativen Flüsse von Kohlenstoff und Stickstoff adäquat zu repräsentieren.

In der aktuellen Literatur werden mögliche Gründe für beobachtete Variabilitäten diskutiert. Dies sind z.B. Prozesse während der Produktion wie Nährstofflimitierung oder überschüssige Aufnahme reichlich vorhandener Nährstoffe, sowie Änderungen in der Artenzusammensetzung des Phytoplanktons. Darüberhinaus kann die Partikelzusammensetzung während der Remineralisierung verändert werden, was als

bevorzugte Lösung von Nährstoffen im Vergleich zu Kohlenstoff bezeichnet wird.

Die Abweichung zwischen den Ergebnissen der vorliegenden Datenanalyse und Analysen gelöster Nährstoffe, die generell konstante Elementverhältnisse ermitteln, ist kein Widerspruch. Untersuchungen an gelösten Nährstoffen betrachten die Elementverhältnisse der regenerierten Nährstoffe auf Isopyknen, wobei über die Tiefe integriert wird, die die jeweilige Isopykne durchlaufen hat. Folglich erzielen diese Untersuchungen tiefenintegrierte anstatt tiefenabhängige C:N Verhältnisse. Sie betrachten das Elementverhältnis der Komponente, die gelöst wurde, während Partikeluntersuchungen sich auf die Zusammensetzung des verbleibenden Partikels beziehen. Beide Verhältnisse stimmen nicht notwendigerweise überein.

Die Auswirkungen systematischer Variationen in der Elementzusammensetzung von POM auf den marinen Kohlenstoffhaushalt wurden mit Hilfe des globalen Ozeanzirkulationsmodells AAMOCC bestimmt. Erhöhte und tiefenabhängige C:N Verhältnisse in sinkendem Material führen zu einer Kohlenstoffanreicherung von 150 Gt in einem Ozean, der im Gleichgewicht mit einer vorindustriellen Atmosphäre ist. Außerdem ergeben sich stärkere Tiefengradienten von DIC als in einem Experiment mit klassischem Redfield Faktor. Die Zunahme entspricht zwar nur 0.5 % des marinen Kohlenstoffinventars, aber gleichzeitig 25 % des vorindustriellen atmosphärischen CO_2 Gehalts. Angenommen, daß der zusätzliche Kohlenstoff aus der Atmosphäre kommt, würde deren CO_2 Gehalt dadurch um 75 μatm verringert. Die Anwendung eines CO_2 Emissionsszenarios zeigt geringfügige Unterschiede zwischen einem 'Redfield' und einem 'non-Redfield' Experiment, wobei die Menge der anthropogenen CO_2 Aufnahme sowie das Muster der DIC Anreicherung übereinstimmen. Die Ergebnisse entsprechen außerdem Modellergebnissen und Messungen anthropogener CO_2 Verteilungen, die in der aktuellen Literatur beschrieben werden.

Genaue Auswirkungen von Global Change (Erwärmung der Oberfläche, stärkere Schichtung, geringere Wassermassenzirkulation) auf die biologische Pumpe sind unbekannt, aber kohlenstoffangereicherte transparente exopolymer Partikel (TEP) können den relativen Anteil von Kohlenstoff am Vertikaltransport erhöhen. TEP wird abhängig von der CO_2 Verfügbarkeit sowie unter Nährstofflimitierung, einer Folge von verringerter Wassermassenzirkulation, produziert. Angenommen, daß TEP vorindustriell eher unbedeutend war und sein Anteil an der globalen POC Produktion bis heute auf 5 % zugenommen hat, bedeutet eine Erhöhung des C:N Verhältnisses von oberflächennahen Partikeln von 7.1 auf 8.1. Diese Zunahme bewirkt einen Anstieg des CO_2 Flusses von der Atmosphäre in den Ozean, der heute etwa zusätzlichen 0.5 Gt C/Jahr entspricht, d.h. einer Verstärkung des aktuellen Flusses um 18 %, wobei Rückkopplungen auf die Atmosphäre allerdings unberücksichtigt sind. Allgemein wird erwartet, daß die Stärke der physikalische Pumpe aufgrund einer schwächer werdenden Ozeanzirkulation reduziert wird. Folglich wird ein Mechanismus, der zu einer Erhöhung des relativen Gehalts an Kohlenstoff in sinkenden Partikeln führt, den Effekt einer geringer werdenden CO_2 Aufnahme des Ozeans mildern, sie aber nicht ausgleichen können.

Summary

The current study investigates systematic variations in the elemental composition of marine particulate organic matter (POM) and their influence on the marine carbon cycle. At the air-sea interface CO_2 gas exchange takes place, and ambient physical and biological processes determine the strength of CO_2 fluxes. This is of major research interest, as the global ocean currently acts as a sink for anthropogenic CO_2, but the amount of this sink, its detailed functionality and persistence are yet unresolved. Mainly two processes determine the CO_2 gas exchange; the physical pump which is dependent on the CO_2 partial pressure gradient between ocean and atmosphere and advection/downwelling. Secondly, the biological pump, which comprises the removal of dissolved inorganic carbon and nutrients from the surface water by particle formation and export flux. Both pumps affect the CO_2 exchange at the ocean atmosphere boundary. Export of organic matter and the subsequent release of carbon and nutrients by remineralization in the water column creates vertical nutrient and carbon gradients, and C:N:P element ratios of sinking material determine the relative magnitudes of the downward phosphorus, nitrogen and carbon fluxes. Biogeochemical models describe the known physical and biological processes of the ocean, and they are used to simulate the mechanism and strength of the respective pump. For simplicity, it is common practice to use the constant Redfield ratio C:N:P (106:16:1) for biogeochemical modeling and flux estimations.

This study yields a close link between data analysis and model implementation. It provides new results on the elemental composition of marine particulate organic matter and inherent systematic spatial and temporal variations. Data of the C:N ratios of particulate material from many independent sources are assembled into a single data collection for joint evaluation. The data set contains 10200 C:N values from sediment trap deployments and from analyses of both small volume and large volume filtrations, where all major oceans and latitudes, oligotrophic and high productive regions as well as areas of seasonal ice coverage are included. From the data analysis it turns out that C:N ratios are highly variable with values below the traditional Redfield ratio (C:N=6.6) to values greatly exceeding it. There are regional differences in the C:N ratios of exported material and in apparent depth dependencies. Furthermore, C:N ratios of particulate matter from single regions exhibit strong seasonal patterns. On a global mean, C:N ratios of particles from the surface water amount to 7.1, and there is a systematic increase with depth of 0.2 units per 1000 m water depth. Both findings, elevated C:N ratios for exported particles just below the euphotic zone and the increase with depth, suggest that higher-than-Redfield and depth dependent C:N ratios should be implemented in biogeochemical models to correctly represent relative strengths of downward carbon and nitrogen fluxes.

In the recent literature, many processes are discussed that can be responsible for the observed variations. There are processes during production like nutrient limitation or excess uptake of certain elements as well as varying species compositions. Additionally, the elemental composition of POM may be modified during particle

decomposition, a process called preferential remineralization of phosphorus and nitrogen in contrast to carbon.

The ascertained discrepancy between results from the present data analysis and studies of dissolved inorganic nutrient fields yielding essentially constant C:N ratios close to the Redfield value is not contradictory. The respective studies investigate regeneration rates of dissolved nutrients on isopycnal surfaces. Thereby an integration over depth variations of the surfaces under consideration is performed, i.e. these studies provide rather depth integrated remineralization ratios than depth dependencies. Furthermore, observations of regenerated nutrients refer to element ratios of the component that has gone into solution, while particle analyses refer to the composition of the remaining particles, and both ratios do not necessarily correspond to each other.

The impacts of systematic variations in elemental compositions of POM, as determined by the present data analysis, on the marine carbon cycle are investigated by using the global ocean carbon cycle model AAMOCC. Elevated and depth dependent carbon to nutrient ratios in sinking material result in a 150 Gt higher steady-state preindustrial oceanic carbon inventory and stronger DIC depth gradients, as compared to a run with the constant classical Redfield ratio. This represents a 0.5 % increase of the total marine carbon inventory only, but corresponds to about 25 % of the preindustrial atmospheric carbon reservoir. Assuming that the increased oceanic inventory was derived from the atmosphere, this would lead to a reduction of the atmospheric CO_2 partial pressure by about 75 μatm. The implementation of rising atmospheric CO_2 concentrations yields only small CO_2 gas exchange differences between the 'Redfield' and 'non-Redfield' experiments. Both, the amount of anthropogenic CO_2 uptake and the pattern of DIC increase, are very similar and they correspond very well with model results and the latter also with measurements of anthropogenic CO_2 concentrations reported by recent literature.

Implications of global change (surface warming, increased stratification, reduced circulation) on the biological pump are speculative. However, transparent exopolymer particles (TEP), which are highly carbon enriched, may increase relative carbon fluxes by the biological pump. TEP are produced CO_2 dependently and largely under nutrient limitation (carbon overconsumption), which is predicted as a consequence of reduced water mass circulation. Assuming a continuous increase from minor global significance of TEP carbon at preindustrial times, to presently a contribution of 5 % to the global oceanic carbon export, yields a rise of the exported C:N ratio of sinking particles from 7.1 to 8.1. This change can lead to a considerable increase of air-sea carbon fluxes of about 0.5 Gt C/yr, enhancing present air-sea CO_2 fluxes by about 18 %. However, this scenario assumes no further oceanic response to global change, but it is predicted that the physical pump will be weakened due to reduced ocean circulation. Thus, any mechanism leading to higher carbon to nutrient ratios of sinking particles, may alleviate the effects of a generally lowering CO_2 sequestration, but it will not be able to outweigh the consequences.

1 Introduction

1.1 Marine Biogeochemistry

Carbon is the basic component of all living organisms, thus it has a key function in biogeochemical cycles. In its gaseous phase, as carbon dioxide (CO_2), it is next to water vapor and methane the most important greenhouse gas in the atmosphere. In the ocean, organic carbon is produced during photosynthesis in the surface water, where dissolved inorganic carbon (DIC) and nutrients (PO_4, NO_3) are transformed into particulate organic matter (POM). Particles sink down whereby carbon and nutritional elements are exported from the euphotic zone into the deeper ocean. The corresponding loss of DIC in the surface water is replaced by upwelling of DIC from deep waters and by atmospheric CO_2 due to equilibration via gas exchange. Both mechanisms, production and sinking of organic matter (biological pump) and solubility in the surface water (physical pump), are the main processes leading to an exchange of CO_2 between ocean and atmosphere [Volk and Hoffert, 1985]. Production and remineralization of sinking particles create vertical gradients of dissolved carbon, nutrient and oxygen concentrations with nutrient depletion in the surface waters and nutrient accumulation in deeper waters, which can be seen in Figure 1.1 (A and B). While DIC, inorganic phosphorus and nitrogen are released during particle remineralization, oxygen is consumed. This results in oxygen depleted zones in the subsurface layers of the water column (see Figure 1.1 (C)). Carbon and nutrient profiles show different depths of maximum concentrations, i.e. they underly different remineralization processes. In general, phosphorus and nitrogen are remineralized faster from the particles than carbon, leading to a deeper transport and thereby more efficient downward transport of carbon in contrast to phosphorus and nitrogen [Christian et al., 1997]. Due to the uptake of CO_2 from the atmosphere, the storage of dissolved inorganic carbon in deep water and the burial of particulate organic carbon in seafloor sediments, the global ocean may act as a net sink for carbon. Quantifying the oceanic carbon uptake is currently a major research goal with respect to the increase of anthropogenic CO_2 emissions and their potential for global warming. The oceanic carbon reservoir is about sixty-times larger than that of the atmosphere [Ittekkot, 1993], therefore the oceans are of fundamental importance in the global carbon cycle.

The global ocean is a complex dynamical system, underlying physical forcings and biological processes, that permanently transport, mix and redistribute energy, heat and biogeochemical properties. On large spatial scales these processes are quite well known, leading to characteristic ocean currents like e.g. the Antarctic Circumpolar Current (ACC) and the Gulf Stream [Tomczak and Godfrey, 1994] as well as to the distinct water mass distributions of the Atlantic Ocean [Dietrich et al., 1975] as shown in Figure 1.1 (B). However, on a finer spatial resolution and over longer time scales the current knowledge is still limited. The global ocean transports large amounts of heat and thereby regulates the world's climate. The current oceanic

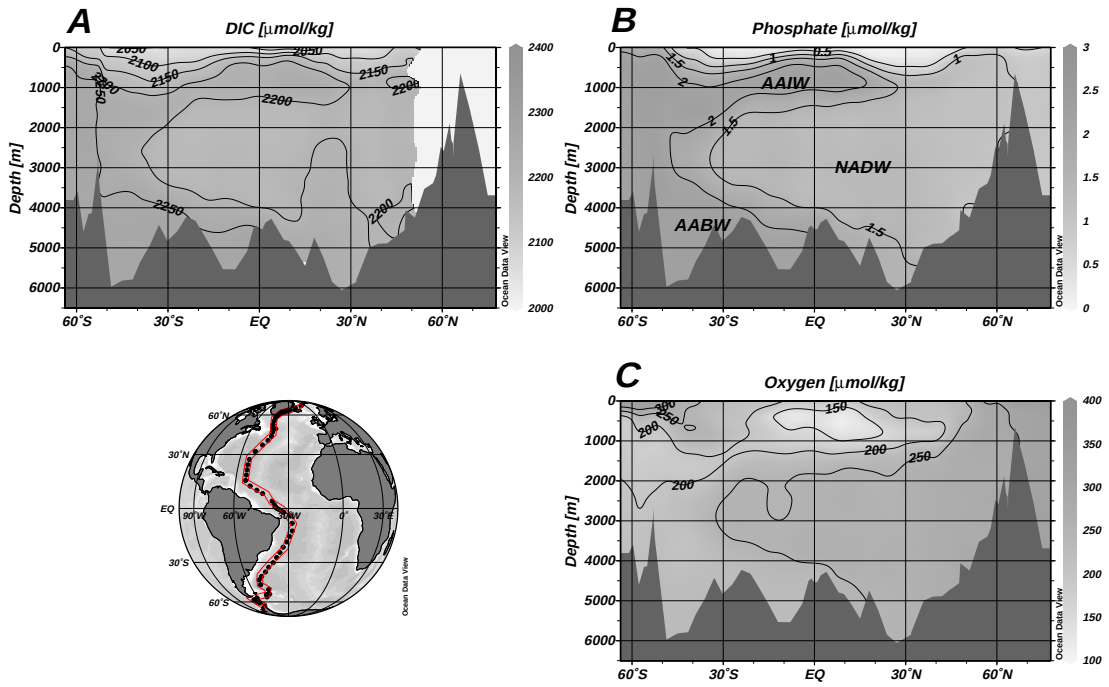

Figure 1.1: Distribution of DIC (A), Phosphate (B) and Oxygen (C) along the GEOSECS (Geochemical Ocean Sections Study) transect in the western Atlantic. Characteristic water masses are shown in panel (B), NADW: North Atlantic Deep Water; AAIW; Antarctic Intermediate Water; AABW: Antarctic Bottom Water. Data are from GEOSECS [1998].

circulation pattern is very constant since the last glacial period, which is supposed to be responsible for the relatively constant global mean temperatures during this interval of about 8000 years [Broecker, 1997]. But the global circulation is also very sensitive to changes in temperature, salinity and wind forcing, and relatively small changes therein may result in strong impacts, which consequently will be able to shift the world climate significantly [Rahmstorf, 2002].

Many reasons have been discussed to be responsible for climate variability on geological time scales, e.g. astronomical forcings like changes in solar radiation and the earth's orbital parameters (precession, obliquity and eccentricity), which occur quasi periodically. Changes of large scale atmospheric and oceanic circulation patterns have also been suggested as well as changes in the concentration of atmospheric trace gases, e.g. the CO_2 concentration, as CO_2 is one of the major greenhouse gases. Ice core records from Antarctica have shown that the atmospheric CO_2 partial pressure during the last 400000 years has varied between 180 and 300 μatm and correlated very well with global temperature records, as shown in Figure 1.2 [Barnola et al., 1999; Petit et al., 1999; CDIAC, 2002]. It is not clear whether increasing atmospheric CO_2 concentrations force global warming or if they occur as a consequence, but a close connection between both phenomena has been confirmed. However, there seems to be a natural control mechanism, which prevented the atmospheric

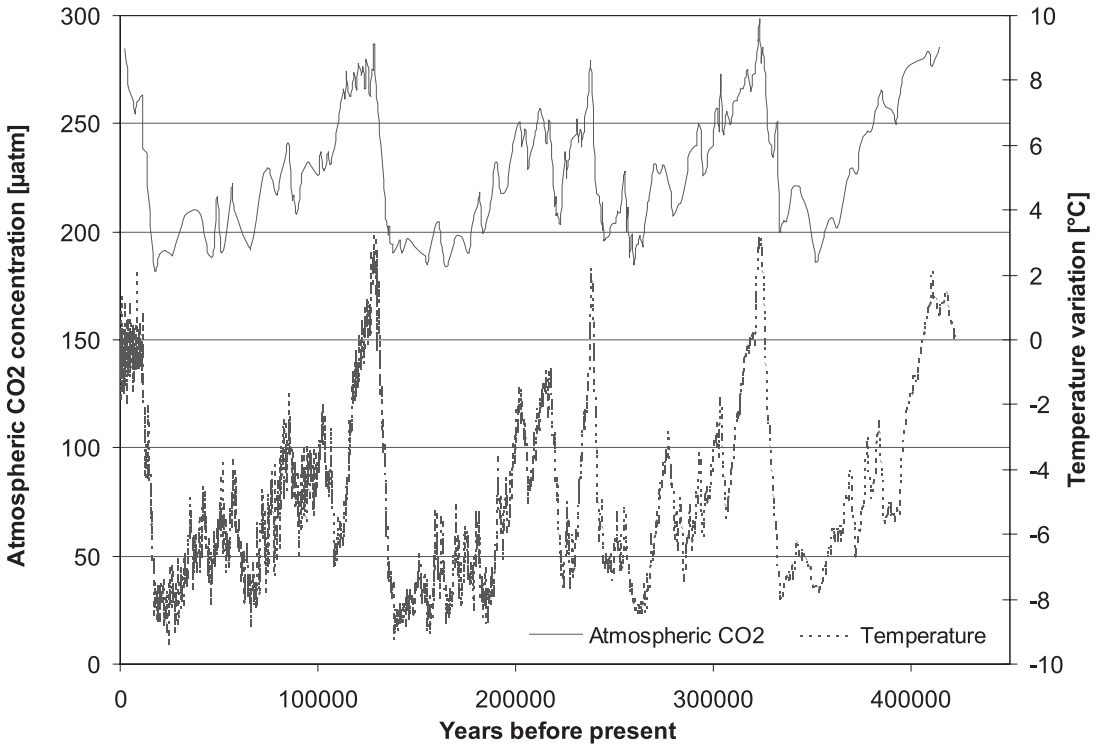

Figure 1.2: Atmospheric CO_2 concentrations and global mean temperatures during the last 400000 years from the vostok ice core according to Barnola et al. [1999].

CO_2 partial pressure from exceeding a value of 300 μatm, sustainably.

Anthropogenic greenhouse gas emissions provide the possibility of human impacts on climate change. Large efforts have been undertaken to gain a better understanding of the global carbon cycle and the paleoclimatic history, because future predictions for the world climate require a reasonable understanding of the past conditions and interactions. Since the beginning of industrialization the atmospheric CO_2 partial pressure has increased from 280 μatm to 370 μatm [Neftel et al. 1994; Keeling and Whorf, 2002]. This corresponds to an increase in the atmospheric carbon inventory from approximately 600 Gt C at preindustrial times to 750 Gt C, nowadays (Figure 1.3). But this increase of the atmospheric CO_2 concentration only accounts for a fraction of the anthropogenic emissions. Approximately 7 Gt C are emitted annually by burning of fossil fuels, cement production and changes in land use [Siegenthaler and Sarmiento, 1993; Schimel et al., 2001]. The known CO_2 sinks in the atmosphere, terrestrial biosphere and oceans take up only parts of these emissions, and the current net air to sea flux of CO_2 is approximately 2 Gt C per year [Siegenthaler and Sarmiento, 1993; Takahashi et al., 1999]. The remainder, called *missing sink*, amounts to 1.8 Gt C per year [Broecker and Peng, 1993]. Parts of this *missing sink* are believed to be in the oceans. The global carbon cycle with its fluxes and reservoirs is shown schematically for a preindustrial and current situation in Figure 1.3, according to Siegenthaler and Sarmiento [1993].

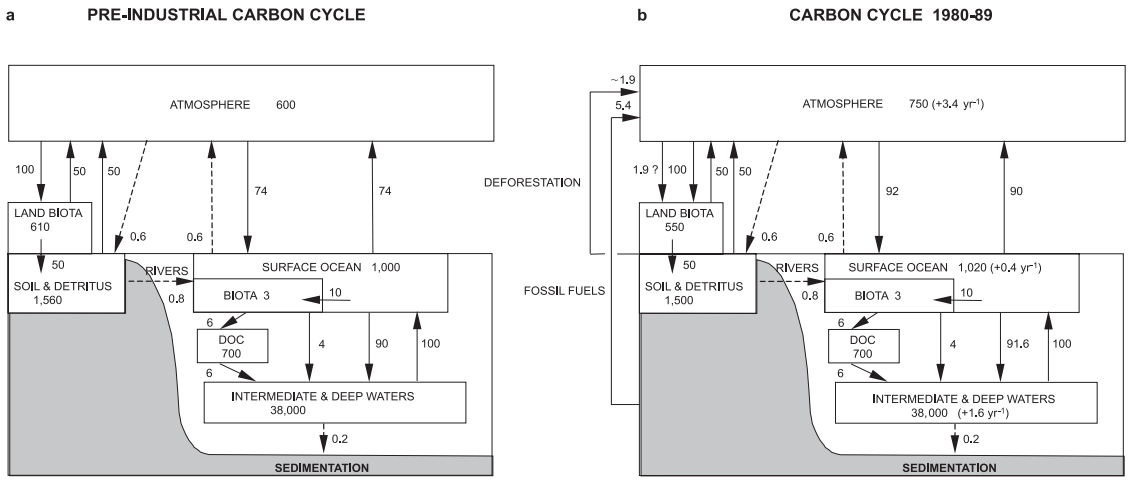

Figure 1.3: The global carbon cycle, reservoirs and fluxes at preindustrial times (a) and after anthropogenic perturbation (b) according to Siegenthaler and Sarmiento [1993].

Three pump mechanisms are identified in the ocean, that affect the air-sea exchange of CO_2, considerably; the *physical pump*, which is also known as solubility pump, the *biological pump* or soft tissue pump and the *carbonate pump*. Detailed descriptions of the respective mechanisms are given by Volk and Hoffert [1985]. The physical pump describes the uptake of atmospheric CO_2 by gas exchange, its solubility in the surface water and subsequent downward transport by deep water formation. Gas exchange and solubility are functions of the gradient between atmospheric and oceanic partial pressure of CO_2, surface water temperature and mixing parameters. Additionally, the efficiency of the physical pump depends on the amount of deep water formation, which is a function of temperature, salinity, stability of water column stratification and ice coverage and formation, respectively. On the one hand, the physical pump can lead to uptake and downward transport of CO_2 in areas of deep water formation, but on the other hand, in the upwelling regions of the ocean, the physical pump supplies the sea surface with DIC enriched deep waters leading to regional net CO_2 outgassing [Wanninkhof, 1992]. In the preindustrial steady state ocean sources and sinks of CO_2 were believed to be almost in equilibrium, i.e. there is no net CO_2 gas exchange.

The biological pump is the second important process for the air-sea CO_2 gas exchange. As this mechanism refers to the flux of particulate organic carbon (POC), it is also called the soft tissue pump. During primary production (PP) in the surface water photosynthesis transforms dissolved inorganic carbon and nutrients into particulate organic matter (POM). The subsequent sinking of particles exports carbon and nutritional elements from the surface to the deep ocean, and the C:N:P element ratios of sinking matter determine the relative magnitude of carbon, nitrogen and phosphorus fluxes. Remineralization of the sinking particles leads to a release of dissolved inorganic carbon and nutritional elements in the water column, while oxygen is consumed. Primary production depends on nutrient availability, temper-

ature, light conditions and vertical mixing. However, the strength of the biological pump, does not depend on the primary production, but on the amount of particle export. Export production (EP) is defined to be the amount of carbon and nutrients, being exported from the euphotic zone by sinking particles, balanced by the upwelling of dissolved inorganic carbon and nutrients. According to results from satellite observations of ocean color and model assumptions the annual amount of primary production corresponds to 43.5 Gt C per year [Behrenfeld and Falkowski, 1997], and results from inverse modeling suggest that the global carbon export out of the euphotic zone amounts to 10 Gt C per year [Schlitzer, 2002].

Many efforts have been undertaken to describe the mode of action and efficiency of the biological pump, which is very complex. Berger [1989] estimates the efficiency of transferring particulate organic carbon from the surface to the sediments. For open ocean areas he predicts that only 10 % of the organic carbon produced during primary production are exported from the euphotic zone to the deep ocean. Most of this material is remineralized in the water column, and only a fraction of 10 % of the exported material (i.e. 1 % of the primary production) reaches the sea floor. At the sea floor, benthic organisms respire organic carbon, and only about 0.03 % of primary production is actually archived in sedimenteds.

Behrenfeld and Falkowski [1997] use ocean color measurements from satellite data to derive surface water chlorophyll concentrations. From those data, by the application of conversion algorithms, values of primary productivity for the global ocean are derived. This method is profitable, because satellite data provide a large spatial and temporal coverage, i.e. there are global measurements for at least the last decade. A map of global primary production according to Behrenfeld and Falkowski [1997] is shown in Figure 2.1. Eppley and Peterson [1979] empirically derived a relationship between the export production (EP) and primary production (PP), called f-ratio. While primary production refers to the total amount of carbon that has been produced during photosynthesis, the export production is the amount of carbon that effectively has been exported out of the euphotic zone, mostly by sinking particles. However, there is still large uncertainty about the exact amount of carbon export fluxes in the ocean.

The third mechanism important for the air-sea carbon exchange is the carbonate pump, which is also called the counterpart to the biological pump. The carbonate pump refers to the production of organisms with carbonate shells, mostly calcite and aragonite. Due to complex interactions in the marine carbonate system, the removal of bicarbonate, which is the main carbon source for calcification, leads to an increase in surface water pCO_2 and thus probably to CO_2 outgassing. For the net effect on the surface water pCO_2 it is important to regard the ratio of organic to inorganic carbon fixation by the respective organism [Antia et al., 2001]. While a strong soft tissue pump results in large amounts of organic carbon export, and thus positive air-sea fluxes of CO_2, a strong carbonate pump counteracts this mechanism and maintains negative air-sea CO_2 fluxes [Riebesell et al., 2001].

1.2 Particulate Organic Matter (POM)

Photosynthesis in the surface ocean produces both dissolved and particulate organic matter (DOM, POM), and the focus in the current study is on sinking particles. Marine particulate organic matter is defined to be the fraction of organic substances larger than 0.45 μm [Cauwet, 1978], however, in most studies GF/F or GF/G filters are used with a pore size between 0.7 - 1μm. It is not a homogeneous pool, but a mixture of living phytoplankton, zooplankton and detritus, which consists of faecal pellets of zoolankton, plus dead phytoplankton and zooplankton [Edwards, 2001] at different stages of decomposition and of various shapes. With respect to particle fluxes, POM has to be divided into suspended and sinking material. Suspended matter is very small and can be very old, as a consequence of its long residence time in the water column [Druffel et al., 1992; 1996]. It is supposed to be largely degraded, i.e. nutrient depleted. Due to its non-sinking behavior, suspended matter does not contribute to the downward export of material and in this respect it is of minor importance. Sinking particles, caught by sediment traps, are larger in size. Due to their relative high sinking rates, they are the main carrier of nutrients and carbon from the surface into the deep ocean.

During primary production phytoplankton is produced in very small sized cells and organisms that do not sink on their own, except for species like *Fragilariopsis kerguelensis*, where single cells merge to longer chains, most probably as a protection against zooplankton grazing. Grazing of zooplankton is one of the main transform mechanisms for the packaging of suspended matter to make particles sink downwards [Strom et al., 2001]. Some zooplanktous organisms like e.g. *Euphausia superba* produce faecal pellets with a high sinking velocity. For some time, this was assumed to be the main way of producing sinking particles and thus export fluxes. In some ocean regions, e.g. the Norwegian Sea and in higher latitudes in general, this process still seems to be the most important mechanism for the repackaging of particles for export fluxes. Another way of compacting phytoplankton and detritus has been proposed, which is the aggregation of particles to marine snow. Particles stick together and thereby increase their size. This mechanism is dependent on the probability of particle collisions, which is a function of particle size and concentration [Alldredge and Gotschalk, 1989; Kjørboe et al., 1994]. Furthermore, particle stickiness, dependent on the physicochemical properties of the particle surface, has to be considered for the aggregation of marine snow [Engel, 2000]. Transparent exopolymer particles (TEP) are one class of particles, important for aggregation to occur. They are extracellular particles, that originate from phytoplankton exudates, especially polysaccharides [Alldredge et al., 1993; Logan et al., 1995]. These transparent extracellular gel particles stick together and form larger aggregates that capture phytoplankton cells and detritus as well. As TEP alone has a densitiy close to that of seawater it does not increase the aggregate's density, but mainly the size [Engel and Schartau, 1999]. However, due to its high stickiness, particle components of higher densities (inorganic shells, lithogenic matter) may be attached

to TEP, leading to an increase of the aggregates density and subsequent particle export.

Particulate matter found in the ocean is not necessarily of pure marine origin. There are considerable inputs of terrigenous material by eolian dust deposition and river discharge, respectively. These terrigenous contributions can either be mineral or organic. A detailed description of lithogenic material analysed from sediment trap data in the northeast Atlantic, for instance, is given by Ratmeyer et al. [1999]. Dust storms in desert areas of the Sahara and central Asia are the major sources of lithogenic dust depositions. There is lithogenic material deflated from the desert areas in the order of 1.4 Gt per year [Duce et al., 1991] to 2 Gt per year [Schütz and Sebert, 1987], which is mostly deposited in the oceans and thereby supply the surface ocean with iron. Iron is supposed to be the limiting micro nutrient in some open ocean areas e.g. in the Southern Ocean and the northeast and equatorial Pacific Ocean [Martin et al., 1990; 1991]. By this means, mineral dust deposition enhances particle export by stimulating biological production due to iron fertilization. This seems to be essential in areas with high abundance of macro nutrients (nitrate, phosphate) and low chlorophyll concentration, the so called HNLC areas [Cullen, 1991] like the Southern Ocean and the northeast and equatorial Pacific. Secondly, due to the higher density of lithogenic material, i.e. increased mineral ballast, particle sinking rates are increased [Armstrong et al., 2002] and scavenging of marine biomass by lithogenic particles appears [Ittekkot, 1993; Hebbeln et al., 2000]. Vice versa, the lithogenic material can also be trapped by the organic mucus of phytoplankton as reported by Honjo [1982] for a coccolithophorid bloom in the Panama Basin. However, the results from both explanations are increased particle settling rates due to lithogenic ballast. Iron fertilization experiments have shown, that adding iron to the surface water is likely to increase biological production [Coale et al., 1996], but a subsequent enhanced downward export of biogenic material has not been ascertained, yet. Possibly, it is the combination of an iron fertilized biomass production together with lithogenic ballast, which has forced enhanced carbon sequestration, as it is supposed to have taken place during glacial periods [Mahowald et al., 1999], leading to a significant lowering of atmospheric pCO_2 during glacial periods, as indicated by ice core records [Barnola et al., 1999] and discussed by Martin [1990] and Ittekkot [1993].

1.3 Element Ratios

The Redfield Ratio

Redfield [1934] and Redfield et al. [1963] determined that during primary production phytoplankton biomass is produced in constant molar elemental ratios of C:N:P:O of 106:16:1:-138; i.e. dissolved carbon, nitrogen and phosphorus are fixed into organic particles while oxygen is released. Their investigations included the analysis of

dissolved nutrients and measurements on particles in incubation experiments and in the field. Redfield et al. [1963] also reported species specific, seasonal and regional variations, but they concluded that on a global annual mean the element ratio corresponds to the value as cited above. This element ratio is called the classical Redfield ratio. It is considered to be valid for marine biomass in a phytoplankton bloom during exponential growth [Redfield et al., 1963]. The Redfield ratio is widely accepted as constant in space and time and applied as such in biogeochemical modeling.

Analyses of Dissolved Nutrient Fields

Several more recent studies based on the analysis of dissolved nutrient fields supported or slightly revised the classical Redfield ratios [Takahashi et al., 1985; Peng and Broecker, 1987; Minster and Boulahdid, 1987; Boulahdid and Minster, 1989; Anderson and Sarmiento, 1994; Arrigo et al., 1999]. For the determination of particulate element ratios from dissolved nutrients there are two approaches applied. The first one is measuring the nutrient drawdown during a phytoplankton bloom, which is the difference in nutrient concentrations before and after the bloom. The preformed nutrient concentration, i.e. the initial concentration of the respective tracer in the surface water before biological production occurred, can either be calculated or measured. Thus, some studies use measured winter values as the preformed nutrient concentration. The net nutrient drawdown by biological production corresponds to the difference between winter values and postbloom values, whereby upwelling of remineralized nutrients during winter deep mixing is taken into account [Arrigo et al., 1999]. The second way of analyzing dissolved nutrient ratios is the determination of nutrient regeneration ratios, i.e. nutritional elements that have been remineralized from the particles. A detailed description of this method is given by Körtzinger et al. [2001]. The method uses temperature and salinity as conservative tracers on isopycnal or neutral surfaces of carefully selected water masses to avoid changes in nutrient concentrations as a consequence of water mass mixing. In a first step, the apparent oxygen utilization (AOU), i.e. the difference between the in situ oxygen concentration and the oxygen saturation value is determined. Regressions of potential temperature versus oxygen concentration are made for the water masses under consideration. From the intersection of the respective regression line with the value of oxygen saturation, which is a function of temperature, the preformed concentration of oxygen (saturation value) can be derived. The concentration of regenerated dissolved nutrients is then determined using regression lines of oxygen concentration versus nutrient concentration. Here, the concentration of the preformed nutrients can be derived from the extrapolation of the regression line to the (preformed) oxygen saturation value. The regenerated nutrient concentration is the difference between the calculated preformed concentration and the in situ measurement. Having done this for several nutrients and carbon, respectively, allows the derivation of elemental ratios of regenerated nutrients.

The studies mentioned above are based on the detection of changes in dissolved

nutrient concentrations due to remineralization in carefully selected water masses. While restricted regions with special climatic conditions and nutrient levels can exhibit strong non-Redfieldian behavior at least temporariliy (e.g. Arrigo et al., 1999), all studies using basin-wide or global dissolved nutrient, carbon and oxygen distributions reveal remarkably constant (in space and time) elemental ratios with numerical values that agree well with the classical Redfield ratios. Larger differences are only found for the oxygen to phosphorus ratios, with values of about 170 instead of 138 [Broecker et al., 1985; Takahashi et al., 1985; Minster and Boulahdid, 1987; Boulahdid and Minster, 1989; Anderson and Sarmiento, 1994]. A study of temporal changes in the regeneration rates of dissolved nutrients by Pahlow and Riebesell [2000] has shown that in single ocean basins and on decadal time scales changes in the element ratios of dissolved nutrients may occur, suggesting that the marine carbon cycle is currently not in steady state.

Particle Measurements

A more direct approach for studying the elemental ratios of POM is the direct determination of the C, N and P content of particulate material obtained by filtrations and sediment traps. The most common sampling method is filtration of one to four liters of seawater over filters of a pore size between 0.7 and 1 μm. Such filtration data are relatively easy to obtain and provide a good regional and vertical data coverage. However, due to the small amounts of filtrated water the yield of particulate material is generally low, and particulate organic nitrogen (PON) and phosphorus (POP) are often close to the detection limit. In addition, the small POM samples are easily affected by contamination. Bishop et al. [1999] used in situ pumps for the filtration of POM from up to 20 m^3 of seawater. These samples yield large amounts of particulate material and are therefore supposed to be of very high quality.

Sediment traps, usually deployed for some months or up to two years, collect sinking material. While filter samples represent conditions at the time of sampling, sediment trap data provide integrated information over the whole deployment period with a temporal resolution between a few days to months, whereby seasonal variability near the surface or in deeper water masses can be detected. However, sediment traps might not capture the vertical particle flux quantitatively due to non-ideal trapping efficiencies and the composition of the material might be altered due to remineralization in the sampling cups [Gardner et al., 1983; Wakeham et al., 1993; Gust et al., 1994; Noji et al., 1999; Kähler and Bauerfeind, 2001; Scholten et al., 2001].

The elemental composition of marine particulate organic material has been studied extensively in the past [Holm-Hansen et al., 1966; Gordon, 1971; Copin-Montégut and Copin-Montégut, 1978; Honjo, 1980; Knauer and Martin, 1981; Honjo et al., 1982; Wefer et al., 1982; de Baar et al., 1983; Copin-Montégut and Copin-Montégut, 1983; Karl et al., 1984; Karl et al., 1988; Tréguer et al., 1990; Haake et al., 1993;

Hecky et al., 1993; Honjo et al., 1995; Arrigo et al., 1999; Honjo et al., 1999; Honjo et al., 2000; Hebbeln et al., 2000; Hebel and Karl, 2001; Hernes et al., 2001]. Although variations in particle compositions were found, all these studies concluded that their results were not significantly different from the classical Redfield ratios or spatial limitations did not allow general conclusions. Some studies discussed probable reasons for varying elemental ratios and came up with two major ways of explanation for deviations from the classical Redfield ratio: changes during particle production and changes during subsequent remineralization processes.

During production, variations in elemental compositions may be related to ambient CO_2 concentrations and nutrient availability [Sakshaug and Holm-Hansen, 1977; Burkhardt and Riebesell, 1997; Burkhardt et al.,1999]. Ample supply of phosphate and nitrate can lead to luxury consumption, e.g. particles may incorporate more nitrogen than essentially necessary, which leads to low C:N ratios [Droop, 1973; Elfiri and Turpin, 1985; Roelke et al., 1999]. Under nutrient limitation (phosphate and nitrate), particles may take up less nitrogen, i.e. they are able to incorporate relatively more carbon, leading to elevated C:N ratios [Gervais and Riebesell, 2001]. Changes during remineralization can occur as preferential remineralization of nutrients, i.e. phosphorus and nitrogen are released more easily from the particles than carbon and become faster available for new production. Although this process has not been observed directly, the idea was supported many times by measuring significant differences between dissolved and particulate elemental ratios [Thomas et al., 1999; Hupe and Karstensen, 2000; Osterroht and Thomas, 2000; Körtzinger et al.,2001]. Preferential remineralization can explain the process called carbon overconsumption [Toggweiler, 1993], describing the fact that more DIC is consumed by biological production than it can be explained by the application of the Redfield stoichiometry to the drawdown of nitrogen and phosphorus [Sambrotto et al., 1993; Michaels et al., 1994].

Pure mineral dust inputs are not supposed to influence the particle's C:N:P elemental compositions, as they do not contain organic substances. However, there may be terrigenous organic and inorganic components attached to lithogenic particles. Terrestrial biomass is mainly produced with C:N ratios higher than the Redfield ratios. Furthermore, terrestrial biomass has passed a long way of transport and decomposition until reaching the ocean [Kononova et al., 1966]. Therefore it is supposed to be strongly nutrient depleted, i.e. it has extraordinary high elemental C:N ratios. Such contributions are able to shift the elemental composition of formerly pure marine material to values of a higher relative carbon content. Another source of lithogenic components found in sediment traps is resuspended material from the seafloor. Due to benthic carbon decomposition, such contributions found in marine particulate material will shift particle elemental compositions to lower C:N ratios.

The explanations show that particles found in the ocean are a mixture of a large number of different sources, with many factors controlling their composition and element ratios. Hebel and Karl [2001] reported that sediment trap material does

not consist of pure phytoplankton, and as the aggregation to marine snow and/or repackaging to faecal pellets is needed for particle export, it is not surprising that deviations from the Redfield ratio, which originally should describe freshly produced material [Redfield et al., 1963] in a phytoplankton bloom at maximum growth rate, may appear.

Biogeochemical Models

Biogeochemical models combine physical, chemical and biological processes in the ocean to explain the distribution of property fields. Furthermore, they are used to make simulations for past and future developments. However, there is still large uncertainty e.g. about carbon export production. Results from the Ocean Carbon-Cycle Model Intercomparison Project (OCMIP) and from inverse modeling show that different models predict global carbon export fluxes between 8.6 and 25.5 Gt C per year [Najjar et al., in preparation; Schlitzer, 2002].

Elemental ratios are implied in the models to parameterize marine carbon and nutrient fluxes, and to calculate the oceanic storage capacity for carbon. Most of the major biogeochemical models use spatially and temporally constant elemental ratios according to Redfield et al. [1963], although there is observational evidence that particle compositions underly systematic variations. Consequently, the application of the Redfield ratio for flux estimations may underestimate carbon fluxes substantially.

1.4 Objectives

The aim of this study is to provide a new global perspective on the elemental composition of POM in the ocean and its implication on the global carbon cycle. An important aspect of this study is the very tight link of data analysis and model implementation. While large variations in particle compositions have been found in previous investigations using different methods, the spatial and/or temporal limitations of the respective data did not allow the derivation of general conclusions on basin-wide or global scales. In the current study, next to a global trend there will be regional and depth related variations in particle compositions investigated. Therefore, many independent measurements of C:N elemental ratios from particulate matter have been compiled into a large data collection for joint evaluation. Processes leading to variations in the elemental compositions will be explained. The results from the current data analysis will be discussed in comparison with results from analyses of dissolved nutrient fields. Furthermore, suggestions for the application in biogeochemical modeling will be given to yield better estimates of marine carbon and nutrient fluxes. A model approach will be presented, showing that systematic changes in particle compositions have a significant influence on marine biogeochemical cycles and the CO_2 exchange at the ocean-atmosphere boundary.

2 Elemental Composition of POM: Data Analysis

2.1 The Data Set

In this study, more than 10200 C:N measurements on particulate material from sediment trap and filter samples were compiled, covering large parts of the global ocean. Most of the data are from major research projects like *SFB 261* (Sonderforschungsbereich 261, University of Bremen) and *JGOFS* (Joint Global Ocean Flux Study), published in the internet. Only a minor contribution is from unpublished data. Detailed information about the individual data sets and their sources are given in Table 2.1. All data sets include data of particulate organic carbon (POC) and particulate organic nitrogen (PON). Several filtration data sets also include dissolved nutrients and chlorophyll concentrations of the ambient water. Most sediment trap data sets include particle fluxes in addition to element ratios. The global distribution of the resulting data set is shown in Figure 2.1 overlain on a global productivity map based on satellite observations [Behrenfeld and Falkowski, 1997]. Figure 2.1 shows that there are data from all major oceans, and many different hydrographic and biogeochemical provinces are covered. Data are available from oligotrophic regions like the Sargasso Sea as well as high productive areas in coastal and equatorial upwelling regions, in the Pacific, Indian and the Atlantic Ocean. Zones with seasonal ice cover in polar regions, areas of high nutrient and low chlorophyll *(HNLC)* concentrations in the South Atlantic and the northeast Pacific and furthermore the monsoon region of the Arabian Sea are also represented in the data set.

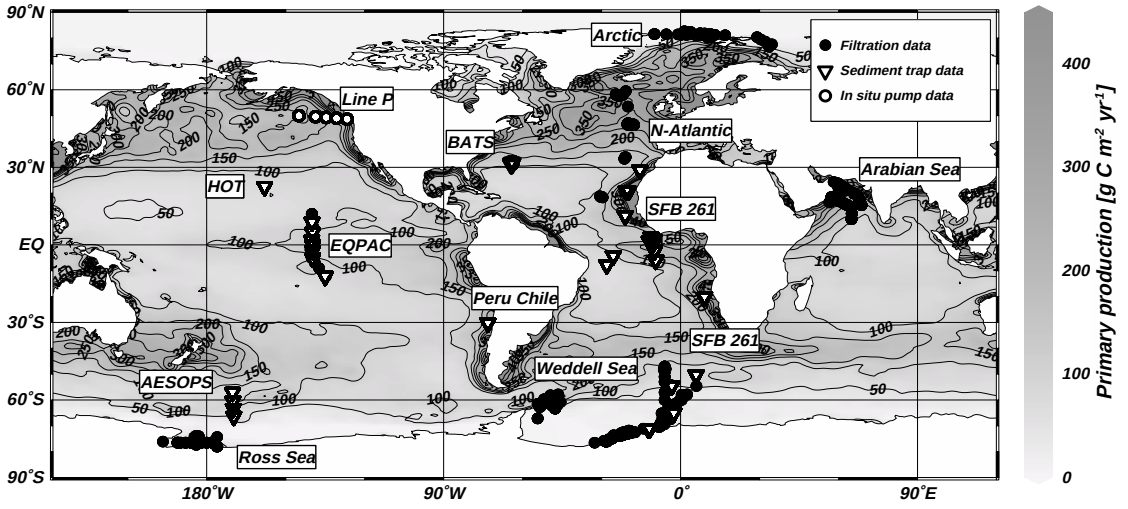

Figure 2.1: Sample locations of the C:N data collection overlain over the marine primary production map of Behrenfeld and Falkowski [1997].

Table 2.1: General overview and references of individual data sets used for this study.

Name	Cruise/Station	Type	No. of Samples	Project	References
AESOPS	MS-1, MS-2, MS-3, MS-4, MS-5	Traps	58	JGOFS	Honjo et al., 2000
Arabian Sea	ttn 043, ttn 045, ttn 049, ttn 053	Filter	944	JGOFS	http://usjgofs.whoi.edu/jg/dir/jgofs/
Arctic	ARK XIII/2	Filter	227	AWI	unpublished data
BATS	BATS trap 150, OFP 500, OFP 1500 OFP 3200, SCIFF/OFP	Traps	922	JGOFS	http://www.bbsr.edu/users/ctd/traplist.html
BATS	BATS bloom, BATS core, BATS valid	Filter	2896	JGOFS	http://www.bbsr.edu/users/ctd/batdataex.html
EQPAC	tt007	Filter	287	JGOFS	http://usjgofs.whoi.edu/jg/dir/jgofs/
EQPAC	eqpac	Traps	305	JGOFS	Honjo et al., 1995
HOT	HOT	Traps	206	JGOFS	http://usjgofs.whoi.edu/jg/dir/jgofs/
Line P	Line P	Pump	769	JGOFS	http://www.meds-sdmm.dfo-mpo.gc.ca/jgofs/ jgofs_cd/datasets/varela/readme.htm
North Atlantic	Nabe atl II, Meteor 10-1, Meteor 10-2	Filter	727	JGOFS	http://usjgofs.whoi.edu/jg/dir/jgofs/ (Nabe); and unpublished data
Peru/Chile	CH1-3, CH3-1, CH3-2, CH 4-1	Traps	80	JGOFS	Hebbeln et al., 2000
Ross Sea	NBP 96-4A, NBP 97-1, NBP 97-3	Filter	728	JGOFS	http://usjgofs.whoi.edu/jg/dir/jgofs/
SFB 261	BO1, BO2, BO3, CB1, CB2, CB3, CB4, CB5, CI1, CI2, CI3, CI4, CV1, CV2, EA1, EA2, EA3, EA4, EA5, EA8, GB2, GBN3, GBN6, GBZ4, GBZ5, KN1, KN3, PF3, PF5, WA1, WA2, WA3, WA4, WR1, WR2, WR3, WR4, WS3, WS4	Traps	897	SFB 261	Fischer and Wefer, 1996; Wefer and Fischer, 1993 and unpublished data
Weddell Sea	ANT III/3, ANT V/2, ANT VII/2, ANT X/6	Filter	1009	AWI/ JGOFS	Nöthig, 1987; Scharek, 1990; Bianchi et al., 1992; Rutgers van der Loeff et al., 1997

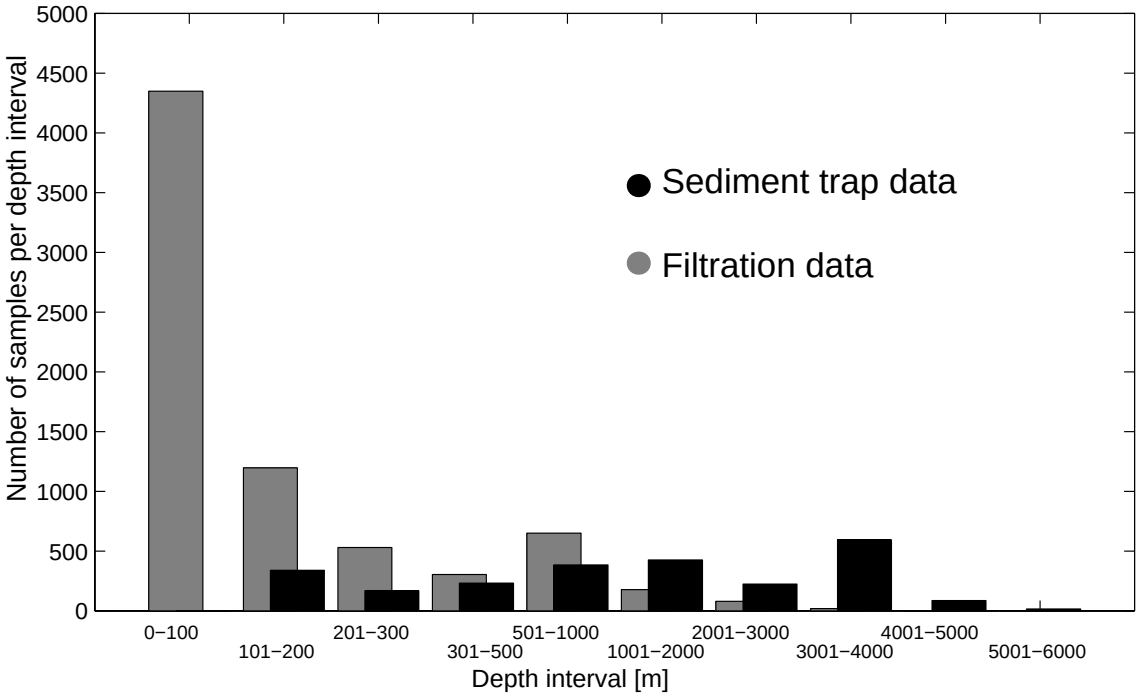

Figure 2.2: Sample distribution over depth in the water column.

The data collection contains data from sediment trap samples as well as from filter samples obtained from small or relatively large (in situ pumps) volumes of seawater. Approximately 75 % of the values in the data set are from filtrations while 25 % are sediment trap data (Figure 2.1). Filtration data are mostly from the upper water column with a mean depth of 200 m. Sediment trap samples are taken at deeper levels with an average depth of 1500 m (Figure 2.2). Sediment traps are typically deployed over time periods from months to one or two years, and provide time-series measurements. Filtration data, on the other hand, represent point measurements in space and time, and thus exhibit spatial and temporal variability caused by individual production and remineralization events. Figure 2.3 shows the seasonal resolution, i.e. the number of samples per month, for both methods, filter samples and sediment trap data. Sediment traps are distributed evenly over the whole year, whereas filtrations show large differences between single months. The spatial distribution of data is patchy as there are some regions with many data, as e.g. the *BATS* site (Bermuda Atlantic Time-series Study) in the Sargasso Sea, where a time-series of more than twenty years has been recorded, and 35 % of all data in the current study are from this site. Another reason for the spatially inhomogeneous distribution is disproportionate depth coverage at some locations. At the *HOT* site (Hawaiian Ocean Time-series) in the subtropical north Pacific, e.g. there are only data from the upper 500 m available, and from the *AESOPS* site (Antarctic Environment Southern Ocean Process Study) in the subpolar south Pacific there are only data from a depth level of 1000 m $\pm$ 50 m. Therefore, single subdata sets are overrepresented in estimating global averages, which has to be taken into account

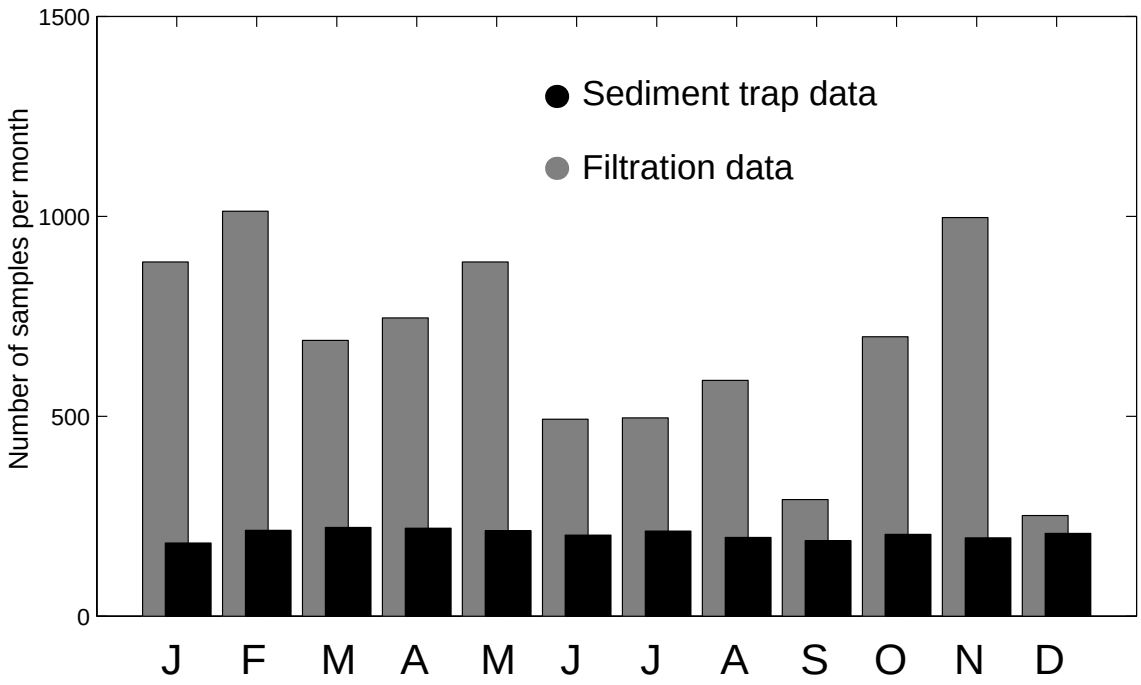

Figure 2.3: Number of samples per month.

for further interpretations.

All data are transferred from their original formats into ODV-collections (Ocean Data View) [Schlitzer, 2002] to facilitate joint evaluation. The following analysis focuses mainly on C:N ratios, because these data are most abundant. Throughout this study, C:N ratios are given in molar units. Weight ratios in the original data sets were converted to molar units using the atomic weights for carbon (12) and nitrogen (14). Arithmetic means ($\bar{x}$) of C:N ratios, standard deviations (s) and standard mean errors ($s_{\bar{x}}$) are calculated for different depths or regional data subsets. A t-test is applied to test whether the occurring differences are statistically significant. With a level of confidence higher than 95 %, corresponding to a level of significance of 0.05, deviations are supposed to be statistically significant. Regression analyses are made by linear least squares fits. The statistical analyses follow procedures from Sachs [1997] and Lozan and Kausch [1998].

2.2 General Trend

The investigation of data about the elemental composition of POM reveals that C:N ratios are highly variable with systematic deviations from the classical Redfield ratio into both directions. For a global overview all available values of POC versus PON (n = 10224) are displayed in Figure 2.4. Despite the large scatter, the data show that POC:PON ratios are generally higher than the classical Redfield ratio, which is evident especially for higher POC and PON values. The global mean C:N

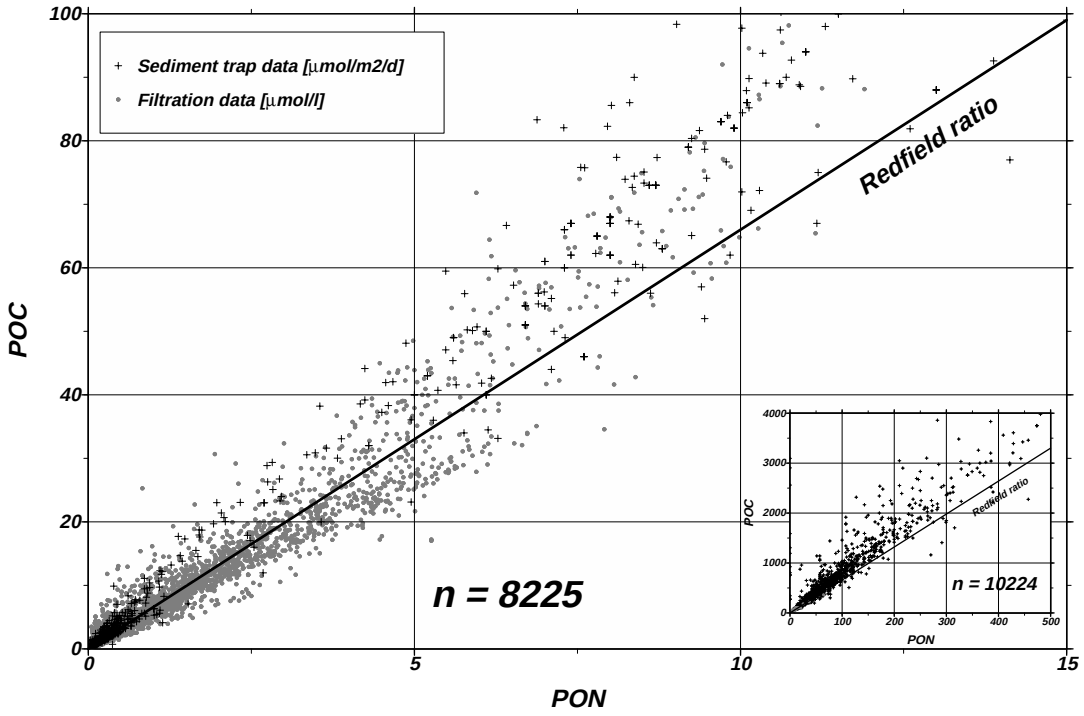

Figure 2.4: Particulate organic carbon (POC) displayed versus particulate organic nitrogen (PON) for all data from all depths. The solid line indicates the classical C:N Redfield ratio of 6.6. The small panel shows the whole range of data, whereas the large panel displays the range of low POC and PON values, only.

molar ratio for all data and all depths (note that data are not evenly distributed over depth, see Figure 2.2) is 8.2 $\pm$ 0.1 with values reaching from 3 to up to 60. Some minimum values lower than 3 were found (n = 45) in the Arabian Sea during the whole year and at all depths. This ratio is even lower than the C:N ratio of pure bacterial biomass. Substances with C:N ratios lower than three can not be explained, therefore these data were excluded from further analyses.

The large database, which comprises data from different sampling techniques, permits a detailed evaluation of both C:N ratios and analytical methods. As it was proposed before, data from different sampling strategies may gather different types of particles exhibiting systematic variations in their elemental compositions. A direct comparison of data from the two sampling approaches (filtrations and sediment traps), can be made at the site of *BATS* in the Sargasso Sea, where both methods were applied at the same time and position in the upper 500 m of the water column. In Table 2.2 mean C:N ratios of data from the 1989-1999 period for both sample types are shown for four depth levels, 150 m, 200 m, 300 m and 500 m (n = 997), respectively. Sediment trap data are representative for the given depth, while filtration samples were taken from a depth range 10 m above and below the reference

Table 2.2: Comparison of sediment trap data with filtration data at the *BATS* site, 150-500 m depth: mean C:N ratios, standard deviation (s), number of samples (n) and level of significance.

	Filtration data			Sediment trap data			Level of
depth	**C:N**	**s**	**n**	**C:N**	**s**	**n**	**significance**
150 m	7.7	2.8	164	7.0	1.4	115	0.01
200 m	8.0	2.8	141	7.6	2.8	113	n.s.
300 m	9.8	3.0	110	8.9	2.8	112	0.05
500 m	9.9	3.1	118	8.1	3.2	124	0.001

level. C:N ratios from filter samples turn out to be systematically higher than those from sediment trap data. In the depth of 150 m the C:N ratio of filtration data is 7.7, while sediment trap data show a C:N ratio of 7.0. The discrepancy increases towards greater depth, and in 500 m depth the C:N ratio of filter samples is 9.9 in contrast to 8.1 from the sediment trap data. The differences between the filter and trap samples from the *BATS* site are statistically significant on all examined depth layers except for 200 m. Both data types show standard deviations of similar magnitude, ranging from 1.4 to 3.2, indicating that the scatter is similar for both sampling types. Also, in situ pump data (not shown separately) exhibit similar variances as compared with small volume filter samples, suggesting that the variability in the data is mostly due to natural variability and not caused by analytical procedures. A detailed comparison between in situ pumps and small volume filtrations revealed no significant differences in the range of C:N ratios nor in the standard deviation. Therefore, in the following, in situ pump data and small volume filtrations are treated alike.

2.3 C:N Depth Dependence

For the study of depth dependencies, all available sediment trap C:N ratios (n = 2462) are plotted versus depth as shown in Figure 2.5. The determination of depth related variations of particulate elemental compositions refers to sediment trap data only, because these samples contain truly sinking material, whereas filter samples may largely consist of suspended material [Altabet, 1988]. Furthermore, sediment trap data are more evenly distributed over depth than filter data, and they span longer time intervals, allowing the calculation of annual mean values and the detection of seasonal trends. Also shown in Figure 2.5 is the C:N versus depth regression line (solid) and the classical C:N Redfield value of 6.6 (dashed line). Despite the relatively large scatter, the regression line clearly shows an increase of C:N values with depth. This increase of particulate C:N ratios with depth in the water column (based on 2462 sediment trap samples) can be described by the equation:

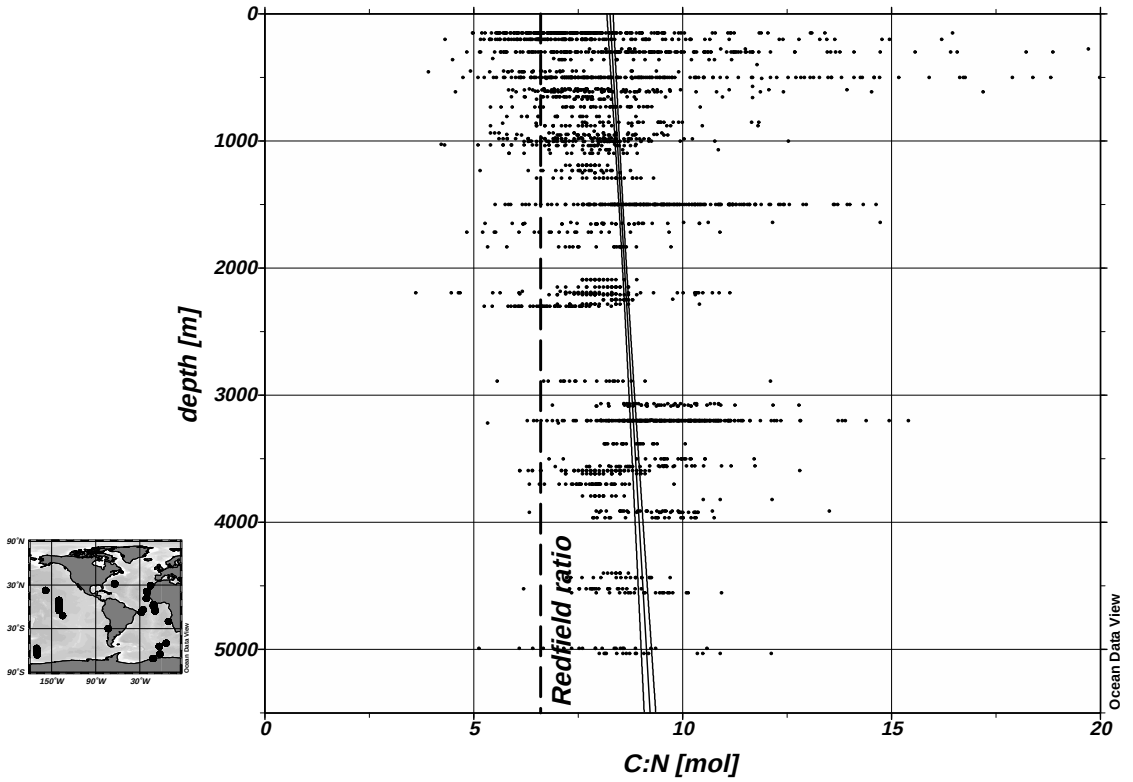

Figure 2.5: C:N ratios of sediment trap samples versus depth. The dashed line indicates the Redfield ratio of C:N (6.6), the solid black line is the regression line for the increase of C:N ratios with depth. The curved lines mark the mean error of the regression line.

$$C:N(z) \;=\; 8.26\ (\pm 0.1) \;+\; 0.17\ (\pm 0.1) \;\cdot\; z\ [km] \tag{2.1}$$

The mean C:N ratio of sinking POM in the surface water is about 8.3, which is significantly higher than the classical Redfield ratio. Additionally, C:N ratios are increasing over depth with a rate of almost 0.2 per 1000 m water depth. Because the shallowest traps were deployed in 150 m water depth, the C:N value for the surface water is obtained as an extrapolation of deeper values. There are regional differences in the absolute values of C:N ratios as well as in the rates of increase over depth. In Table 2.3 and Figure 2.6 these increases are shown for some regions that exhibit larger than average depth increases of C:N values, such as the Sargasso Sea, the South Atlantic and the low-latitudinal Atlantic.

As a consequence of spatially and temporally inhomogeneous data distribution, individual regions may influence the global mean values disproportionately. This may be the case for the *BATS* data which make up roughly 35 % of all sediment trap data points. Also, there are numerous data from the *HOT* time-series, including 10 years of investigations in the subtropical North Pacific, which have a significant impact on global mean values. These data cover the depth interval between 150 and

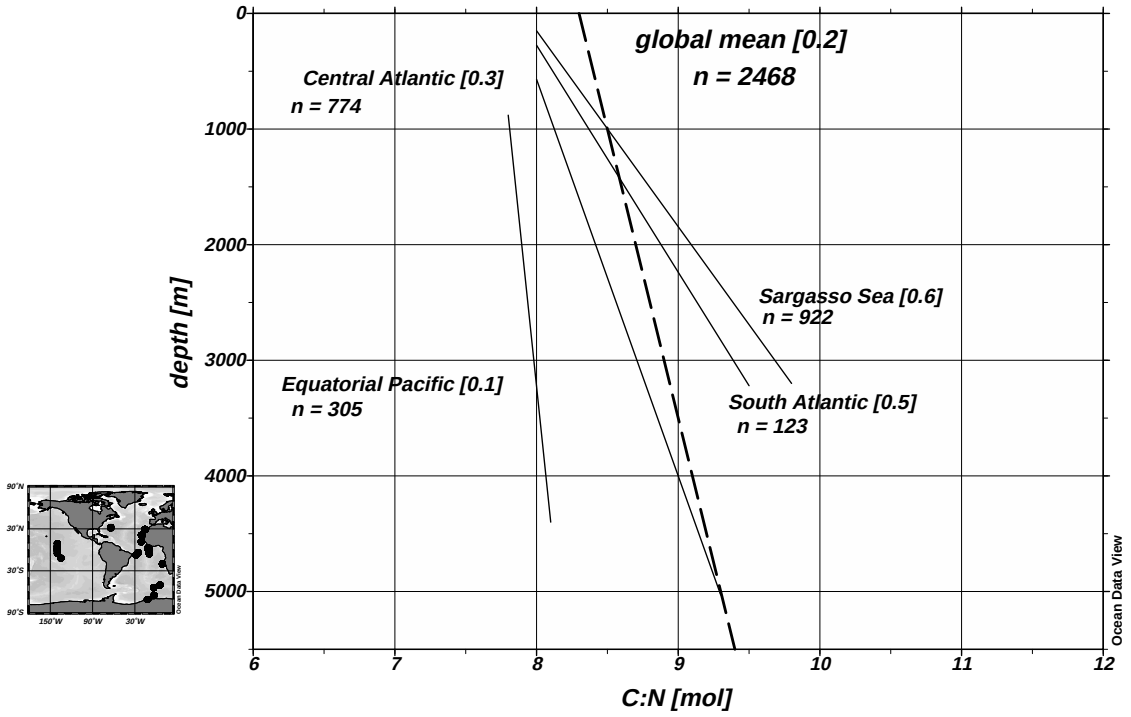

Figure 2.6: Rates of increase over depth of C:N ratios of sediment trap samples from different ocean basins. Numbers in brackets are the rates of increase per 1000 m depth interval and the dashed thick line indicates the global mean. The vertical extent of the lines represents the depth interval covered at the respective sampling area.

500 m only, but with a total of 206 single data points they amount to 10 % of all sediment trap data. The mean C:N ratio of the *HOT* data amounts to 10.2 with a standard deviation s=4.58 (see Table 2.4) which is a much higher mean value than the classical Redfield ratio and other data from similar depth intervals. This deviation results in a significant shift of global mean C:N ratios towards higher values in near-surface waters and simultaneously it reduces the rate of increase of C:N ratios over depth markedly. If the *HOT* data are excluded from the data set the depth dependence is described by:

$$C:N(z) \;=\; 7.8\ (\pm 0.1) \;+\; 0.31\ (\pm 0.1) \;\cdot\; z\ [km] \qquad (2.2)$$

Compared to equation 2.1 the surface C:N values are now significantly lower and the rate of increase with depth is higher. Table 2.4 shows mean C:N ratios of sinking particles (sediment trap samples) from selected regions and depth ranges. Higher than Redfield C:N ratios are found almost everywhere and increasing C:N ratios over depth are also detected in most cases. However, note that there is a statistically significant decrease of C:N ratios near the bottom (e.g. East Atlantic and all samples). This effect will be discussed in more detail below.

Table 2.3: Linear least squares fits of C:N ratios as functions of depth for sediment trap data from selected regions with large vertical data coverage.

Name	Depth Range	Regression Line	n
Sargasso Sea	150 - 3200 m	C:N = 7.9 + 0.6 · z [km]	922
Atlantic (30°N-20°S)	570 - 5030 m	C:N = 7.8 + 0.3 · z [km]	774
South Atlantic	275 - 3220 m	C:N = 7.9 + 0.5 · z [km]	123
Equatorial Pacific	880 - 4400 m	C:N = 7.7 + 0.1 · z [km]	305

Table 2.4: Mean values of C:N ratios, standard deviations (s) and number of samples (n) for sediment trap data from selected regions. Bold numbers indicate significant deviations from the Redfield ratio of 6.6.

	E-Atlantic (SFB 261)			**W-Atlantic (SFB 261)**			**S-Atlantic (SFB 261)**		
depth [m]	**C:N**	**s**	**n**	**C:N**	**s**	**n**	**C:N**	**s**	**n**
0-500							**7.77**	2.32	58
501-1500	**8.13**	1.06	276	**7.39**	0.72	92	**8.75**	2.23	45
1501-2500	**8.31**	1.66	93				6.12	1.79	12
2501-3500	**9.00**	1.19	98				11.91	7.34	8
3501-4500	**9.28**	1.07	139						
4501-5500	**8.01**	0.63	20	**8.72**	1.23	56			
	Sargasso Sea (BATS)			**S-Pacific (Peru/Chile)**			**N-Pacific (HOT)**		
depth [m]	**C:N**	**s**	**n**	**C:N**	**s**	**n**	**C:N**	**s**	**n**
0-500	**7.92**	2.93	480				**10.24**	4.6	206
501-1500	**9.54**	1.76	183						
1501-2500				**6.83**	0.71	40			
2501-3500	**9.69**	1.35	259						
3501-4500				**7.84**	0.61	40			
4501-5500									
	S-Pacific (AESOPS)			**Eq. Pacific (EQPAC)**			**All sediment trap data**		
depth [m]	**C:N**	**s**	**n**	**C:N**	**s**	**n**	**C:N**	**s**	**n**
0-500							**8.55**	3.58	744
501-1500	6.7	1.0	58	**7.7**	0.7	68	**8.28**	1.62	722
1501-2500				**8.0**	0.6	140	**7.87**	1.26	285
2501-3500							**9.55**	1.71	365
3501-4500				**8.0**	0.8	97	**8.63**	1.14	276
4501-5500							**8.53**	1.15	76

2.4 Lithogenic Contribution

Marine sinking particles consist of marine produced particulate organic matter, but may carry substantial amounts of lithogenic material of eolian dust input, river discharge or from resuspension from the seafloor. The content of lithogenic matter from sediment trap samples is calculated as Lithogenic = Total - Opal - Carbonate - $2C_{org}$, i.e. it is not determined directly as lithogenic material, but calculated from other parameters. On a global mean, sediment trap samples consist of 25 %

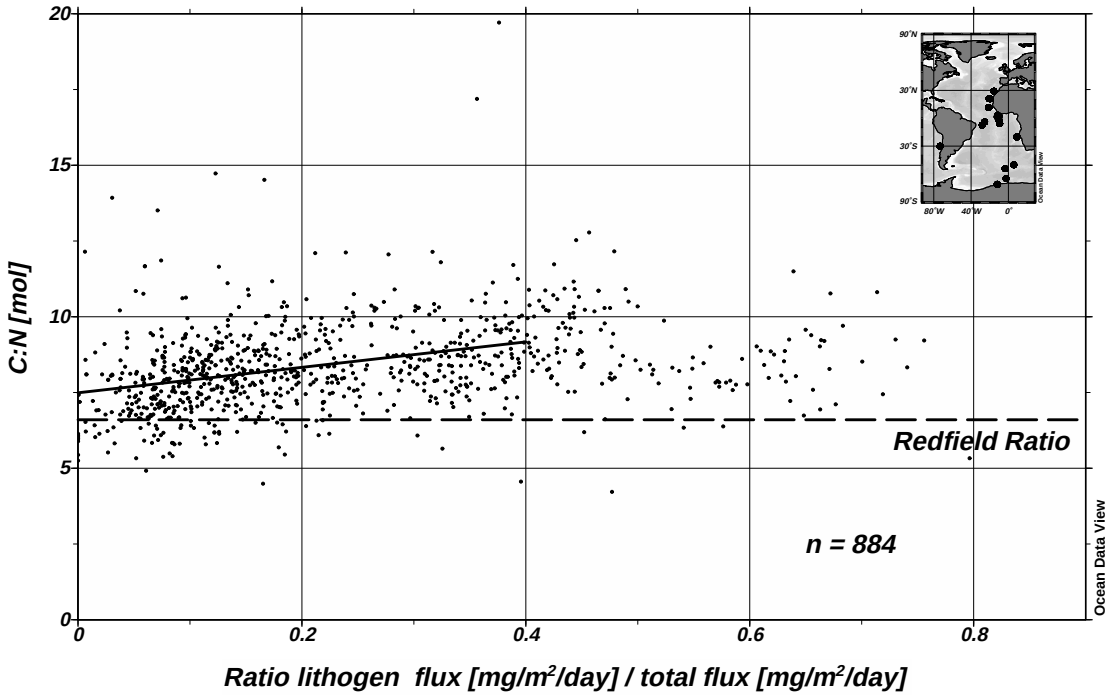

Figure 2.7: C:N ratios of sediment trap samples versus relative flux of lithogenic material. The dashed line indicates the classical Redfield ratio of 6.6, while the solid line is the regression line for particles fluxes with less than 40 % lithogenic contribution.

lithogenic material, and in some cases lithogenic fluxes reach up to 90 % of total flux rates. These lithogenic contributions can influence elemental ratios significantly [Wefer and Fischer, 1993]. In Figure 2.7, C:N ratios of sinking POM are displayed versus the relative contribution of lithogenic material to the total flux for data from the Atlantic Ocean and the southeast Pacific Ocean, including all stations where data of lithogenic fluxes were available. For small and moderate lithogenic contributions, there is a positive correlation between lithogenic fluxes and C:N ratios, with an increase of 0.4 units per 10 % increase of lithogenic fluxes. To separate the C:N values of marine particles from bulk particle values, a correction procedure was applied to eliminate the effect of the lithogenic component. In a first step all data with lithogenic fluxes higher than 40 % were omitted. For the remaining data, the C:N signal of the lithogenic contribution was estimated from the slope of the regression line of C:N ratio vs. relative lithogenic flux (Figure 2.7), and the values were corrected to zero lithogenic contribution.

For some data of more open marine sites, which did not include appropriate parameters for lithogenic fluxes, this correction procedure could not be used (*BATS, HOT, AESOPS, EQPAC*). However, there is evidence from associated aluminum measurements (used as a proxy for lithogenic contributions) that most of these data do not need correction due to very low lithogenic fluxes, i.e. they can be used as such for the derivation of a C:N depth dependency. These arguments seem to ap-

Table 2.5: Comparison of lithogenic and corresponding aluminum fluxes from sediment trap data between different regions.

Name	Lith. fluxes $g/m^2/yr$	Al-fluxes $mg/m^2/yr$	% lithogenic of total fluxes	Reference
AESOPS	0.05 - 0.12	4.1 - 59.4	0.2 - 6.9	Honjo et al., 2000
EQPAC		1.2 - 42.4		Honjo et al., 1995
NE-Atlantic (lowest)	4.2 - 7.7		22 - 70*	Ratmeyer et al., 1999
NE-Atlantic (highest)	11.4 - 20.5		22 - 70*	Ratmeyer et al., 1999
Arabian Sea	2.9 - 10.5	219 - 284	9 - 13	Honjo et al., 1999

*from this analysis

ply to the *AESOPS* data set, where in addition to detailed aluminum flux rates, lithogenic fluxes are given as annual mean values, and for the *EQPAC* sediment trap data, where only aluminum fluxes are given. The comparison of aluminum flux rates of these two data sets with data from the literature [Honjo et al., 1995; Honjo et al., 1999; Ratmeyer et al., 1999; Honjo et al., 2000] reveals that lithogenic fluxes in these two sub data sets are in fact negligible. This comparison is displayed in Table 2.5. aluminum fluxes in both cases (*AESOPS* and *EQPAC*) are in the range of 1.2-60 $mg/m^2/yr$. At the site of *AESOPS* this corresponds to annual lithogenic fluxes between 0.05 and 0.12 $g/m^2/yr$. Comparing these values with data from the subtropical Northeast Atlantic [Ratmeyer et al., 1999] and to data from the Arabian Sea [Honjo et al., 1999] shows that firstly, the relatively low lithogenic fluxes from the Northeast Atlantic exceed those from *AESOPS* by far and secondly, the amount of aluminum fluxes from the Arabian Sea are also much higher than aluminum fluxes from the *AESOPS* and *EQPAC* data sets. Therefore, lithogenic fluxes at the *AESOPS* and *EQPAC* sites can be neglected in the following approach for the investigation of pure marine particulate organic matter.

The corrected C:N ratios and those that did not need correction (n = 1123) are displayed in Figure 2.8 versus depth in the water column. It is found that there is still an increase of C:N ratios with depth of about the same rate as it has been determined for the uncorrected values shown in Figure 2.4. However, the corrected C:N values are now closer to the classical Redfield ratio than the uncorrected values. The increase of C:N ratios of what is considered as pure marine sinking particulate organic matter corresponds to the following equation:

$$C:N(z) \;=\; 7.14\ (\pm 0.1) \;+\; 0.18\ (\pm 0.1) \;\cdot\; z\ [km] \tag{2.3}$$

The C:N ratio of pure marine sinking particles for the surface water is just above 7.1 and the increase over depth amounts to 0.2 per 1000 m. As the shallowest trap for this analysis is in 275 m depth the C:N ratio for particulate material at the surface was inferred by extrapolation.

The depth dependence of C:N ratios from particles without lithogenic components can also be achieved without correction, by the application of bulk particle flux data

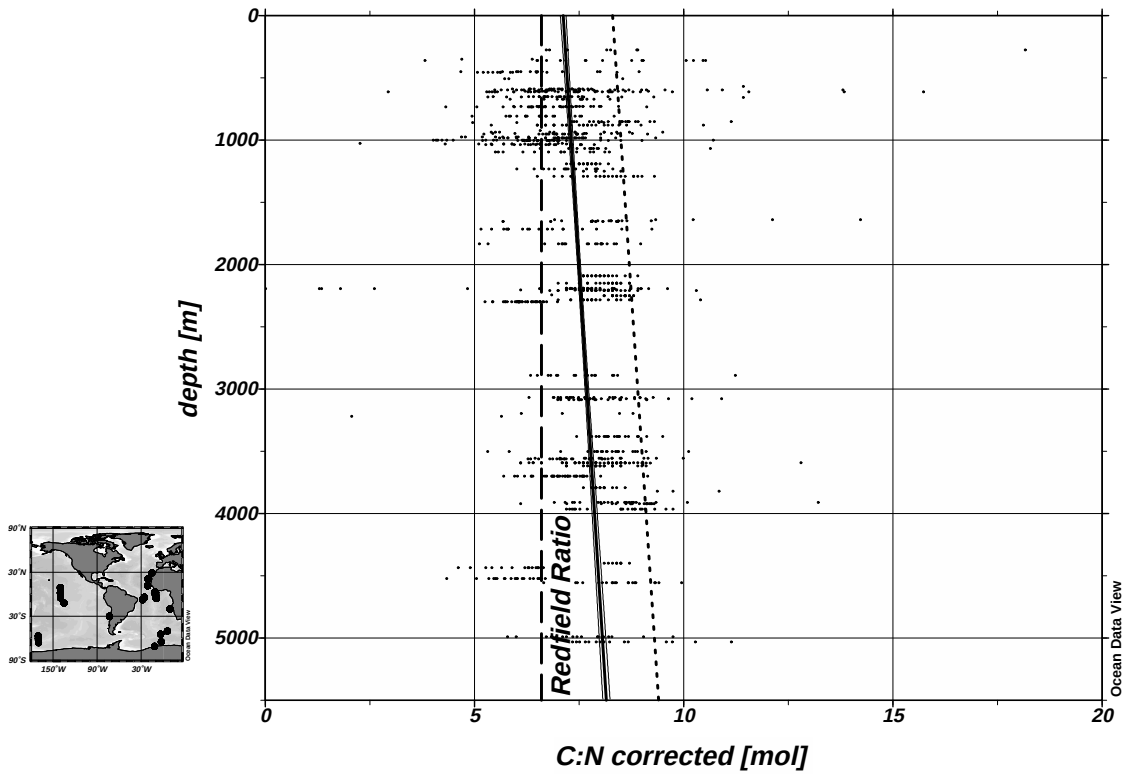

Figure 2.8: C:N ratios of sediment trap samples corrected for lithogenic contributions (see text) versus depth. The dashed line indicates the Redfield ratio of C:N (6.6), the solid line is the regression line for the increase of C:N ratios with depth (equation 2.3)and the curved lines mark the mean error of the regression line. The dotted line shows the increase of C:N ratios with depth of uncorrected sediment trap data (equation 2.1).

where lithogenic contributions are negligible. Therefore, all samples with lithogenic fluxes lower than 10 % are chosen from the global data collection and only the data from the *AESOPS* and *EQPAC* sites are included as well, where lithogenic fluxes are low as explained above. After plotting the respective C:N ratios versus depth, the resulting increase with depth is of comparable magnitude to the one obtained from the corrected data with a slightly higher surface value of 7.4 and a rate of increase with depth of 0.2 per 1000 m depth. The number of samples has slightly increased in contrast to the corrected values (n=867), and the errors are in the same order of magnitude as in the analyses made before.

$$C : N(z) \;=\; 7.4\ (\pm 0.1) \;+\; 0.22\ (\pm 0.1) \;\cdot\; z\ [km] \tag{2.4}$$

Relations of elemental ratios versus depth show for may different approaches, that the C:N ratios of POM are significantly higher than the classical Redfield ratio and that there are increasing ratios over depth in the water column on a global annual mean, and also for single regions.

The higher than Redfield C:N ratios and the depth dependence obtained in the present study can be extrapolated to carbon to phosphorus ratios, assuming constant N:P ratios equal to the Redfield ratio of N:P = 16. In this case, corresponding to a C:N ratio of 7.1 the C:P ratio for particles near the surface amounts to 114 (traditional Redfield C:P = 106). The increase with depth is 3.2 molar units per 1000 m depth interval leading to a C:P ratio of 130 in 5000 m water depth.

2.5 Temporal Changes

Seasonal Trends

In large regions of the world, biological production is characterized by strong seasonal patterns [Longhurst, 1998]. In mid and high latitudes, marine primary production can be limited by seasonal changes of insolation leading to light limitation, and furthermore to changes in water temperature as well as seasonal ice coverage. In lower latitudes, e.g. a monsoon system changes wind and (surface) water circulation patterns vice versa twice a year, which also affects biological production, significantly. These forcings, combined with regionally specific nutrient abundance and general oceanic circulation systems lead to regionally distinct patterns of biological production. These patterns are reflected e.g. in highly seasonal particle flux rates and possibly also in seasonal changes of particle compositions.

In the present data set, time-series measurements that are long enough to allow the determination of seasonal trends, are available at three locations. One location is the Hawaiian Ocean Time-series (*HOT*), where sediment trap data are available from the upper 500 m of the water column, for the period from 1989 until 1999. The second location is the *BATS* site in the Sargasso Sea, where filtration and sediment trap data were gathered simultaneously. Here, the determination of seasonal signals data from the time interval from 1992 until 1997 and the depth layer from 150 until 500 m water depth are chosen. The deeper sediment traps and filter data are left out, because seasonal variations are expected to occur mostly in the surface and subsurface layers. The third area is the South Atlantic Ocean, investigated by sediment trap deployments, covering the time interval from 1988 until 1992. Sediment trap deployments were made here at three stations in the eastern Weddell Sea, reaching from 54^o S to 71^o S, and from 250 until 500 m water depth.

Sediment trap data from the *HOT* site in the oligotrophic subtropical North Pacific do not reveal seasonal signals, neither for total or organic carbon fluxes, nor for the accompanying C:N ratios. For the time period from 1989 until 1995, where the depth range from 150 until 500 m was investigated, there is a very high scatter of both, the total and the organic carbon flux rates. The total fluxes have an average value of 45.07 mg/m^2/day ($\pm$ 1.95, n=159) and the organic carbon fluxes show a mean value of 18.13 mg/m^2/day ($\pm$ 0.83, n=163). At the same time the C:N ratios are also highly variable and significantly elevated compared to the classical Redfield

ratio with a mean value of 10.68 (± 0.39, n=163). The large scatter of particle fluxes and of particulate C:N data from the *HOT* site shows that though a seasonal signal cannot be ascertained here, both the fluxes and the C:N ratios are also not evenly distributed over the year. This indicates high temporal variability on time scales of weeks to months.

In the Sargasso Sea data of total particle fluxes reveal seasonal changes, as shown in Figure 2.9. The total flux rates are displayed here, because data of organic carbon fluxes are not available from the *BATS* site. The highest particle fluxes appear during winter, each year from December until March, and they reach maximum values up to 470 mg/m^2/day during January. However, during the rest of the year the total fluxes are significantly lower, especially from April to November, where the average amounts to 61.1 mg/m^2/day (± 2.6, n=210).

The C:N elemental composition of particles also shows a clear seasonal pattern. In Figure 2.10 this is displayed for the C:N ratios of organic particles from both, filtration and sediment trap data. At the beginning of each year, average C:N ratios decrease to their lowest values, which appear from March until May. In May, the lowest monthly mean C:N ratio of 6.48 (± 0.20, n=19; sediment trap data) occurs. From then on, the C:N ratios of sediment trap samples increase to their maximum in August with a mean value of 8.31 (± 0.43, n=25), from which they decrease again to the low winter values. The difference between the minimum and maximum mean monthly values in May and August, respectively, is statistically significant. The seasonal progression of the C:N ratio from filtration data is similar, but slightly more pronounced. The lowest mean value of C:N ratios from filter samples is in February with a value of 6.58 (± 0.37, n=56), which is slightly but not significantly higher than the corresponding sediment trap value. The seasonal increase of C:N ratios from filter samples begins in April, a little earlier than it was determined for the sediment trap data, and the according C:N ratios reach maximum values in September, which is two months later than the peak of sediment trap data. The monthly mean C:N ratio of the filtered material in September is 10.35, but there is also a relatively large error (± 0.88, n=32). However, this filter maximum in September is significantly higher than the highest mean value of sediment trap samples, and there is also a statistically significant difference between the maximum and the minimum mean values from filter samples. Comparing the seasonal progression of sediment trap and filtration data shows next to the higher scatter of filtration data, which can be seen in the larger standard mean errors, that the C:N ratios obtained from filter analyses are also systematically higher than the C:N ratios measured from sediment trap samples.

In the South Atlantic particle flux data from sediment traps also show strong seasonal changes that are even more pronounced than in the Sargasso Sea (Figure 2.11). The total flux rates are shown again to allow the comparison with the *BATS* data, even though data of organic carbon fluxes are available. However, the organic carbon flux data reproduce the same pattern as the total flux rates do, they are only

lower by a factor of about 10. The highest particle fluxes in the southern hemisphere occur during the summer season, especially in January and February, when they reach peak values of 1300 mg/m^2/day. There are moderate flux rates at the end of the summer season in March, with values up to 500 mg/m^2/day, but during the rest of the year, particle fluxes are very low. From May until the end of October they have a mean value of 30 mg/m^2/day ($\pm$ 5.01, n=48), which is even much lower than particle fluxes during the season of low particle flux in the Sargasso Sea.

The accompanying C:N ratios in the South Atlantic also reveal high seasonal variability, which is shown in Figure 2.12. During the productive summer season, from January until April, C:N ratios reach their maxima with the highest monthly mean value of 9.81 ($\pm$ 0.60, n=5) in April. From May on they decrease strongly and scatter around the Redfield ratio from June until November. During this time the minimum C:N ratio occurs in June with a monthly mean value of 5.79 ($\pm$ 0.69, n=4), which is significantly lower than the maximum value measured in April. In the beginning of spring (November), the C:N ratios start to increase again observably towards the high summer values.

The relation of C:N ratios versus particle flux rates in data from the *BATS* site (Figure 2.13, sediment trap data only) shows that highest particle fluxes coincide with relatively low C:N ratios, around the classical Redfield ratio. The largest scatter can be found for C:N ratios during lower particle flux rates. The data from the South Atlantic show an opposite behavior in the relation of particle fluxes to element ratios, which is shown in Figure 2.14. During times of high flux rates the C:N ratios of sinking particles are always significantly higher than the Redfield ratio. When particle fluxes are low, C:N ratios also reveal the largest range of scatter, as it is found for data from the *BATS* site.

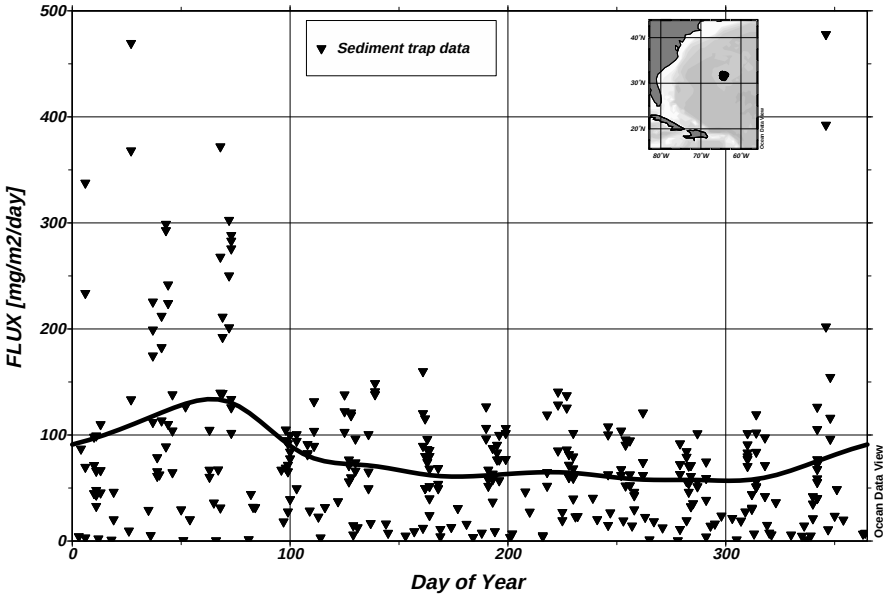

Figure 2.9: Seasonal variation (1992-1997) of total particle flux rates at the *BATS* site in the Sargasso Sea. Samples are from 150 m down to 500 m water depth (n=316). The black line shows the monthly mean values of total particle fluxes.

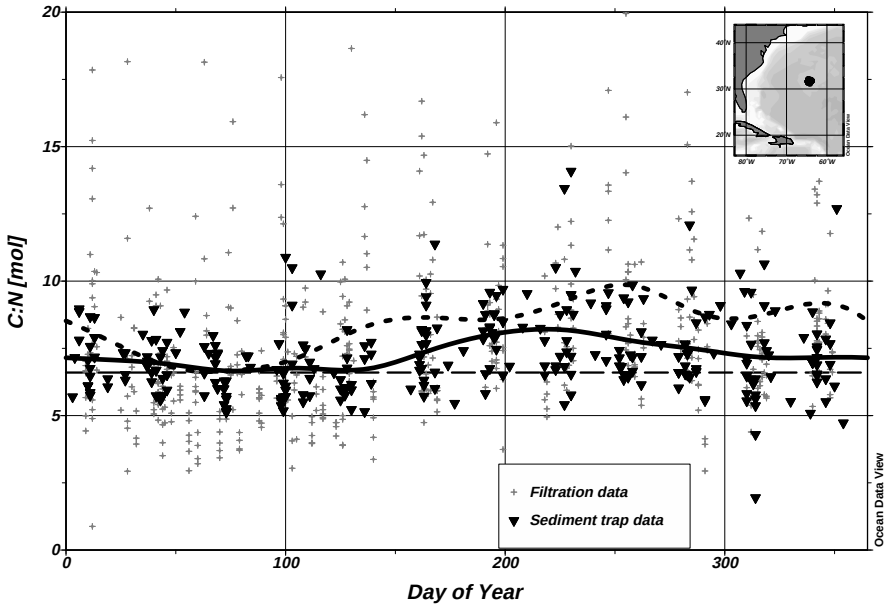

Figure 2.10: Seasonal variation (1992-1997) of C:N ratios at the *BATS* site in the Sargasso Sea. Samples are from 150 to 500 m depth. The gray crosses are filtration data, triangles mark sediment trap data (n=806). The dashed line is the classical Redfield ratio for C:N (6.6), the solid black line shows the monthly means of sediment trap data and the dotted black line is the monthly mean from filtration data.

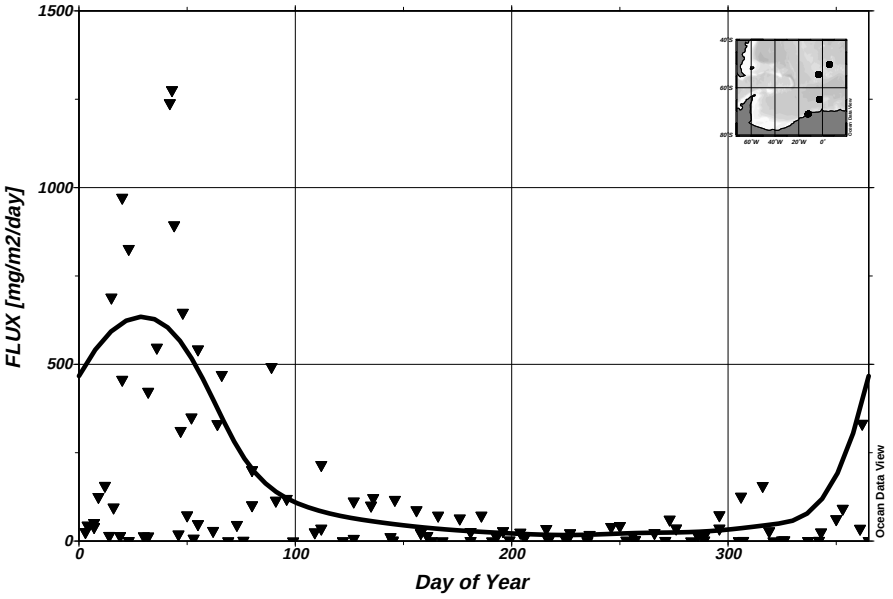

Figure 2.11: Seasonal variation (1988-1993) of total particle flux rates in the South Atlantic. Samples are from 250 until 500 m depth (n=107) The black line shows the monthly averages of particle fluxes.

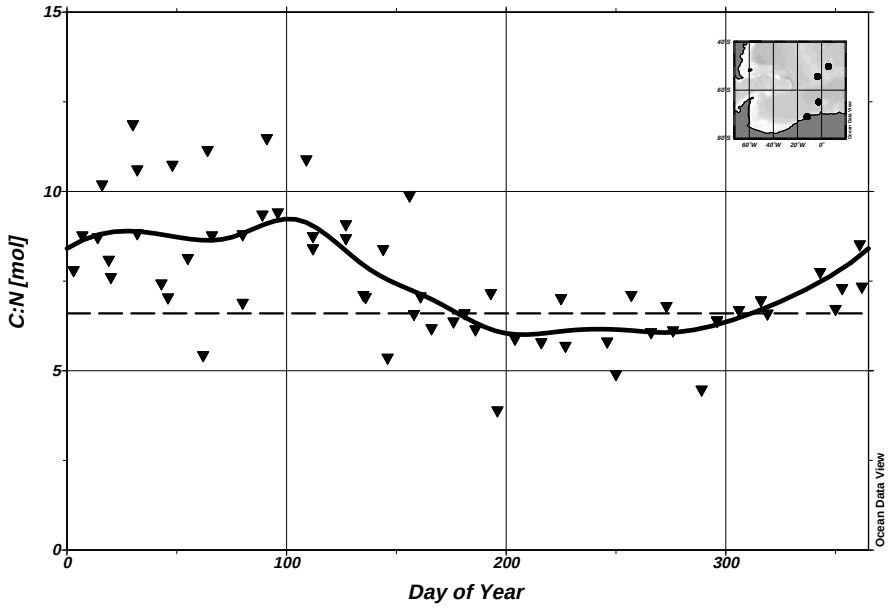

Figure 2.12: Seasonal variation (1988-1993) of particulate C:N ratios in the South Atlantic. Samples are from 250 until 500 m depth (n=60). The black line shows the monthly averages of C:N ratios.

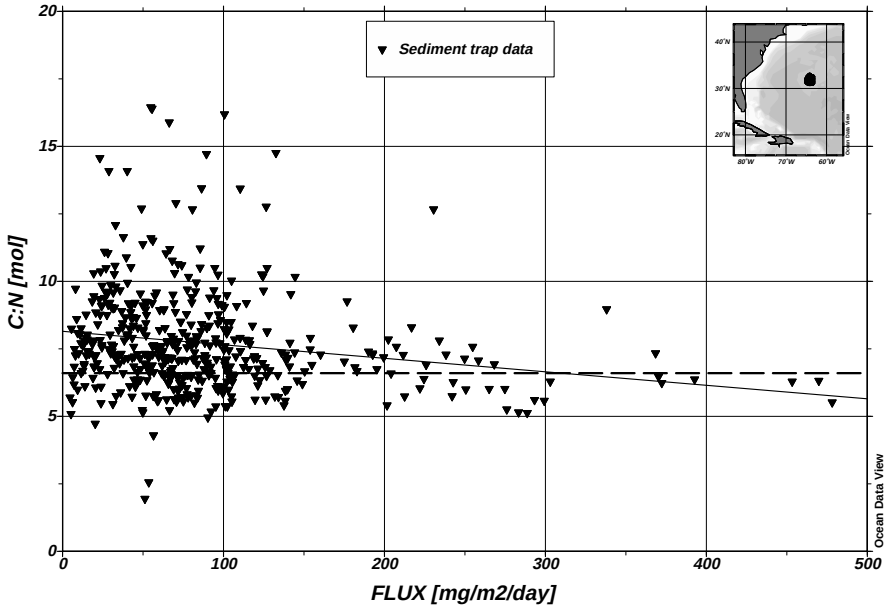

Figure 2.13: Relation of C:N ratios versus flux rates of shallow sediment trap samples at the *BATS* site in the Sargasso Sea until 500 m depth (n=476). The black line is the regression line of C:N ratios versus particle fluxes.

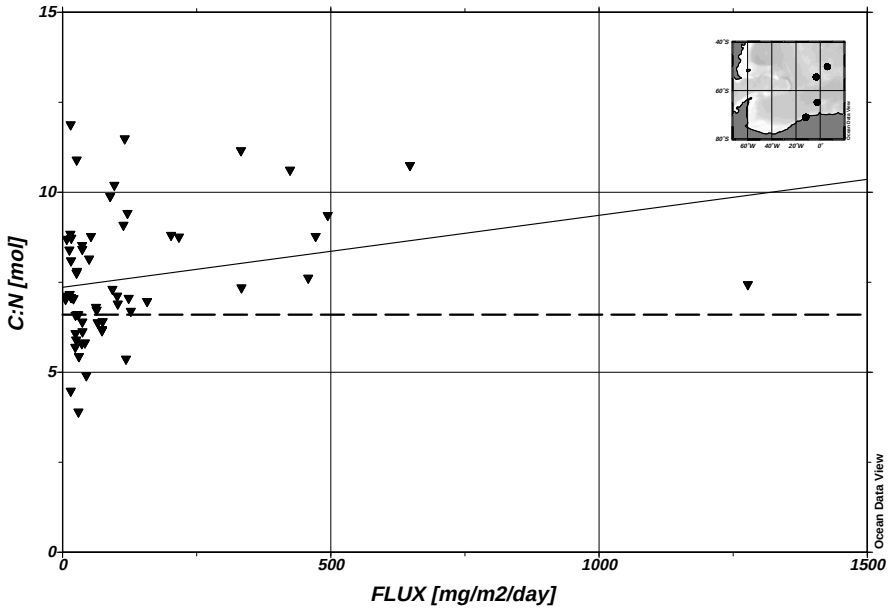

Figure 2.14: Relation of C:N ratios versus flux rates of sediment trap samples from the South Atlantic until 500 m depth (n=60). The black line is the regression line of C:N ratios versus particle fluxes.

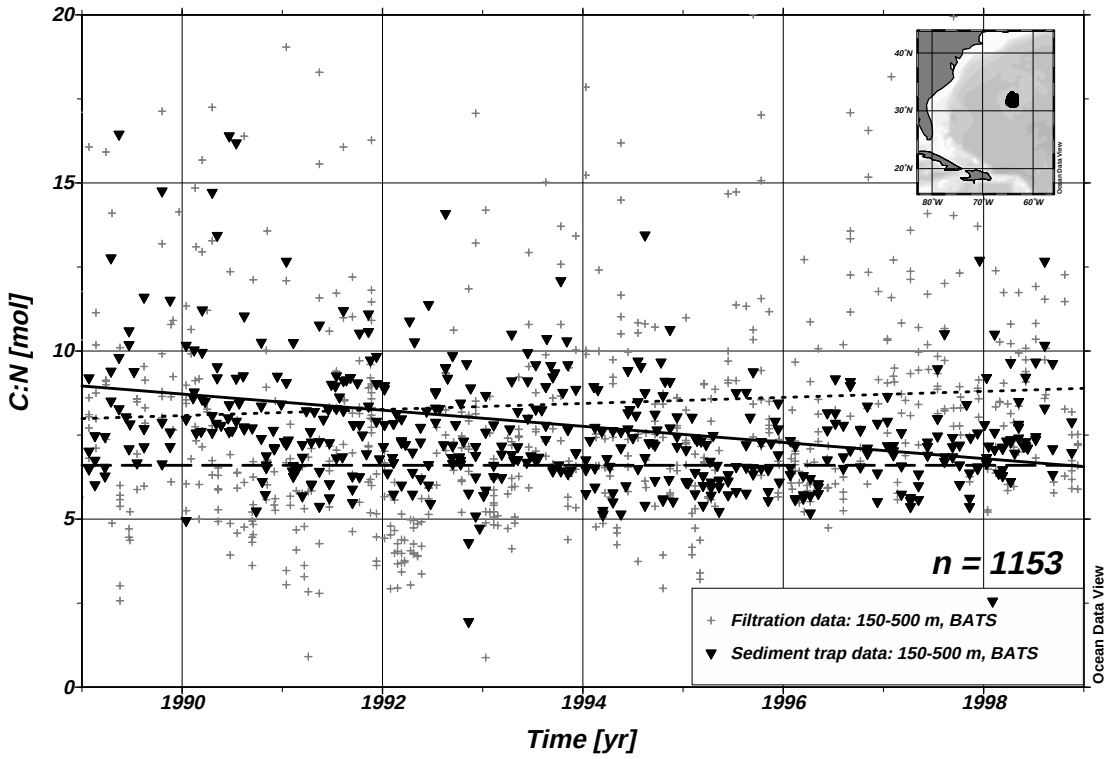

Figure 2.15: C:N ratios from filtration and sediment trap samples displayed versus time at the *BATS* site in the Sargasso Sea, 150-500 m depth. The dashed black line is the classical Redfield ratio for C:N (6.6), the solid line shows the multi year trend of C:N ratios from sediment trap data (equation 2.5) and the dotted line represents the trend of C:N ratios over the respective years obtained from filtration data (equation 2.6).

Perennial Variability

At the two long time-series stations, the *BATS* site in the Sargasso Sea and the *HOT* site in the subtropical North Pacific, changes of particulate C:N ratios over several years can be determined. From the *BATS* site, this can be done for both, filter and sediment trap samples. To determine temporal changes in the surface water, data from the depth range of 150 m down to 500 m, for the time interval from 1989 until 1998 are chosen at the *BATS* site, including 716 filtration data and 437 sediment trap data. Even though the time span of the entire time-series at the *HOT* site is longer (1989-1999), the interval from 1989-1995 is chosen for the determination of perennial changes, because during this time the whole depth interval from 150 m down to 500 m was investigated (n=165). For the entire period from 1989-1999, only data from 150 m depth are continuously recorded, which are 95 sediment trap values.

In Figure 2.15 particulate C:N ratios from the *BATS* site between 150 and 500 m depth are displayed versus time. Both sample types show large scatter and mean

values above the traditional Redfield value, whereby the mean C:N ratio of the filtration data is 8.5 (s=4.55, n=716), which exceeds the one of the sediment trap data of 7.7 (s=2.02, n=466), significantly. A trend over several years for the C:N ratios of sediment trap data from the *BATS* site is given by linear regression, showing declining C:N ratios over time of 0.20 units per year. The regression line follows the equation:

$$C:N(t) \;=\; 8.67\ (\pm 0.1) \;-\; 0.20 \;\cdot\; t\,[years\ past\ 1989] \tag{2.5}$$

At the same time the filtration data from this depth interval show a controversial behavior. There is a proceeding increase of the C:N ratios of suspended particles versus time with an amount of 0.09 units per year. This temporal increase from 1989 on is given by the regression line:

$$C:N(t) \;=\; 8.00\ (\pm 0.2) \;+\; 0.09 \;\cdot\; t\,[years\ past\ 1989] \tag{2.6}$$

The sediment trap data from the *HOT* site also reveal a considerable increase of the C:N ratios over the time-series from 1989 until 1995 in the depth interval from 150 m down to 500 m (not shown). The mean C:N ratio over this time interval is 10.68 (s=5.01, n=163) and the increase over time amounts to 0.42 units per year, according to the equation:

$$C:N(t) \;=\; 9.20\ (\pm 0.4) \;+\; 0.42 \;\cdot\; t\,[years\ past\ 1989] \tag{2.7}$$

Analyzing only the shallow traps in 150 m depth for a longer time period, from 1989-1999, however, does not show a clear trend over time during the whole time-series from 1989 until 1999, with a slight increase of 0.02 units per year.

3 Variable Element Ratios of POM: Explanations

3.1 Methodological Discussion

3.1.1 Filter Samples

The analysis of POM using filtrations of low volumes of water (1-2 l) may yield only small amounts of material, leading to analytical problems and corresponding large measurement errors. Furthermore, the sorption of DOM onto the filters has been reported to be a serious problem for filter analyses, especially with very low volumes of filtered water and low POC concentrations. Moran et al. [1999] found that with decreasing volumes of sampled water (< 2 l) and also with decreasing POC concentrations (< 5 μmol/l), the contribution of sorbed DOM to the filters increases, which is then quantified as POC and PON, erroneously. This may lead to an overestimation of POC concentrations up to a factor of five, and consequently to an overestimation of the C:N ratio. However, most of the filter samples in the current study have been processed following the JGOFS sampling protocols [JGOFS, 2002]. According to these protocols at least two liters of water are taken for samples from the upper 250 m of the water column and four liters for samples from below 250 m water depth. Sorbtion blanks are determined during the standard analyses, providing a correction value for the measured POC and PON values. There are 539 filtration values in the current study (8 %), where the determined POC concentrations are low (< 10 μmol/l POC) and where the application of this sorbtion blank correction cannot be approved by the available data documentations. This may result in too high C:N ratios due to systematic measurement errors. The respective data are single values from larger data sets from the Weddell Sea (ANT X/6) and from the North Atlantic (Nabe, Met 10-1, Met 10-2). However, all these data, which are possibly not blank corrected, do not reveal significantly elevated C:N ratios, and they do not affect the main findings of the current data analysis.

The problems of DOM sorption onto the filters and overall too small sample sizes, as it is described above, do not apply to the large volume filtrations using in situ pumps [Bishop et al.,1999]. However, comparing the C:N standard deviations of low volume and large volume filtrations does not reveal a larger scatter of the low volume filtration data. The mean C:N ratio for all small volume filtration data in the current data set is 8.00, with a standard mean error of $\pm$ 0.04 (n=7288), which is even lower than the error of the large volume filtrations, which have a mean C:N ratio of 7.98 with a standard mean error of $\pm$ 0.16 (n=752). This comparison shows that there appear to be no systematic differences in the results of both types of filtration, large volume and low volume, and also the low volume filtration data in the current data collection seem to be of good quality.

3.1.2 Sediment Trap Samples

In the current literature there is a recent discussion about the efficiency of sediment trap samplings. Sediment traps most probably do not gather particle fluxes, quantitatively [Scholten et al., 2001], especially at shallow water depth. It is assumed, that due to turbulence in the water column especially smaller particles are diverted and do not reach the sampling cups, leading to undersampling, while on the other hand, deeper traps may catch too large particle fluxes [Buesseler et al., 1994], possibly due to higher catchment areas of deeper traps in contrast to shallow traps. This means that due to lateral particle transport deeper sediment traps can collect particles from a larger surface area, where phytoplankton blooms produce organic matter to sink downwards, than shallow sediment traps. One method to avoid these biases is the deployment of floating sediment traps as described by Knauer et al. [1979]. The sediment trap data from the *BATS* site in the current study are achieved by this method. Floating traps follow the ocean currents and thereby reduce ambient turbulences. Furthermore, for a correction of vertical particle fluxes, measurements of ^{230}Th, a particle reactive radionuclide, have been applied. From this correction procedure Scholten et al. [2001] concluded that fluxes deeper than 1000 m are represented by the sediment traps very well even without ^{230}Th correction. The particle flux values in the current study are not ^{230}T corrected, but as mainly the element ratios of sinking particles and not the quantity of carbon flux are considered, the ^{230}T correction is not essentially necessary. The element ratios of sinking particles are not expected to change with varying trapping efficiencies. However, for the correlation of C:N ratios versus particle flux rates, the use of corrected particle fluxes is recommended.

Another often discussed problem of sediment trap analyses is dissolution of particles in the sampling cups, which may alter the composition of particulate material within the traps. Poisoning of the water in the sampling cups has been applied to reduce this effect. However, Noji et al. [1999] and Kähler and Bauerfeind [2001] measured dissolved organic material (DOM) from the supernatant of sediment trap samples, and concluded that particle degradation happens as a consequence of zooplankton feeding (swimmers) on particles in the cups, especially in shallow trap deployments. For traps deeper than 1000 m this problem seems to be negligible [Honjo et al., 1995], due to less zooplankton abundance. If there was a constant loss of particulate material to the dissolved phase, short term trap deployments should be much less affected by degradation in the sampling cups. However, v. Bodungen et al. measured by the user of short term deployments C:N ratios that are higher than the classical Redfield ratio, which is in agreement with findings from this study.

Kähler and Bauerfeind [2001] suggest that a substantial change in particle compositions due to such dissolution processes emerges, but the magnitude of these changes is not known. The application of a correction procedure examining both the element ratios of particulate material and the dissolved organic matter, yielded corrected particle element ratios significantly below the Redfield ratio, which also

seems implausible. Kähler and Bauerfeind [2001] also report that the dissolution in the cups appears very fast, i.e. within hours up to a few days. However, if there is any mechanism of dissolution in the cups, altering the C:N ratio of particles therein, this must be a systematic process. A completely stochastic effect is expected to even out all systematic variations, e.g. as they are found for the seasonal changes at the *BATS* site in both, the sediment trap and the filtration data (Figure 2.10). Consequently, it is feasible that a systematic shift towards elevated C:N ratios obtained from sediment trap data occurs due to the preferential remineralization of nitrogen in the sampling cups. Therefore, C:N ratios obtained from particles in shallow sediment traps probably need to be corrected towards the Redfield ratio.

Most sediment trap data in the current study are from deeper trap deployments, below 500 m, where intense grazing by zooplankton is not expected, and the depth dependence found for C:N ratios in this study is largely based on the deeper sediment traps. A possibly necessary correction of the shallow values towards lower C:N ratios, consequently, would result in a stronger increase of C:N ratios towards greater depth.

However, changes of particulate material within the sampling cups of shallow sediment traps can not be fully excluded. Poisoning of the water in the sampling cups is likely to reduce this problem, but it can not exclude further changes. In the following there are a large number of plausible reasons that can explain very well the distinguished regional and seasonal variations as found in the current study, and it is not likely that these systematic variations are the result of systematic dissolution of material in the sediment traps.

3.1.3 Comparison between Sediment Trap and Filter Samples

At the *BATS* site in the Sargasso Sea, filtrations and sediment trap sampling have been carried out simultaneously, which allows a direct comparison of C:N ratios of samples obtained by the two different methods. C:N ratios from both methods of the time interval under consideration (1989-1999) are displayed in Table 2.2 and Figure 2.15. There are seasonal changes in both types of data with a similar progression of lower C:N ratios at the beginning of each year, shifting towards higher values during the summer season, and then decreasing again to the low winter values. Filtration data show a larger scatter than sediment trap data. The mean C:N ratio of filtration data over the 10 year period is 8.5 with a standard mean error of $\pm$ 0.17 (n=716). This large scatter seems to be a consequence of the fact that a filtration measurement is isolated in space and time and secondly that a relatively low amount of material is gained for the analysis. The mean C:N value of filtration data is significantly higher than the mean C:N ratio of sediment trap data from the same period, which amounts to 7.7 ($\pm$ 0.08, n=464). The scatter of sediment trap data is much lower, and this lower scatter seems to be due to the reason that sediment traps measure integrated values over several days up to two weeks, depending on the duration of the sediment trap deployment. Generally, C:N data from filter analyses are systematically higher

than sediment trap data, which can also be seen in Figure 2.10.

The systematic difference between sediment trap and filter samples can be explained by the fact that there are generally different types of particles obtained by each method. Below the euphotic zone, filter samples largely consist of suspended particles that are very small, do not sink, and are partially old and nutrient depleted as a consequence of preferential nutrient remineralization [Müller, 1977; Sambrotto et al., 1993]. On the other hand, sediment trap samples predominantly contain larger, sinking particles that are relatively fresh due to their higher sinking rates. Consequently, sediment trap data are more appropriate than filtration data to estimate C:N ratios of truly sinking particles.

Generally, it can be stated that data obtained from measurements of sampled particulate material represent a more direct measure of the elemental composition of sinking material as compared to the indirect method of analyzing regeneration rates on dissolved inorganic nutrient fields. The discussion has shown that though sediment trap analyses possibly need some improvement, they are most suitable to determine the element ratio of sinking particles in the ocean.

3.1.4 Comparison with Results from Dissolved Nutrient Fields

The main conclusions of the present study, namely that C:N ratios of particulate organic matter increase significantly with depth and are above the classical Redfield value, even at the base of the euphotic zone, are in contrast to results from studies based on dissolved nutrient fields that yield C:N values independent of depth and in close agreement with the traditional Redfield value of 6.6 [Anderson and Sarmiento, 1994; Takahashi et al., 1985].

Anderson and Sarmiento [1994] discussed a number of possible explanations for discrepancies between both analyses on particulate material and dissolved nutrient fields. One is the possible dissolution of material within the sediment traps, which is a general problem and is described above. Plots of the C:N ratios from the compiled database versus sample sequence have not shown any trend to systematically higher C:N values for the first samples of a sequence, which would be expected if dissolution in the cup was altering C:N ratios. Even if degradation in sampling cups increased C:N ratios of the bulk material significantly, this should occur at all depths and thus could not explain the increase of C:N values with depth as shown in Figure 2.5 and 2.8.

Another argument used by Anderson and Sarmiento [1994] is that high C:N ratios would in general be associated with small vertical particle fluxes and would thus not be important for vertical budgets. They argue that the large downward particle fluxes found in productive regions were essentially equal to the Redfield ratio. To test this hypothesis, C:N ratios from the compiled data set were plotted versus downward flux (Figure 3.1). It is found, that even for large POM fluxes, greater

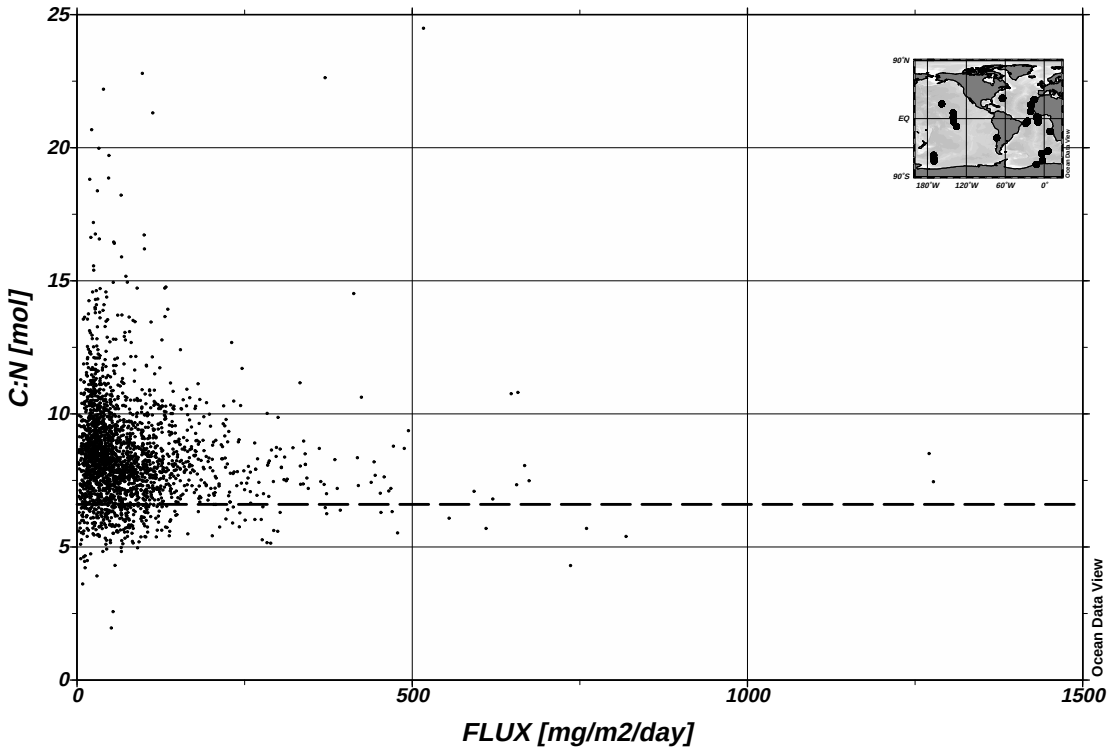

Figure 3.1: C:N ratios of sediment trap data (uncorrected) displayed versus total particle fluxes. The dashed line indicates the Redfield ratio of C:N (6.6).

than 150 mg/m^2/day (Peru/Chile, Namibia, Northwest Africa and equatorial Pacific upwelling regions and Southern Ocean) the average C:N ratio amounts to 8.1, which is significantly higher than Redfield's value.

If particulate C:N ratios increase due to preferential remineralization of nitrogen and phosphorus, as suggested by Müller [1977] the C:N ratio of the component going into solution must be smaller than the C:N value of the particulate matter remaining. It is therefore possible that changes in the dissolved carbon and nitrate fields ΔC:ΔN indicate relatively low C:N ratios of the remineralized part, while at the same time the sinking particulate matter has higher than Redfield C:N values. This can explain the lower C:N values obtained from dissolved nutrient fields, compared to particulate C:N ratios determined in this study. The method applied by Anderson and Sarmiento [1994] and Takahashi et al. [1985] exploits dissolved property changes on isopycnal or neutral surfaces over basin scales. Because these surfaces are not level but cover relatively large depth ranges, the method implicitly involves averaging over the depths of the respective surface under investigation. Therefore, any existing C:N depth dependence is likely to be masked because of depth integration. For the deeper surfaces, the uncertainties of the method grow because of very small gradients in the nutrient fields due to low particle fluxes and remineralization rates. In addition, the Anderson and Sarmiento [1994] results may be questioned

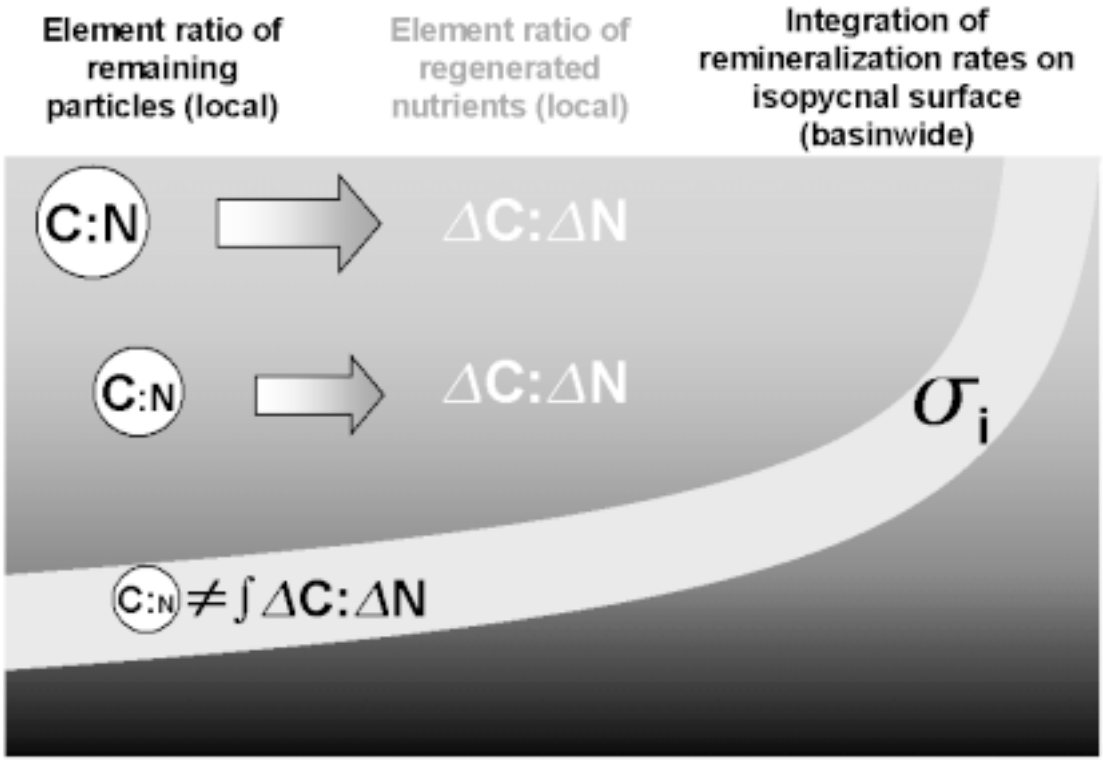

Figure 3.2: Relation of elemental ratios of sinking particles, redissolved nutrients and elemental ratios on isopycnal surfaces. It is shown that increasing C:N ratios of sinking particles can be achieved with constant element ratios of the redissolved nutrients, if the $\Delta C/\Delta N$ ratio of the regenerated nutrients is smaller than the ratio remaining the particulate matter. Changes in the element ratios of dissolved inorganic nutrients on isopycnal surface provide rather a depth integration of redissolved nutrients over depth than depth dependencies.

especially in the deep ocean, because of an unrealistic, assumed correlation between remineralization of organic carbon and $CaCO_3$ (introduced for numerical stability). A simplified relationship between elemental composition of sinking particles to the ratios of redissolved nutrients and remineralization ratios on isopycnal surfaces is illustrated in Figure 3.2.

In summary, it turns out that the sediment trap data shown in this study are most suitable to represent the C:N element ratio of sinking material. These ratios are significantly higher than the traditional Redfield value in the upper water column, and they increase further with depth. In order to reconcile these findings with the results from dissolved nutrient distributions that yielded no depth dependence and essentially Redfieldian values, it is important to realize that in case of preferential remineralization, the elemental C:N ratio of the component that goes into dissolution (and affects dissolved nutrient distributions) is smaller than the C:N ratio of the particulate material being remineralized. As a consequence, the C:N ratios based on

analysis of dissolved nutrient distributions do not necessarily reflect the composition of the particles themselves but rather the change of particle composition due to remineralization. Furthermore, analyses of dissolved nutrients mirror the remineralization of all organic components, including dissolved organic matter (DOM) as well. Consequently, this approach does not refer to sinking particles only, but also to advective transports which are responsible for the export of DOM. Regeneration rates derived from nutrient fields therefore reflect redissolution rates of total organic matter. A parametrization of the elemental composition of particle fluxes can not be achieved in this way.

3.2 Processes influencing Particle Composition

3.2.1 Preferential Remineralization

The analysis of data on the elemental composition of POM reveals systematic deviations from the classical C:N Redfield ratio. A detailed description of the determined variations and their causes is also given by Schneider et al. [2003]. In most of the data compiled here, C:N ratios are higher than the classical Redfield ratio, although large deviations in both directions are detected (Figure 2.4). For sinking particles, determined by sediment trap analyses, the extrapolated surface water C:N ratio corresponds to 8.3, which is significantly higher than the classical Redfield ratio. Furthermore, particulate C:N ratios increase with depth, and this increase amounts to 0.2 units per 1000 m water depth (equation 2.1). There are regional differences in both near surface C:N ratios and depth dependencies (Figure 2.6), but all those regions exhibit C:N ratios significantly higher than the classical Redfield ratio.

Elevated particle C:N ratios have been found in previous investigations, where the large C:N values were explained by preferential remineralization of nitrogen and phosphorus in contrast to carbon [Gordon, 1971; Copin-Montégut and Copin-Montégut, 1983; Tréguer et al., 1990, Anadón et al., 2002]. Anadón et al. [2002] investigated particle compositions from shallow sediment traps (65 m) in the Bellingshausen Sea, close to the Antarctic Peninsula. The sampling interval covered one summer season and particulate C:N ratios showed large variations reaching from values of 5.5 to 16.4, which lead to the conclusion that nitrogen and carbon exports are not strictly coupled. Gordon [1971] found increasing C:N ratios with depth for particulate matter collected by filtrations in the central Pacific, near Hawaii, during a time-series study of 18 months. In his study, the depth range from the surface to 4000 m depth was covered and C:N ratios increased from 7.5 (weight ratios; = 8.8 molar ratios) in 0-250 m depth to 15.1 (weight ratios; = 17.6 molar ratios) for the depth range between 3000 and 4000 m. Gordon [1971] concluded that the increasing C:N values are due to preferential remineralization of nitrogen-rich proteins in contrast to a slower degradation of carbohydrates. Comparable results were presented by Copin-Montégut and Copin-Montégut [1983], who examined particulate

C:N ratios from filtration data collected in the northeastern equatorial Atlantic, the southwestern tropical Indian Ocean, the Antarctic Ocean and the western Mediterranean Sea. They found particulate C:N ratios in the surface water varying between 5-8, and explained these variability with changes in species composition. For deep waters they found increased C:N ratios between 8-15 and larger variances as compared to the surface. Again, the increase of C:N values with depth and the higher variances were explained by preferential remineralization of nitrogen. Tréguer et al. [1990] investigated particle elemental ratios during autumn 1987 in the Scotia Sea by filter analyses. They measured C:N ratios from surface water particles close to the Redfield ratio. However, several profiles from the surface to 4500 m depth revealed increasing C:N ratios from surface values of 6.4 to deep water values of 10.1. From their results Tréguer et al. [1990] also suggested that nitrogen recycling is more rapid than that of carbon due to a preferential loss of nitrogen from the particles during decomposition. Preferential remineralization of nitrogen and phosphorus has also been suggested in studies of dissolved nutrient fields [Sambrotto et al., 1993; Anderson and Sarmiento, 1994; Shaffer et al., 1999; Thomas et al., 1999; Hupe and Karstensen, 2000; Osterroht and Thomas, 2000] .

In the current study, C:N ratios were found to be generally higher than the classical Redfield ratio by all methods applied (sediment traps, low volume and large volume filtrations). This general trend can be explained by the preferential remineralization of nitrogen in contrast to carbon, as it is outlined above. Filter samples may largely consist of suspended particles that are old and nutrient depleted. This nutrient depletion will result in a higher relative carbon content of the respective suspended material.

Sinking particles, gained by sediment traps, are fresher than suspended particles, i.e. less nutrient depleted. This can be seen in the lower C:N ratios compared to filtration data from the same time and depth interval, a fact that was discussed in more detail, above. However, sinking particles have also been partly remineralized when being packaged into faecal pellets and during sinking in the water column. This also explains the higher than Redfield C:N ratios generally found for sediment trap data, even at shallow depths. Furthermore, C:N ratios of sinking particles increase with depth in the water column. On a global mean, the rate of increase amounts to 0.2 units per 1000 m water depth, however, there were regional differences as it is displayed in Table 2.3 and in Figure 2.6. The low C:N increase at the *EQPAC* site from the equatorial Pacific seems to be due to the fact that the fluxes of both total material and organic matter are very constant over the investigated depth interval (not shown). This indicates that obviously only minor remineralization occurs here, which is furthermore mirrored in relatively constant C:N ratios over depth. Whereas other regions (*BATS*, central and south Atlantic) reveal increasing C:N ratios stronger than the global mean, and they also show significantly decreasing total particle fluxes and organic carbon fluxes as well, with increasing water depth, which is a strong indication for proceeding particle decomposition accompanied by preferential nitrogen remineralization.

Elevated C:N ratios with a mean value of 7.77 have been found for particles from shallow traps in the South Atlantic (250-500 m). Shallow remineralization of particles has been suggested based on results of inverse modeling for this area by Usbeck et al. [subm.]. Therefore, preferential nitrogen remineralization will be responsible in this area for the higher than Redfield C:N element ratios.

3.2.2 Nutrient Availability

While changes in the elemental composition of particulate organic material due to preferential remineralization of nitrogen and phosphorus seem to be well documented by the available data, there is also the possibility of obtaining non-Redfield element ratios during particle production. This can result from differences in the availability of ambient nutrients.

Upwelling of nutrient rich deep water is the most important mechanism to supply the surface ocean with the main limiting nutrients for biological production, NO_3 and PO_4, respectively [Toggweiler, 1999]. Whereas dissolved inorganic carbon is plentiful available in the ocean, and never the limiting nutrient for phytoplankton growth. Eolian dust deposition provides the surface water with iron, which is an important micro nutrient. Iron limitation [Martin et al., 1990; 1991] is most probably responsible for limited plankton growth in large regions of the Southern Ocean and the Equatorial and Northeast Pacific, the so called HNLC (high nutrient low chlorophyll) areas [Cullen, 1991], where in spite of high NO_3 and PO_4 abundance primary production is low [de Baar et al., 1995; 1997].

Large regions of the world ocean underly seasonal cycles with variations in the wind field, changing oceanic circulation patterns, variable dust deposition and/or seasonally varying ice coverage. These effects can result in direct and indirect changes in the nutrient availability of the surface water. Mixing of the surface ocean during winter forces upwelling of dissolved inorganic nutrients, the prerequisite for primary production. The subsequent accumulation and export of biomass leads to nutrient depletion in the surface water and possibly to nutrient limitation in advanced stages of the growing season, which then in turn affects the following biological production. Furthermore, reduced upwelling of nutrients can also occur as a consequence of increased stratification due to surface heating during the summer season. All these mechanisms cause changes in surface nutrient concentrations, which can lead to changes in the elemental composition of particulate material, as it was already mentioned by Redfield et al. [1963] and numerous other studies.

Several studies describe deviations from the Redfield ratio during exponential phytoplankton growth, where high C:N ratios are achieved under nitrogen and phosphorus limitation [Gervais and Riebesell, 2001]. On the other hand, significantly lower C:N ratios, may result from luxury consumption in situations when there is plenty of nitrogen and phosphorus available [Droop, 1973; Elfiri and Turpin, 1985; Roelke et al.,

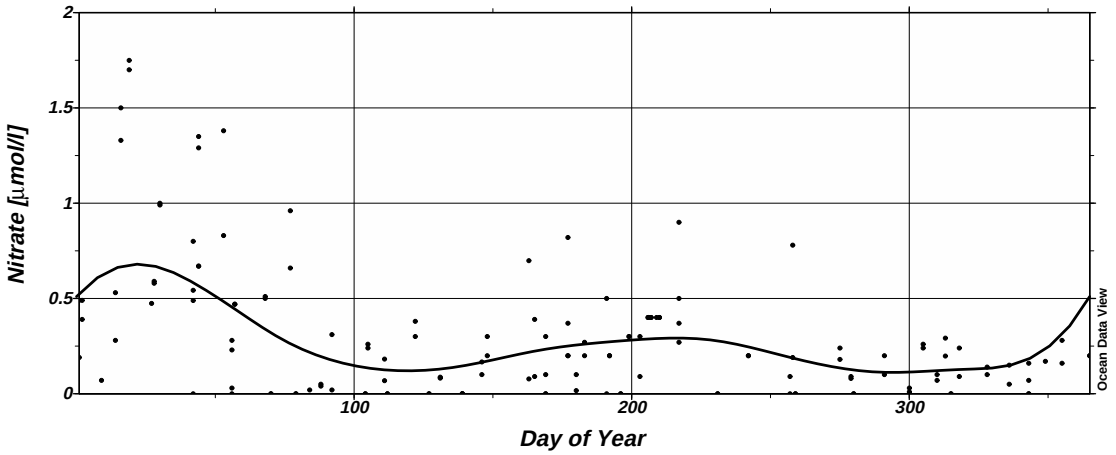

Figure 3.3: Seasonal changes in the surface water (< 20 m) nitrate concentration in the Sargasso Sea. The black line represents the monthly mean averages of the nitrate concentrations.

1999]. Keeping in mind that nutrient availability differs among different ocean areas, this process can lead to regionally varying element ratios of produced particles.

In the current data set nutrient limitation may have influenced particle compositions in the oligotrophic regions of the *BATS* site in the Sargasso Sea and at the *HOT* site in the subtropical North Pacific. In both regions the C:N ratios are generally elevated. The 10 year average C:N ratio of sediment trap samples from the *HOT* site at the depth level of 150 m until 500 m amounts to 10.24 (± 0.32, n=206; see Table 2.4), which is significantly higher than the classical Redfield ratio. Similar elevated C:N values are found for data from shallow traps at the *BATS* site. Here, the 10 year mean C:N ratio for sediment trap samples from the depth range of 150 m down to 500 m amounts to 7.71 (± 0.09, n=466), which is also significantly different from the Redfield ratio. In this region, a pronounced seasonal signal has been distinguished with low C:N ratios close to the Redfield ratio during the most productive season in winter (Figure 2.10), coinciding with the time of highest particle fluxes (Figure 2.9). Seasonal changes in the surface water NO_3 concentration (< 20 m), resulting from nitrogen consumption during biological production, can also be found (Figure 3.3), which most probably are the reason for a seasonally occurring nutrient limitation, influencing the elemental composition of organic particles in this area. The nutrient data are not from the same time as the particle time-series measurements, but they originate from the World Ocean Data Base (WODB) and were measured during two different time periods (1958-1960 and 1991-1992) [WODB, 1998], showing a recurring seasonal signal. The distribution of the nitrate concentration shows that there are generally very low NO_3 concentrations in the surface layer of the Sargasso Sea with an annual mean value of 0.30 μmol/l (± 0.03, n=149), and the values do not exceed a concentration of 2 μmol/l throughout the whole year. During winter, from January until March the NO_3 concentrations are highest with maximum values of 1.75 μmol/l, decreasing after March to values mostly below 0.5 μmol/l later in the

year. The low mean values during April and also during October are significantly different from the maximum concentrations during January. The depletion of nitrogen coming up every year in March shows that nitrogen limitation is an annually recurring phenomenon in this region. It appears in a good temporal accordance with the increasing element C:N ratios of sinking particles, which strongly indicates an influence of nutrient availability on the element ratio of exported particles.

The relation between particle fluxes and C:N ratios in the Sargasso Sea is oppositional to the one found for the South Atlantic. Figures 2.13 and 2.14 show that in the Sargasso Sea the time of highest particle fluxes is when C:N ratios are lowest, and in some cases even lower than the Redfield ratio of 6.6, whereas in the South Atlantic the C:N ratios are high during times of highest particle fluxes. These results show, that different (trophic) regions have different impacts on the marine carbon fluxes. Though there are elevated C:N ratios found in the Sargasso Sea as an annual mean value, the main particle export occurs with element ratios that are close to the Redfield ratio. On the other hand, although there is no apparent nitrogen limitation in the Southern Ocean, the exported particles are carbon enriched, also during the time of highest particle flux rates. This is probably due to the shallow remineralization of particles in this area [Usbeck et al., 2002], combined with preferential remineralization of nutrients at the same time, which can explain the export of generally carbon enriched particles in this area.

The examples of nutrient limitation leading to seasonally changing element ratios in correlation with seasonal variations in the total particle fluxes show that annual mean values of particulate element ratios are inappropriate for the determination of C:N and C:P ratios for sinking particles on a global scale. Thus, for a global synthesis, the element ratios of sinking particles should be weighted by flux rates, which are seasonally varying in most ocean areas. In this way, it is taken into account that areas of strong export fluxes are more relevant for a global carbon budget than areas of low fluxes and/or shallow remineralization. As particle fluxes in many ocean areas are sporadic events, as shown by the large scatter of particle flux rates in Figures 2.9 and 2.11, even short-term variations in element ratios of POM can result in large effects on the downward transport of carbon and nutrients, when coinciding with the time of highest particle export. Therefore, it is important to determine those element ratios that are predominantly exported by sinking particles, including a regional differentiation.

However, a clear distinction between the effects of preferential remineralization and nutrient availability on changes in the element ratio of sinking particles can not be made in the current data analysis. As sediment trap deployments are always below the euphotic zone and particle fluxes consist largely of detrital material, the element ratio of particles found in the sediment traps will always carry a mixed signal of changes in the element ratio during both production and remineralization. Nevertheless, changes in the elemental composition during particle production as a consequence of nutrient availability are very likely to occur, especially in areas of

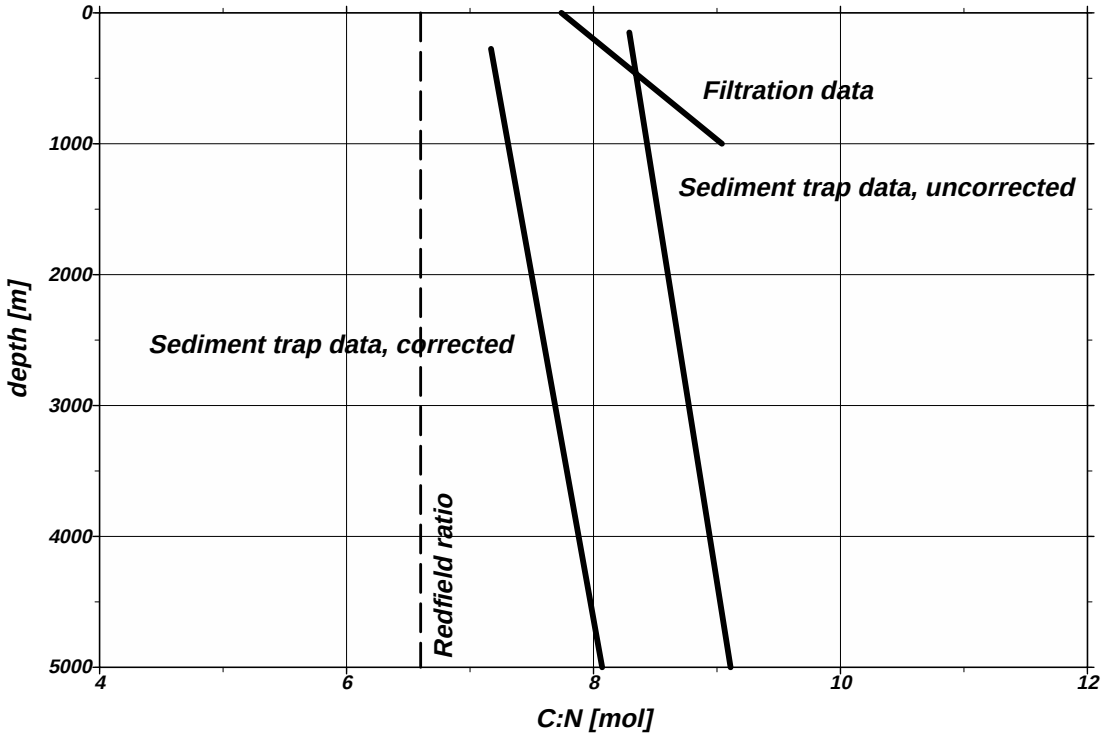

Figure 3.4: Summary of C:N regression lines of different types of POM versus depth. The dashed line indicates the Redfield ratio of C:N (6.6), the solid lines are the regression lines for filter samples, uncorrected and corrected (for lithogenic contribution) sediment trap data, respectively.

nitrogen and phosphorus limitation.

3.2.3 Lithogenic Material

As shown in Figure 2.7 the sampled particles do not consist of pure marine material, but contain lithogenic components which can be either consist of mineral material or terrestrial organic matter. Based on the compiled sediment trap data, lithogenic fluxes appear to be negligible far away from continents or the seafloor, they amount to less than 40 % of the total flux for most of the data set (95 %), and large contributions up to 90 % of the total flux are found in rare and extreme cases, only. Mineral lithogenic material consists mainly of clay particles originating from fluvial and/or eolian input and from resuspension from the seafloor. Terrestrial organic matter is introduced by river discharge, where organic components are attached to mineral particles [Ittekkot et al., 1991], but also from eolian dust input [Fischer and Wefer, 1996; Wefer and Fischer, 1993]. These lithogenic contributions have different C:N elemental ratios, affecting the C:N signals of bulk POM. Clay minerals like illite are able to incorporate ammonia [Müller, 1977], whereas montmorillonite

can adsorb inorganic nitrogen. Thus, contributions of clay minerals are likely to lead to a decrease of C:N ratios, because of the additional nitrogen incorporated by these minerals. On the other hand, river water may carry large amounts of terrestrial organic material. Organic soil C:N ratios are higher than those in marine organic matter [Kononova et al., 1966], therefore, contributions of terrestrial organic material will increase the C:N ratios.

Contributions of terrestrial organic matter might be responsible for the increase of C:N values with lithogenic contribution seen in Figure 2.7. As shown in Table 2.4, near-bottom C:N values for sediment trap data from the East Atlantic and for the whole sediment trap data set are smaller as compared to values from above. Resuspension of minerals from the sediments can explain this observation.

The application of a correction procedure to eliminate the effect of lithogenic contributions, led to significantly smaller C:N ratios for marine produced material as compared to bulk material. The large difference between C:N ratios of uncorrected sediment trap data and the corrected values point out to a probable higher relative carbon contribution of non-marine particles in bulk material fluxes, especially in those areas, where high lithogenic fluxes occur. Comparing the regression lines for different particle type C:N ratios versus depth as displayed in Figure 3.4 shows that marine derived particles are closer to the Redfield ratio, and the extrapolated value for surface water C:N ratios amounts to 7.1, which is only slightly higher than the classical Redfield ratio.

3.2.4 Changes in Species Composition

Sediment trap data from the *BATS* site show temporally decreasing C:N ratios of POM (Figure 2.15). Over the time period from 1989 until 1998 the C:N ratios decrease by about 0.2 units per year, which may be due to a change in species composition. Hood et al. [2001] reported that a high abundance of *Trichodesmium*, a nitrogen fixing cyanobacteria, in the *BATS* area can largely determine DIC drawdown when nitrogen is depleted in the surface water. *Trichodesmium* is able to build up biomass under nitrogen limitation, and the C:N uptake ratio ($\Delta C/\Delta N$) thereby yields values of 14-425 [Orcutt et al., 2001]. A reduction in the contribution of *Trichodesmium* to the total biomass over the time-series as reported by Hood et al. [2001], who compared the results from Orcutt et al. [2001] and Carpenter and Romans [1991], is likely to lower the C:N ratios of particles found in sediment traps at the *BATS* site over the time interval from 1989 until 1998.

The results of declining C:N ratios of POM over the ten year interval (0.2 units per year) from the sediment trap data at the *BATS* site are in contrast to findings from the subtropical North Pacific (*HOT*), where an increase in the element ratios of 0.42 units per year has been found between 1989 and 1995 in the current data analysis. This increase can also be a consequence of a changing species composition, influencing the element ratio of POM in the opposite direction. There is a good

accordance of the results from particle measurements with the element ratio of dissolved organic matter at the *HOT* site. Both increasing C:N and C:P ratios of DOM have been documented by Church et al. [2002] for the same area between 1993 and 1996. They found an increase in the C:P ratio of DOM, which was statistically significant and amounted to 14.6 units per year, and furthermore, there was an increase in the C:N ratio of DOM which was about 0.15 units per year. However, the latter was not statistically significant. Church et al. [2002] explained their results by a change in species composition in the area of investigation over the time-series measurement, resulting in a higher carbon content of DOM.

3.2.5 Transparent Exopolymer Particles (TEP)

Transparent exopolymer particles (TEP) are extracellular gel particles, produced by phytoplankton and bacteria under nutrient limitation, typically at the end of a phytoplankton bloom. They consist largely of carbohydrates and are very sticky, leading to the formation of marine snow, including TEP, phytoplankton, detritus and lithogenic matter. By this means, TEP can enhance downward export fluxes via particle aggregation [Alldredge et al., 1993; Logan et al., 1995; Engel and Schartau, 1999; Engel, 2000; Engel and Passow, 2001]. Phytoplankton may release up to 40 % of photosynthetic carbohydrates as TEP, i.e. that in certain cases TEP can contribute as much carbon to the total particulate matter as conventional particles do [Engel and Passow, 2001]. TEP are highly carbon enriched and C:N values are about 26 [Engel and Passow, 2001], which is much larger than the classical Redfield ratio. The export of TEP via particle fluxes may enhance marine carbon sequestration. What is more important, it is assumed that TEP are also a way of exporting DOM from surface to deep waters. DOM, which is usually not supposed to be exported by particle fluxes, as it does not sink, can be involved in coagulation and sinking processes. This mechanism of carbon enrichment in sinking particles, which does not originally come from the particulate phase, can also explain the process of carbon overconsumption, which was already described by Toggweiler [1993]. By this means, at the end of a phytoplankton bloom considerable amounts of carbon enriched TEP are produced, supporting particle aggregation. During aggregation there is also DOM enclosed in marine snow, which is exported downwards by sinking aggregates. The element ratio of such marine snow aggregates can not be explained by the Redfield stoichiometry for POM.

However, there are no estimates about the relevance of TEP on a global scale. Most investigations were made in shelf areas or are mesocosm experiments, but production of TEP in open ocean areas is also possible. Some estimates for TEP production in the North Atlantic are given by Engel and Passow [2001].

What makes TEP very important in the context of global change is its CO_2 dependent production, as well as the occurrence under nutrient limitation. Engel [2002] reported a positive non-linear relationship between TEP production and the pCO_2

of ambient water. Though the maximum production is almost reached at current CO_2 concentrations, there is the possibility that the existence of TEP has become more important since industrialization. Associated with global change, TEP may force changes in the exported elemental ratios and thereby changes in the marine carbon sequestration.

In the current data analysis, some samples will most probably also contain TEP and the element ratio of TEP is then associated to the one measured for POM, leading to elevated C:N ratios. As TEP production largely occurs under nutrient limitation, it may also explain the elevated C:N ratios found at the *BATS* and *HOT* sites. Especially the increase of C:N ratios in summer in the Sargasso Sea support the idea of an increasing contribution of TEP to sinking particles under proceeding nutrient limitation. The generally high C:N ratios found in sediment traps in the subtropical North Pacific, showing no seasonal trend, can be explained as results from prevailing nutrient limitation over the whole year. This can be accompanied by a considerable contribution of TEP to sinking particles leading to the elevated C:N ratios found in sediment trap material. However, the increasing contribution of TEP to total production dependent on the ambient CO_2 concentrations can not be validated by the current study. Time-series measurements of ten years and longer at both the *BATS* and the *HOT* site do not reveal reliable trends towards increasing C:N ratios over time. What is even more important, there is a slight decrease in the C:N ratios in particles from the *BATS* site from 1989 until 1998. A probable reason why this relation can not be validated by the current data analysis is that the CO_2 dependent TEP production has already reached its maximum at the current CO_2 concentrations [Engel, 2002].

4 Depth Dependent Element Ratios in a Global Carbon Cycle Model

4.1 Implications for Biogeochemical Modeling

The preceding data analysis and the discussion have shown that the elemental compositions of POM deviate systematically from the classical Redfield ratio and that there are a large number of processes that can influence the particle composition into different directions. As the classical Redfield ratio was actually supposed to describe the elemental composition of freshly produced phytoplankton [Redfield et al., 1963] it is not surprising that significant and systematic deviations have been determined in the data analysis of this study. Processes like grazing, aggregation and repackaging transform detritus, freshly produced particles and other components into sinking matter. These processes do not only modify particle shape, but also its chemical and thus elemental composition as they are part of the biological food web. Therefore, one has to distinguish between the elemental composition of particles for primary production (PP) and for export production (EP), especially when implemented in biogeochemical models.

Presently, the majority of global physical/biogeochemical models used to simulate marine nutrient and carbon cycles does not take into account the preferential remineralization of nitrogen and phosphorus and the increase of POM elemental ratios with depth, as determined by this and other studies. In contrast, most models implement depth independent C:N ratios for particulate organic matter, which, according to the results of this study will result in a too large export into the deep ocean of nitrogen relative to carbon. As a consequence, these models might underestimate nitrate concentrations in the upper ocean, which might cause too small productivity and downward carbon fluxes in the models.

One model approach by Shaffer et al. [1999] implemented depth dependent C:P remineralization rates in a simple carbon cycle model (HILDA). C:P ratios from the analysis of regenerated nutrients were applied for the particle elemental compositions, resulting in C:P ratios of 100 from the surface to 750 m depth, increasing to a value of 130 in 1500 m depth and staying constant further down. The model results obtained from this investigation show that the fractionation during remineralization in the modern ocean may reduce atmospheric pCO_2 by 20 μatm below the level it would have without fractionation. By this means, the increase with depth of the carbon to phosphate ratio of sinking particles leads to a strengthening of carbon fluxes towards greater water depth. As a consequence, there is a higher CO_2 uptake in the surface ocean, which then in turn reduces the atmospheric pCO_2. The results from Shaffer et al. [1999] indicate that the implementation of depth dependent C:N ratios for sinking particles according to equation (2.3) significantly affects the uptake of atmospheric CO_2 by the ocean.

However, the element ratios for sinking particles in the study of Shaffer et al. [1999] are obtained from analyses of dissolved inorganic nutrient fields and seem to underestimate the carbon flux in the upper ocean by the application of a C:P ratio of 100 until 750 m water depth, which is even slightly lower than the classical Redfield ratio (106) and significantly lower than the C:P ratio, which has been derived in the current study. Here, assuming a Redfield N:P ratio of 16, the C:P ratio amounts to 114 for sinking particles at the base of the euphotic zone (z_{EP}) and 116 at 750 m water depth. Consequently, the application of depth dependent C:P ratios for sinking particles in the study of Shaffer et al. [1999] results in a relative increase of carbon to nutrient fluxes towards greater depth, but the amount of total carbon export will be underestimated due to the too low C:P ratios in shallow water depth, representing the initial composition of exported particles at the depth of the euphotic zone.

To correctly represent relative carbon to nutrient ratios of marine particle fluxes, in the current study the AWI Adjoint Model for Oceanic Carbon Cycling (AAMOCC) will be used to implement a C:N ratio of 7.1 and a C:P ratio of 114 (assuming a constant Redfield N:P ratio of 16) for particles at the base of the euphotic zone. Furthermore, depth dependent element ratios will be taken into account, like an increase of the C:N ratio with depth of 0.2 units per 1000 m water depth, which corresponds to equation 2.3, and 3.2 units per 1000 m for the corresponding C:P ratio. This elevated carbon to nutrient ratio for sinking particles at the base of the euphotic zone together with increasing relative carbon contents with depth is a first approximation, which will on a global scale more adequately represent marine particle fluxes than the classical Redfield ratio for C:N and C:P.

For a prediction of future marine carbon fluxes under global change, the possibility of temporally variable element ratios will be taken into account. The CO_2 dependence of TEP, and its enhanced production under nutrient depletion is expected to influence the element ratio of sinking particles on a global scale, significantly.

4.2 The AAMOCC Model

The model applied in this study is the AWI Adjoint Model for Oceanic Carbon Cycling (AAMOCC), which is described in Schlitzer [1993; 1995; 2000; 2002] and de las Heras and Schlitzer [1999]. The model is a 3-D ocean circulation model simulating distributions of dissolved inorganic carbon (DIC), nitrate (NO_3), phosphate (PO_4), oxygen (O_2), total alkalinity (TALK) and dissolved organic phosphorus (DOP) in addition to the hydrographic parameters temperature and salinity. The tracer distributions are obtained by solving sets of linear equations arising from property conservation. The model includes advection/diffusion, and there is gas exchange for the tracers CO_2 and O_2 at the air-sea interface.

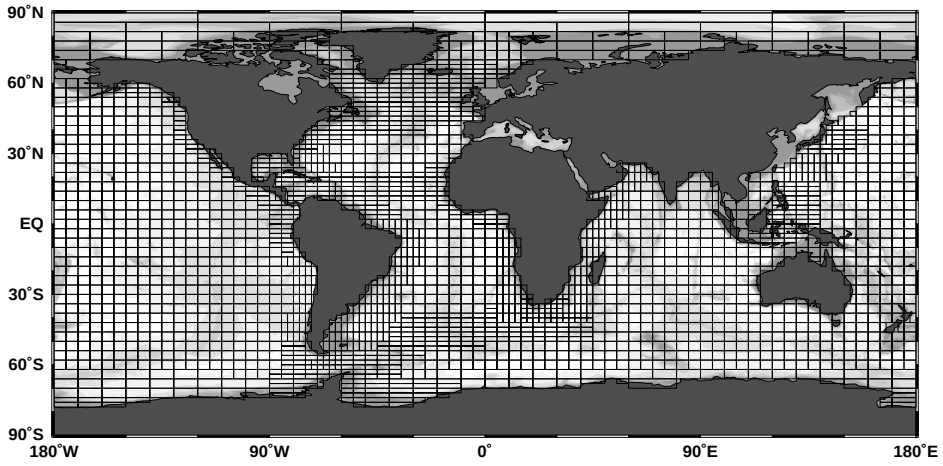

Figure 4.1: Model grid.

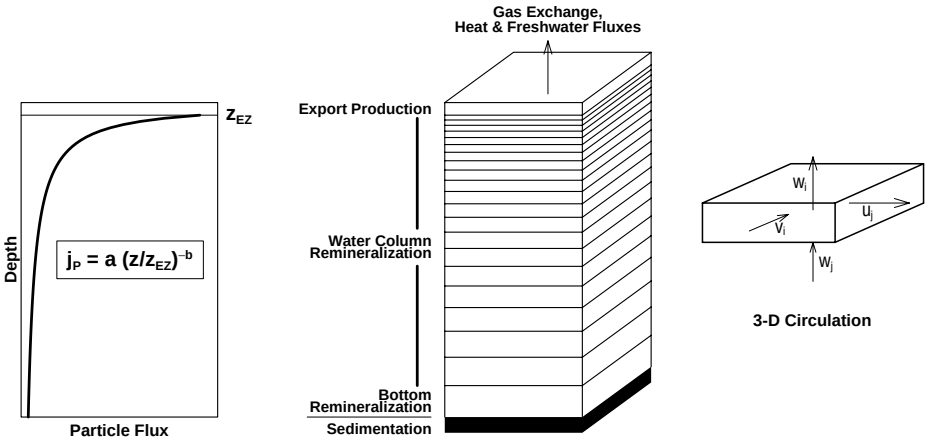

Figure 4.2: Vertical resolution of the model grid, exemplified particle flux curve (left) and model box with velocity vectors (right).

The horizontal resolution of the model grid is variable from 2.5 × 2 degrees in low latitudes to 60 × 4 degrees in high latitudes with a predominant resolution of 5 × 4 degrees, as shown in Figure 4.1. Vertically there are up to 26 levels with increasing layer thickness towards depth (Figure 4.2). At the surface, the euphotic zone is divided into two layers of 61 and 72 m, respectively, i.e. the lower boundary of the euphotic zone in the model is at 133 m depth. Layer thicknesses increase towards depth with a maximum value of 500 m in the deep ocean. For reasons of computational efficiency, the full resolution of 44388 boxes is lowered to 24344 clusters by horizontally merging two or more boxes into one cluster, while the vertical resolution is maintained. The non-uniform gridding and the cluster formation allow calculations with a higher resolution in areas of high current velocities and/or strong property gradients than in areas with less dynamics, without the need to apply the higher resolution to the entire model domain.

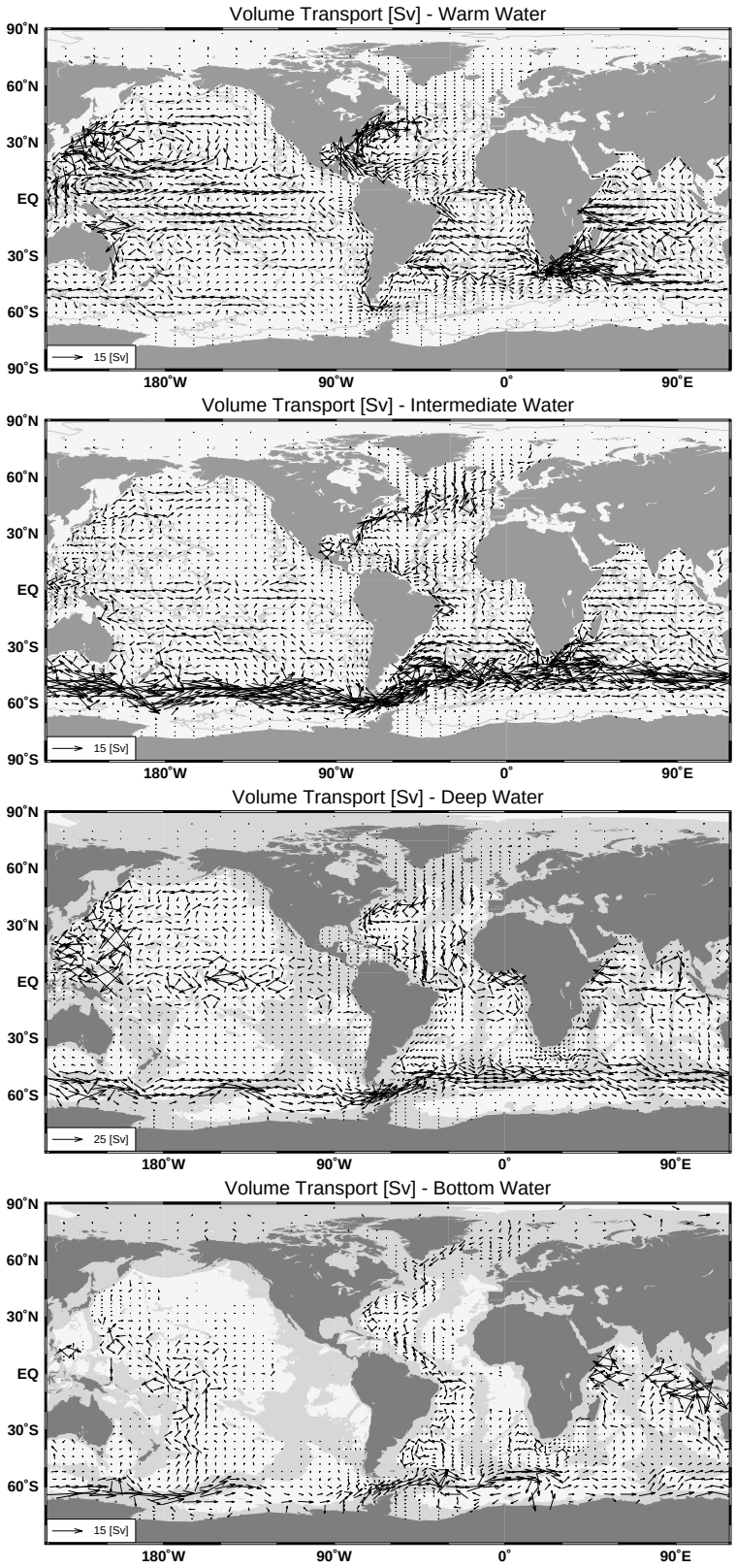

Figure 4.3: Model volume transport in Sverdrup (1 Sv = 10^6 m^3/s) of surface water (surface-σ_0=26.8), intermediate water(σ_0=26.8-σ_2=36.75), deep water (σ_2=36.75-σ_3=45.9) and bottom water ($> \sigma_3$=45.9) water masses, respectively.

The flow field used in the model (Figure 4.3) is obtained by the Adjoint Method, where the ocean flow field is iteratively and systematically varied to simulate property distributions of temperature, salinity and dissolved nutrients that are consistent with data. Furthermore, the horizontal velocity shear is constrained to be close to geostrophic shear values, which were also estimated from the data. The model does not resolve seasonal variations, but the optimized flow field obtained by the Adjoint Model reproduces all major ocean currents. The model flows of all water masses, divided into four depth intervals, are displayed in Figure 4.3, where the lengths of arrows indicate volume transports, given in Sverdrup (1 Sv = 10^6 m^3/s). In the surface water, down to a potential density of σ_0=26.8, the main surface ocean currents are visible, like the Equatorial Current and the North Equatorial Counter Current in all major oceans. Furthermore, the western part of the Gulf Stream in the Atlantic Ocean and the anticyclonic subtropical gyres in the Pacific Ocean are reproduced. The flow pattern of the intermediate water clearly marks the Gulf Stream in the North Atlantic and the Antarctic Circumpolar Current (ACC), which flows in an eastward direction around the Antarctic and is the strongest ocean current with a volume transport of 124 Sv (model result), which corresponds very well to the value of 128 $\pm$15 Sv given by Tomczak and Godfrey [1994]. In the deep and bottom waters, the ACC can also be seen as the most pronounced ocean current. Furthermore, in the bottom water the pathways of the Arctic Bottom Water (ABW), flowing in the western part of the North Atlantic in a southward direction, and the Antarctic Bottom Water (AABW) with two threads of northward directions, one in the eastern part of the South Atlantic and one in the western part of the South Atlantic. While the eastern flow of the AABW is restricted by the Walfish Ridge, the western thread exceeds the equator until about 20^oN. More detailed descriptions of the major ocean currents and water mass transports are given by Dietrich[1975] and Tomczak and Godfrey [1994].

In the current study the model flow field and initial tracer distributions are taken from a former optimization experiment, and only the forward simulation part of the model is applied. The time dependent advection diffusion equation is discretized using a weighted-mean scheme. For the time integration an implicit scheme is used. The length of each time step is 0.1 years, which yields comparable results to a model experiment with time steps of 0.05 years, which was approved in advance.

Unlike in ecosystem models, which simulate the interactions and feedbacks of biological food webs, explicitly, in the present model the effects of such processes are simulated by sources and sinks for dissolved carbon and nutrients. In the euphotic zone particle production takes place leading to a sink for dissolved inorganic carbon and nutrients, whereby 75 % of the production takes place in the top layer of the euphotic zone and 25 % are produced in the next layer underneath.

Below the euphotic zone particle fluxes through the water column are calculated based on remineralization rates of dissolved carbon and nutrients, i.e. they act as a source of dissolved nutrients, as shown in Figures 4.2 and 4.4. The functions of

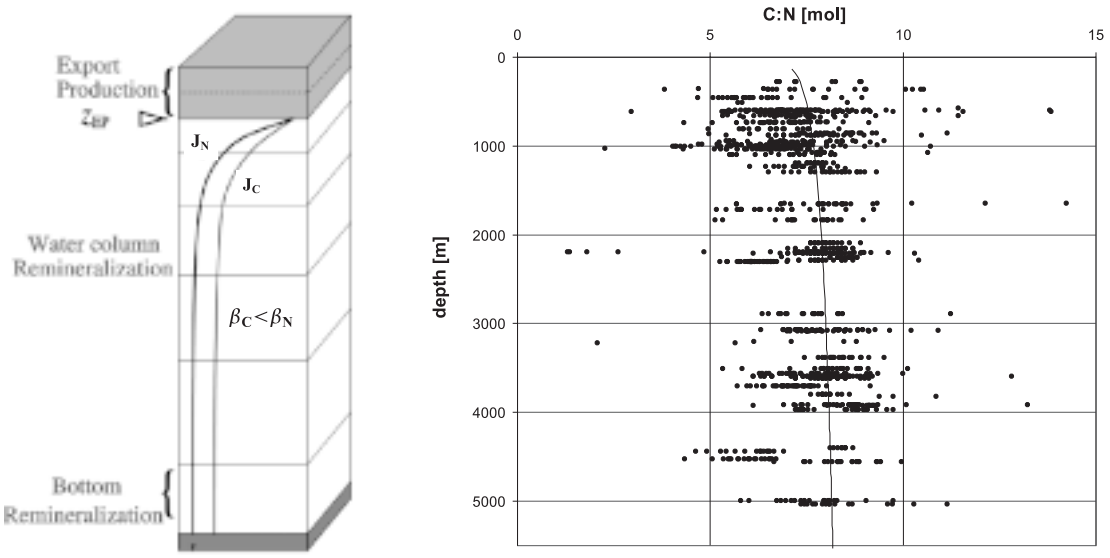

Figure 4.4: Model column (left) with the euphotic zone in the two uppermost layers and particle flux curves indicating different remineralization ratios for the elements nitrogen (N) and carbon (C), respectively (z_{EP} = depth of the euphotic zone). The right panel shows the depth dependence of C:N ratios of POM, indicated by the black line on top of the data as in Figure 2.8. Though in the model the C:N depth dependence is difficult to be implemented linearly (as proposed by equation 2.3) the resulting curve fits the data very well.

Suess [1980] and Martin et al. [1987] are applied leading to model particle fluxes of the following form:

$$J(x,y,z) \;=\; \alpha(x,y) \;\cdot\; z^{-\beta(x,y)} \qquad z \geq z_{EP} \tag{4.1}$$

J(x,y,z) is the particle flux at a given location (x,y,z) while the functions α and β describe the export production and the shape of the remineralization curve for each model column. These two parameters, α and β, have also been optimized by the Adjoint Method for each model column to achieve particle fluxes resulting in property distributions close to the data. At the base of the euphotic zone the particle flux J is equivalent to the export production (EP). The annual carbon export production in the model amounts to 10 Gt C.

Figure 4.4 shows a schematic model column with the euphotic zone in the two uppermost layers, where biogenic particles are formed. Particle fluxes are defined from the base of the euphotic zone, downward. In the bottom box all arriving particles are remineralized, and sedimentation is not considered. A variant of the model including sedimentation processes is described by Usbeck [1999]. The left panel of Figure 4.4 shows schematic particle flux curves for carbon and nitrogen, for a case with different remineralization parameters β for the elements C and N. A decreased remineralization of carbon leads to an increase of carbon fluxes to depth

as it is indicated by the right curve ($\beta_C < \beta_N$).

The gas exchange for CO_2 and O_2 at the air-sea boundary is implemented in the model using the difference between the saturation concentration C_{sat} and the concentration at the sea surface C_{surf} for the respective tracer. Consequently, air-sea gas exchange rates are given by:

$$F = k_w \cdot (C_{sat} - C_{surf}) \tag{4.2}$$

The factor k_w is the gas transfer velocity for the individual tracer. It is seasonally variable and a function of wind speed and its variance. As the model does not resolve seasonal variations, the annual mean value of the gas transfer velocity k_w is applied, derived from Wanninkhof [1992].

Modifications of the Model

Modifications in the model code have been carried out in order to allow a change of the elemental composition of POM with depth, as suggested by the data analysis in section 2 (equation 2.3). This includes higher than Redfield C:N values at the base of the euphotic zone as well as an increase during remineralization in the water column. Furthermore, the atmospheric CO_2 concentration is implemented to vary time dependently, to simulate the uptake of anthropogenic CO_2 by the ocean since the beginning of industrialization.

To achieve C:N ratios for the particles at the base of the euphotic zone corresponding to the results of the current data analysis (equation 2.3) the C:N element ratio for the particle export, i.e. at depth of the euphotic zone, is set to the value of 7.1 for most experiments. In the original model the classical Redfield ratio for C:N of 6.6 was applied, which was done in the current study during some experiments to achieve a reference tracer distribution, which is used for comparison with results obtained by those experiments including variable element ratios and to estimate the effects of the respective variations.

The N:P element ratios are implemented in the original model using the classical Redfield N:P ratio of 16. They are kept constant in space and time like this in the current study. Consequently, deriving the corresponding C:P ratio by the use of a C:N ratio of 7.1, leads to a C:P ratio for particles at the base of the euphotic zone of 114 in contrast to the classical Redfield C:P ratio of 106.

Depth dependent C:N ratios as found in the current data analysis are implemented in the model by adjusting the parameter β, which determines the shape of the vertical particle flux curve for a given element. In the original model, the values for β were identical for all elements C, N and P. Here, the parameter β_C for carbon is modified. Using a smaller value for carbon as compared to nitrogen ($\beta_C < \beta_N$) results in a deeper remineralization of carbon in contrast to nitrogen and leads

to depth dependent C:N element ratios. Even though there was a linear depth dependence proposed from the data analysis, it was not possible to implement this into the model due to computational reasons. A factor of 0.963 was empirically determined for the modification of the parameter β_C. By this means, multiplying β_C with 0.963 results in a depth dependent curve for the C:N ratios, as shown in the right panel of Figure 4.4. The resulting curve fits both, the C:N ratios of particles at the base of the euphotic zone (7.1) and in 5000 m water depth (8.1) as they were determined beforehand. It can also be seen in Figure 4.4, that this non linear depth dependence represents the data very well.

The second modification of the original model is the implementation of time varying atmospheric CO_2 concentrations for some of the model experiments discussed below. Former model studies and some of the reference experiments in the current study are performed with a constant preindustrial atmospheric CO_2 partial pressure of 278 μatm. For the time from 1765 to 1990 atmospheric CO_2 data are taken from ice core records [Neftel et al., 1994] and the Mauna Loa CO_2 record [Keeling and Whorf, 2002]. The S650 scenario [IPCC, 1997] is applied, to simulate the development for the future, which continues the atmospheric CO_2 data records and exhibits an increasing atmospheric CO_2 partial pressure until the year 2200 with a maximum of 650 μatm.

4.3 The Experiments

Seven experiments have been carried out to determine the implications of variable element ratios in sinking particles on the marine carbon cycle. Table 4.1 gives an overview of the experiments and the most important parameters, which have been varied, like atmospheric CO_2, C:N ratio at the base of the euphotic zone (z_{EP}), depth dependence, time interval and the source of the used initial fields of the tracers DIC, NO_3, PO_4, O_2, TALK and DOP. Four experiments are performed with a constant preindustrial atmosphere, and in three experiments variable atmospheric CO_2 concentrations are applied.

To determine the difference of the carbon inventories between a steady state ocean with particle fluxes following the Redfield ratio and a steady state ocean with particle fluxes including both, higher than Redfield and depth dependent element ratios of sinking particles, two model approaches will be presented in the following chapter. The effect of increasing atmospheric CO_2 concentrations will be compared between both steady state oceans, the one with Redfield ratio particle fluxes and the one with higher than Redfield and depth dependent particle fluxes. Here, the air to sea CO_2 flux rates and the distributions of anthropogenic CO_2 for the two systems will be determined and compared.

One major question is whether the determined variations in particulate element ratios by the preceding data analysis are CO_2 dependent or whether export fluxes

Table 4.1: Parameters for atmospheric CO_2, C:N ratio at the base of the euphotic zone (z_{EP}), C:N depth dependence, simulation period and the initial tracer fields for the seven experiments (A-G), carried out in this study.

Exp.	Atmosphere	C:N ratio at z_{EP}	C:N depth dependence	simulated time	initial tracer field from
A	278 μatm	6.6	no	5000 years	Optimization
B	278 μatm	7.1	no	1000 years	A
C	278 μatm	6.6	yes	1000 years	A
D	278 μatm	7.1	yes	8000 years	A
E	S650	6.6	no	1770-2200	A
F	S650	7.1	yes	1770-2200	D
G	S650	7.1 - 8.1	yes	1770-2200	D

have occurred with these ratios at all times, i.e. from preindustrial to present times. There is no indication for long term (preindustrial to present) changes in the data of the compiled collection. However, recent observations suggest that changes on time scales of several years seem to occur in the ocean. One example are the slightly decreasing C:N ratios recorded from 1989 until 1998 at the *BATS* site in the Sargasso Sea, and the slight increases of C:N ratios at the *HOT* site in the subtropical North Pacific. From both trends no global conclusions can be drawn and the two areas are oligotrophic regions with low annual net carbon export, i.e. they are of minor importance for the global carbon export. There are no data available from longer time-series measurements in the high productive ocean areas. Consequently, it has to be assumed that also in a steady state preindustrial ocean, on a global mean, carbon to nutrient element ratios of sinking particles may have been elevated as determined in the current study .

A potential positive response of the element ratios of sinking POM to increasing anthropogenic CO_2 emissions and global change is the CO_2 dependent production of transparent exopolymer particles (TEP). Elevated surface water CO_2 concentrations and wide spread nutrient limitation increase TEP production [Engel, 2002; Engel et al., 2002], and one can speculate that a larger contribution of TEP carbon to global POC production will result in a carbon enrichment relative to nitrogen and phosphorus of sinking particles. A model simulation of this scenario will be presented in the following, even though there is no evidence from the current data analysis for significant temporal changes of this kind.

Steady State Experiment with Element Ratios according to the Redfield Ratio (A)

For reference purposes an equilibrium model experiment (A) has been conducted to simulate the long-term steady state property field under preindustrial atmospheric

CO_2 conditions. In this steady-state system there is no net air-sea gas exchange. To obtain a steady state, the model is run with the flow field, export production and tracer distributions from a former optimization experiment over a time interval of 5000 years. For this run the atmospheric CO_2 partial pressure is kept constant at preindustrial levels (278 μatm). The elemental ratios for biological production and remineralization are set to the classical Redfield ratios.

For the equilibrium state the net CO_2 gas exchange rate is required to be smaller than 0.01 Gt C per year, which is reached after 3000 years. All other tracers also reached their equilibrium after 3000 years, i.e. changes in the mean concentration of the respective tracer are less than 1 % during the last 500 years of the simulation. For example, the change in the mean DIC concentration from the year 2500 until the year 3000 of the simulation amounts to 0.5 μmol/kg, corresponding to 0.02 %. Consequently, at the end of the experiment, after 5000 years, the differences have further decreased, i.e. there are no mentionable changes in the mean concentrations of all tracers and the net CO_2 gas exchange is zero.

The distributions of DIC, NO_3, PO_4, O_2, TALK and DOP from this equilibrium run are later used as initial fields for three experiments to study the ocean's response to changes in particle composition at the base of the euphotic zone and deeper carbon remineralization and for one experiment with variable atmospheric pCO_2.

Model Response to Changes in the Element Ratio of sinking POM (B and C)

To test the response of the model to modifications in the C:N ratio of sinking particles at the base of the euphotic zone and to a deeper remineralization of carbon in contrast to nitrogen, two experiments are carried out. The atmosphere is kept constant at preindustrial values over the whole simulation interval of 1000 years in both experiments, and start values of DIC, NO_3, PO_4, O_2, TALK and DOP are taken from the results of experiment A, the reference run. In experiment B the C:N ratio for particles at depth of the euphotic zone is set to 7.1 in contrast to 6.6 in experiment A, while no further changes for the remineralization are made, i.e. the C:N ratio stays constant with depth. In experiment C the C:N ratio is kept constant at a value of 6.6 like in the reference model, but the parameter β_C is decreased by a factor of 0.963 to achieve a deeper carbon remineralization in contrast to nitrogen and phosphorus. As both experiments start with tracer distributions from the reference experiment (A), but changes in the element ratios are implemented now from the beginning on without smooth transition, these experiments are not expected to follow a natural behavior of marine particle fluxes. However, the intention is to test the response of the model to the applied changes. Therefore, only the effects on the CO_2 gas exchange will be regarded in these two experiments.

Steady State Experiment with Element Ratios from this Study (D)

Experiment D has been carried out to find a steady state solution for a preindustrial ocean with element ratios of particle fluxes comprising elevated C:N ratios at the base of the euphotic zone and depth dependent C:N ratios. This experiment represents the constraint that particle composition has been at all times as determined by the preceding data analysis in section 2 (equation 2.3). Start values of the tracers DIC, NO_3, PO_4, O_2, TALK and DOP in experiment D are taken from the reference experiment A and the atmosphere is kept constant at the preindustrial CO_2 levels of 278 μatm. For the C:N ratios of particles at the base of the euphotic zone a value of 7.1 is applied and deeper carbon remineralization in contrast to nitrogen and phosphorus is achieved by using a smaller β_C value (β_C=0.963 $\cdot$ β_N). This setup now represents a full implementation of the main results from the presented data set, as given by equation 2.3. The experiment is run for 8000 years to reach equilibration for all tracers and the CO_2 gas exchange. Again, the equilibrium was reached after 3000 years with a net CO_2 gas exchange lower than 0.01 Gt C per year and with changes in the mean inventory of all respective tracers of less than 1 % during 500 years of simulation.

The DIC inventory of this experiment (D) is later compared with the DIC inventory of the reference experiment (A). Furthermore, the results of experiment D are used as start values for two experiments of time dependent simulations with variable atmospheric CO_2 concentrations.

Time Dependent Simulation with Redfields Element Ratio (E)

To determine the response to increasing atmospheric CO_2 concentrations of a preindustrial equilibrium ocean with the element ratio according to the Redfield ratio, experiment E has been performed. The start values of the tracers DIC, NO_3, PO_4, O_2, TALK and DOP are taken from experiment A, and a variable atmosphere is now implemented to reflect anthropogenic CO_2 emissions. The experiment starts in 1770 and ends in 2200. Atmospheric CO_2 data for the first phase until 1990 are taken from ice core records [Neftel et al., 1994] and from the Mauna Loa CO_2 record [Keeling and Whorf, 2002]. The further atmospheric CO_2 development is implemented using the S650 emission scenario [IPCC, 1997], which continues the data records and reaches a maximum of the atmospheric CO_2 partial pressure of 650 μatm in the year 2200. In Figure 4.5 the progression of the atmospheric CO_2 concentration and the element C:N ratio of particles at depth of the euphotic zone for the experiment E is displayed for the whole simulation period from 1770-2200.

Experiment E is used to calculate the global net air to sea CO_2 flux and corresponding changes in both the global mean DIC concentration and the distribution of anthropogenic CO_2 in the ocean.

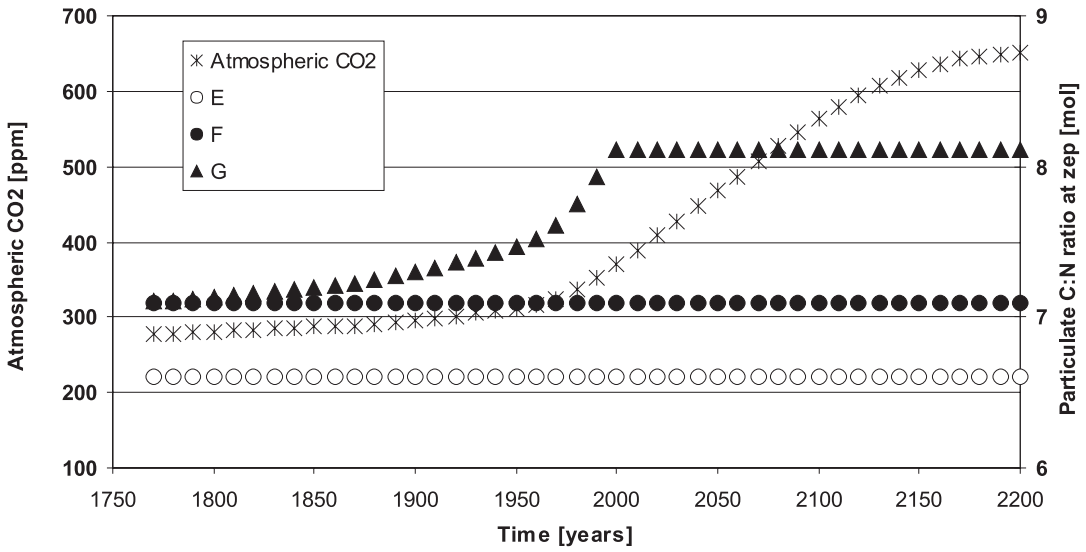

Figure 4.5: Scenarios for the atmospheric CO_2 concentration (black stars, left scale) and particulate elemental C:N ratios (right scale) for sinking particles at the base of the euphotic zone for the experiments E (open circles), F (black dots) and G (black triangles) over the simulation interval from 1770-2200.

Time Dependent Simulation with Element Ratios from this Study (F)

A second experiment for the determination of changes in the marine carbon cycle due to increasing atmospheric CO_2 concentrations is realized in experiment F. The response of a preindustrial steady state ocean where sinking particles have element ratios according to the results from the current data analysis (equation 2.3) to variable atmospheric CO_2 concentrations is estimated. The C:N ratio of particles at the base of the euphotic zone is 7.1, and there is an increase of the C:N ratio with depth in the water column, as displayed in the right panel of Figure 4.4. The initial fields of the tracers DIC, NO_3, PO_4, O_2, TALK and DOP are taken from experiment D, and the atmospheric CO_2 follows the S650 scenario. The experiment is run from the year 1770 until 2200, and the temporal change of the atmospheric CO_2 and the C:N ratio of particles at the base of the euphotic zone are displayed in Figure 4.5.

The resulting air to sea fluxes of CO_2, the corresponding changes in the mean oceanic DIC inventory and the pattern of anthropogenic CO_2 distribution are calculated and compared to the results from experiment E.

Time Dependent Simulation with CO_2 dependent Element Ratios (G)

Particle fluxes with CO_2 dependent element ratios are implemented in experiment G. This experiment follows the hypothesis of an increasing contribution of TEP (transparent exopolymer particles) since the beginning of industrialisation to global

POC production due to increased availability of carbon and presumably to increased limitation in nitrate and phosphate. TEP are particulate carbohydrate products of photosynthesis (primary production) and as the rate of photosynthesis is dependent on the abundance of CO_2 or DIC, this is valid for the TEP production as well. In contrast to cell growth, TEP production is not primarily nutrient limited, and therefore a general CO_2 dependence can emerge.

TEP is reported to be produced largely under nutrient limitation and with a linear CO_2 dependence [Engel, 2002]. Furthermore, it is highly carbon enriched with a mean C:N ratio of 20-26 [Engel and Passow, 2001; Mari et al., 2001]. Descriptions of the amount of TEP carbon produced in a phytoplankton bloom can reach up to 50 % of organic carbon production by TEP. However, TEP production is reported mainly for coastal and shelf areas and it is supposed to happen predominantly under nutrient limitation, which appears neither globally nor in every phytoplankton bloom. For the CO_2 dependent production it seems that currently saturation is almost reached [Engel, 2002].

The start values of the tracers DIC, NO_3, PO_4, O_2, TALK and DOP are taken from experiment D. Element ratios for sinking particles at the beginning of the experiment are taken in accordance to the results from the data analysis as shown in Figure 4.4, i.e. the C:N ratio of sinking particles at the base of the euphotic zone is 7.1, increasing with depth of about 0.2 units per 1000 m water depth, which leads to a C:N ratio of 8.1 for particles in 5000 m depth. The C:N ratio of particles at depth of the euphotic zone now is implemented CO_2 dependently, i.e. it increases with an increasing atmospheric CO_2 concentration, and the atmospheric CO_2 proceeds as shown in Figure 4.5.

Assuming only a minor contribution of TEP to particle fluxes at preindustrial times on a global scale, and a CO_2 dependent increase to a 5 % contribution of TEP-carbon to global POC production in the year 2000, results in a C:N ratio of particles at depth of the euphotic zone of 8.1 for the year 2000. From then on, this value is kept constant until the end of the simulation in the year 2200 (Figure 4.5). Overall, the increase of the particulate C:N ratios from 1770-2000 corresponds to 0.004 units per year. During the decades from 1980 until 2000, it amounts to 0.02 units per year which is still considerably lower than the increase found for sediment trap data from the *HOT* site (+0.23 units per year) during the years from 1989-1995. The depth dependent carbon remineralization is kept constant over time during this simulation, i.e. from the year 2000 on particle fluxes consist of C:N element ratios of 8.1 at depth of the euphotic zone, increasing to a value of 9.1 in 5000 m water depth. Therefore, the parameter β_C, determining the remineralization depth scale (equation 4.1), is decreased by a factor of 0.963 as described above.

The resulting air to sea CO_2 fluxes and the increase of the oceanic DIC inventory, which means the distribution of anthropogenic CO_2 in the ocean, are compared to results from experiment F. Thus, possible effects of CO_2 dependent element ratios of sinking particles under the influence of a changing atmosphere are determined.

4.4 Model Results

4.4.1 Steady State Experiments

Experiment A

Experiment A is supposed to be the reference experiment providing start values for all further experiments with element ratios for particle fluxes according to the traditional Redfield ratio. Calculated to equilibrium, there is no net air-sea gas exchange at the end of the simulation, and the mean concentrations for the following tracers of the model domain are

- DIC = 2227 μmol/kg
- NO_3 = 31.2 μmol/kg
- PO_4 = 2.16 μmol/kg
- O_2 = 164 μmol/kg
- TALK = 2366 μmol/kg
- DOP = 0.01 μmol/kg.

Experiments B and C

Experiments B and C are performed to test the reaction of the model to changes in the element ratio of particles at depth of the euphotic zone (B) and to deeper remineralization of carbon (C). Figure 4.6 shows the resulting global net air-sea flux of CO_2. There are considerable positive air-sea fluxes of CO_2 at the beginning of the simulation, especially for experiment B, where about 0.37 Gt C per year are taken up by the ocean 10 years after changing the particulate element ratio from 6.6 to 7.1. The air-sea CO_2 flux in experiment C is also positive, but much smaller (ca. 0.1 Gt C per year). The largest effect of deeper carbon remineralization occurs with a delay of about 30 years, so that the deeper carbon transport of sinking particles, which underly decreased carbon remineralization, is a relatively slow process leading to a relative depletion of the surface ocean with respect to DIC. While in experiment B air-sea CO_2 fluxes are highest at the beginning and then decreasing exponentially, in experiment C there are increasing air-sea CO_2 fluxes until 30 years after the change in the carbon remineralization and from then on the fluxes are also decreasing exponentially.

After 1000 years, in both experiments air-sea CO_2 fluxes are smaller than 0.04 Gt C per year, i.e. there is no considerable effect left, and the ocean is approaching a new steady state. The results show that a change in the elemental ratio of sinking particles at the base of the euphotic zone has a significantly larger effect on the

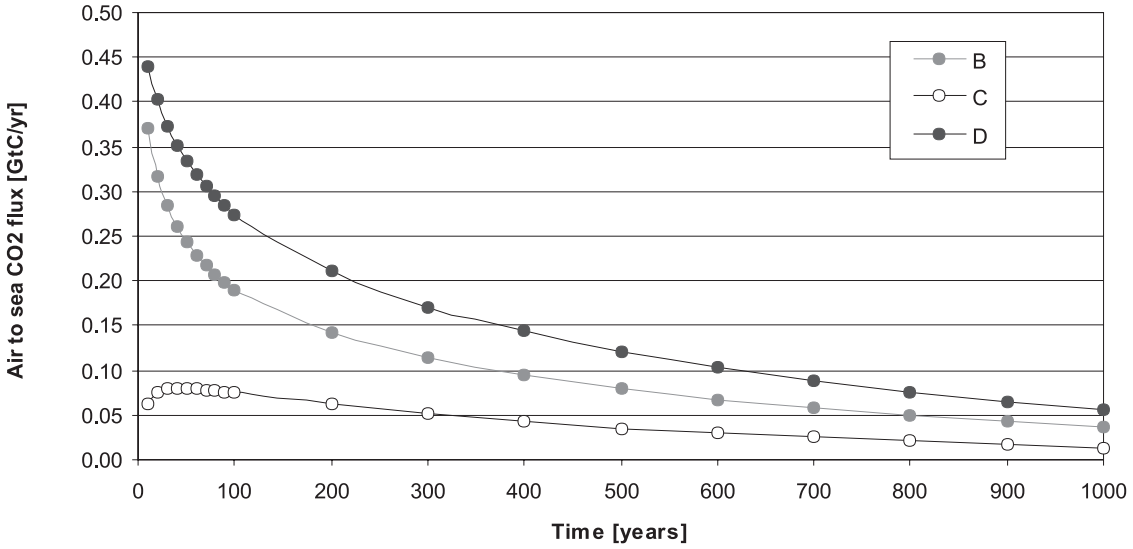

Figure 4.6: Global net air-sea flux of CO_2 in Gt C per year for the sensitivity experiments B, C and D, for a time period of the first 1000 years. Positive values indicate net CO_2 uptake by the ocean.

air-sea CO_2 flux than the additional effect of C:N ratios increasing by 0.2 units per 1000 m water depth.

Experiment D

In experiment D both features, higher than Redfield C:N element ratios at the base of the euphotic zone and increasing C:N ratios towards greater depth are implemented. The experiment is run for 8000 years to reach a steady-state with negligible net air-sea CO_2 fluxes. At the beginning there is a considerable uptake of CO_2 by the ocean as shown by Figure 4.6, with air-sea fluxes of 0.3-0.4 Gt C per year during the first 100 years of the simulation. After 1000 years there are only minor air-sea fluxes in the order of 0.05 Gt C per year, but after 3000 and also after 8000 years ocean and atmosphere are equilibrated, i.e. the global net air-sea CO_2 flux is lower than 0.01 Gt C per year.

The positive air to sea CO_2 fluxes until steady state lead to an increase of the global mean concentrations of DIC in contrast to the Redfield ratio equilibrium run (A), now corresponding to 2236 μmol/kg (ΔDIC=9 μmol/kg). The concentrations of the other tracers PO_4, O_2, NO_3, TALK and DOP remain constant at the values determined in experiment A. In addition to the constant mean inventories there are also no changes in the distributions of those tracers during the simulation.

The increase of the DIC concentration in experiment D compared to experiment A, corresponds to an accumulation of an additional 150 Gt C in the ocean, which appears small compared to the total oceanic carbon inventory of $36 \cdot 10^3$ Gt C

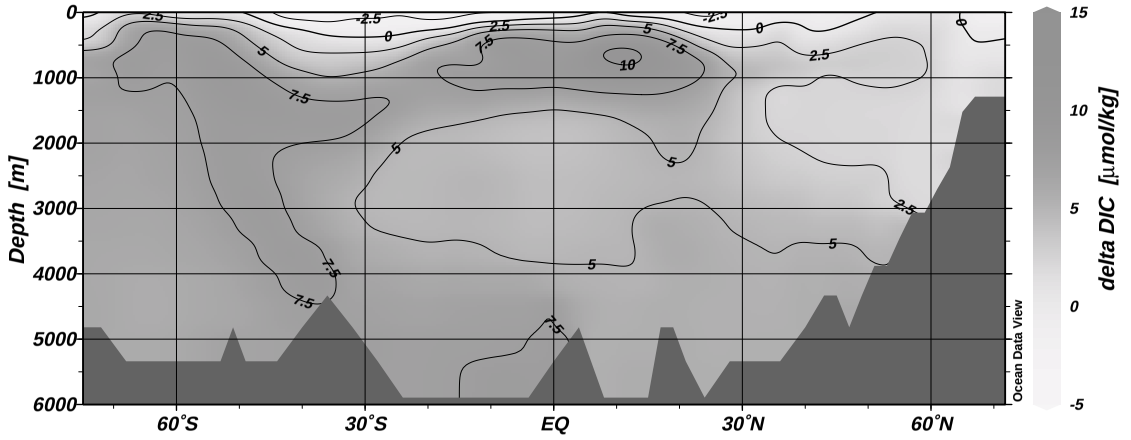

Figure 4.7: Increased DIC concentrations in the Non-Redfield equilibrium experiment (D) in contrast to the Redfield ratio equilibrium ocean (A) on a north to south section in the Atlantic Ocean along 25^o W.

(model result). However, the 150 Gt C correspond to about 25 % of the preindustrial atmospheric CO_2 inventory of about 600 Gt C [Siegenthaler and Sarmiento, 1993] (Figure 1.3), and if removed from the atmosphere would reduce the atmospheric pCO_2 by approximately 75 μatm.

Stronger vertical DIC gradients than in experiment A appear in experiment D. The differences in the tracer distributions of DIC between the two equilibrium experiments (A and D) are displayed in Figure 4.7 on a meridional section in the Atlantic Ocean along 25^o W. Positive values represent larger DIC concentrations in the experiment D, negative values show decreases. Most areas show higher DIC concentrations, but at the surface, there are also large areas with a lowering of DIC. This reduction is due to the higher uptake of carbon during particle production (C:N = 7.1 compared to Redfield ratio C:N = 6.6) and the smaller carbon remineralization parameter β_C, resulting in deep carbon remineralization and a more effective carbon export mechanism.

The distribution of additional DIC mirrors the general water mass circulation pattern of the Atlantic Ocean (compare Figure 1.1), which can be seen clearly in the increasing DIC concentrations following the North Atlantic Deep water (NADW) southward and the Antarctic Intermediate Water (AAIW) in a northward direction. In the South Atlantic there is upwelling of DIC enriched deep water leading to significant increases in the surface water DIC concentrations between 50^o S and 65^o S. Though there is no net gas exchange at equilibrium, areas of lower surface water DIC concentrations will be stronger CO_2 sinks while areas of higher DIC concentrations will be enhanced sources in the Non-Redfield equilibrium ocean.

4.4.2 Time Dependent Simulations

Based on the two different equilibrium experiments (A and D) three further scenarios have been simulated to estimate the oceanic carbon uptake in response to increasing atmospheric CO_2 concentrations. Therefore, the atmospheric CO_2 partial pressure is implemented varying in time, based on ice core [Barnola et al., 1999] and atmospheric measurements [Keeling and Whorf, 2002] and the S650 emission scenario [IPCC, 1997].

Experiment E

Experiment E is based on the results from experiment A, the equilibrium run with particle fluxes according to the Redfield ratio, i.e. the C:N ratio of particles at the base of the euphotic zone is 6.6 and stays constant at this value over depth and over time. Table 4.1 specifies the major parameters for the experiment and Figure 4.5 shows the S650 atmospheric CO_2 scenario and the progression of the C:P elemental ratio for particles at the base of the euphotic zone, which is kept constant during the simulation of experiment E.

At the beginning of the simulation there is a moderate increase of atmospheric CO_2, growing more rapidly after 1950 (Figure 4.8). From 1770 until 1950 the uptake of CO_2 by the ocean is moderate and increasing with time, while the air to sea fluxes are lower than 1 Gt C/yr. From 1950 on the air-sea CO_2 fluxes increase exponentially to about 2.6 Gt C in the year 2000. This increase proceeds further until the year 2080, where maximum fluxes of about 3.8 Gt C per year are reached. From then on there are still positive, but decreasing air to sea CO_2 fluxes, following a less steep increase of the atmospheric CO_2 concentration from about the year 2100 on.

The net uptake of CO_2 by the ocean is accompanied by continuously growing mean DIC concentrations, displayed in Figure 4.9. From preindustrial values up to the year 2000 the mean oceanic DIC concentrations have grown from 2227 μmol/kg DIC to 2236 μmol/kg today, and in the year 2200 the mean concentrations are significantly higher than preindustrial and today's values, and they will amount to 2278 μmol/kg.

The increase in oceanic DIC concentrations in the ocean is not evenly distributed over the global ocean, but shows a pattern, which is related to the main ocean circulation. Figure 4.10 shows on a north to south section along 25^o W in the Atlantic Ocean the changes of DIC concentrations between given times of the simulation (1800, 1900, 2000 and 2100) and preindustrial values. The increase represents the uptake of anthropogenic CO_2 (aCO_2) in the ocean. Note that the scales for the different panels are different by factors of 10 to 100.

The strongest DIC concentration changes occur at the sea surface, where gas exchange takes place. In the year 1800, the surface water DIC increases are small

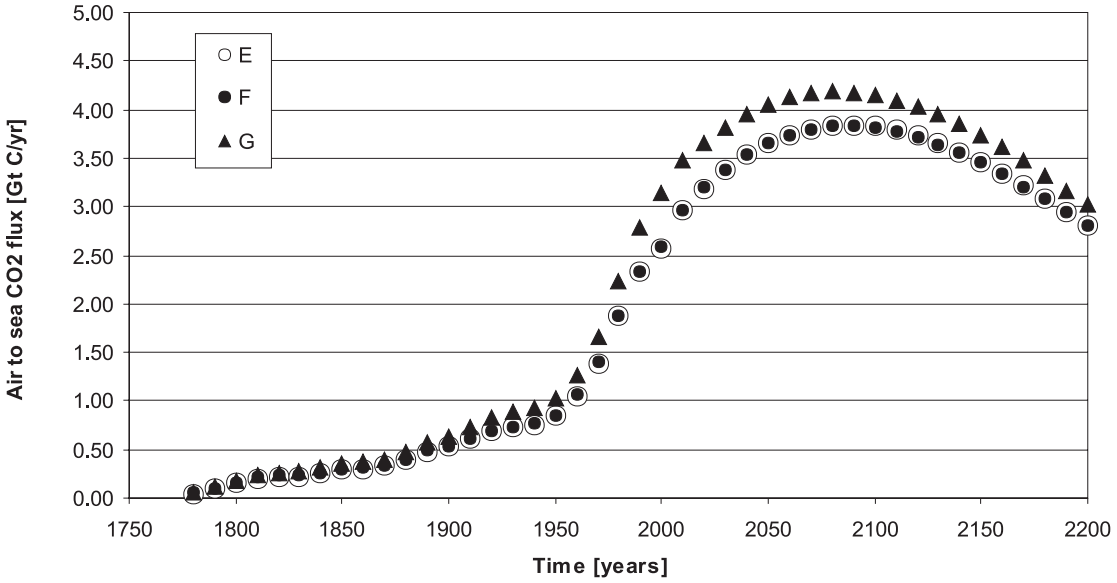

Figure 4.8: Annual net air-sea flux of CO_2 in the experiments E (open circles), F (black dots) and G (black triangles).

(about 1 μmol/kg), and the water masses below 1000 m depth are almost unaffected, but the DIC increase intensifies with time.

There are increasing DIC concentrations following the pathway of the North Atlantic Deep Water (NADW) which forms in the Nordic and Labrador Seas and flows southward in a depth range between 1000-3000 m. Equatorial upwelling and upwelling in the Southern Ocean cause a shallowing of the CO_2 isolines close to the surface. In the year 2000 the surface water anthropogenic CO_2 concentrations in the North Atlantic amount to 40-50 μmol/kg, and there are about 10 μmol/kg in the North Atlantic Deep Water on 30^o N in 2000 m water depth. For the year 2100 there is a distinct difference in surface water DIC concentrations predicted by the model which amounts to 150 μmol/kg. This corresponds to a relative increase of 7 %.

Experiment F

In analogy to experiment E, experiment F has been carried out to determine the response of a steady state ocean to increasing atmospheric CO_2 concentrations. Outgoing from the second equilibrium ocean (experiment D), higher than Redfield and depth dependent element ratios for sinking particles are implemented in the current experiment, representing the depth dependence of C:N ratios as displayed in Figure 2.8. The atmospheric behavior is identical with the preceding experiment (E) and is shown in Figure 4.5.

The resulting net air-sea flux of CO_2 in experiment F follows almost exactly the one

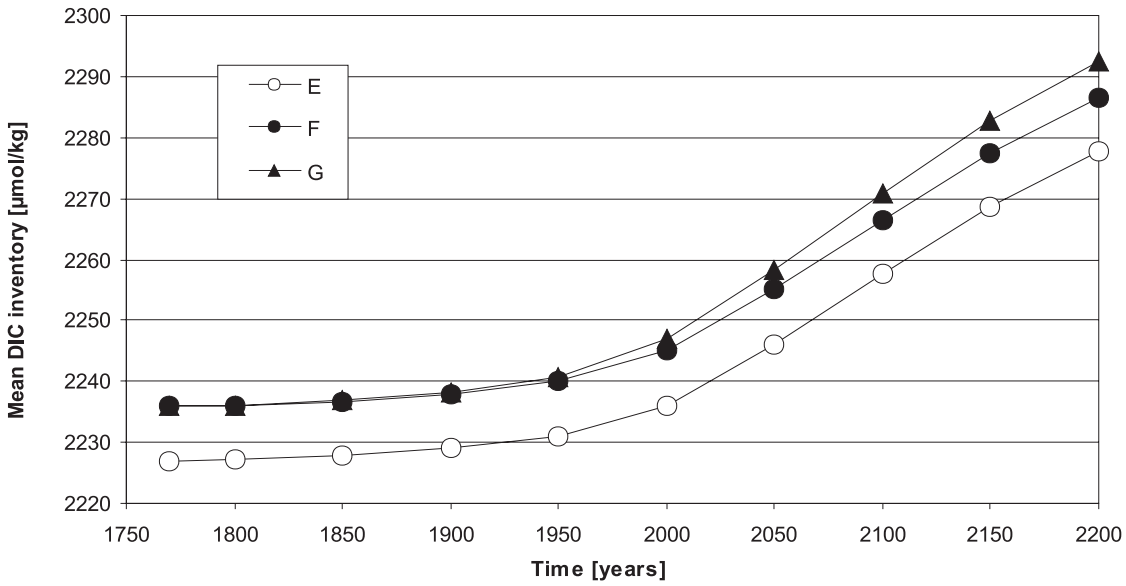

Figure 4.9: Increase of the global mean DIC concentrations in μmol/kg for the experiments E (open circles), F (black dots) and G (black triangles).

of the experiment E (Figure 4.8). The differences are lower than 0.01 Gt C per year, as it is shown by the black dots in Figure 4.11. However, there is a difference to experiment E in the increase of the mean DIC concentration (Figure 4.9). Starting with a global mean DIC concentration of 2236 μmol/kg, the simulation ends in the year 2200 with a global mean DIC concentration of 2287 μmol/kg. The offset between the mean DIC concentrations of the experiments E and F is constant over the simulation period and amounts to 9 μmol/kg ($\approx$ 150 Gt C) at all times, i.e. except for the generally higher carbon inventory there is no mentionable difference in the uptake rates of CO_2 in experiment F, compared to experiment E.

Furthermore, the pattern of anthropogenic CO_2 uptake and distribution, which is the difference between the DIC concentration at the beginning (1770) and the end (2200) of experiment F is the same as for experiment E, which is shown in Figure 4.10. Therefore, there is no difference neither in the uptake rates of anthropogenic CO_2 nor in the spatial distribution between the two experiments, E and F. These results show that the element ratios of sinking particles do not influence the current uptake of anthropogenic CO_2, assuming constant behavior since preindustrial times.

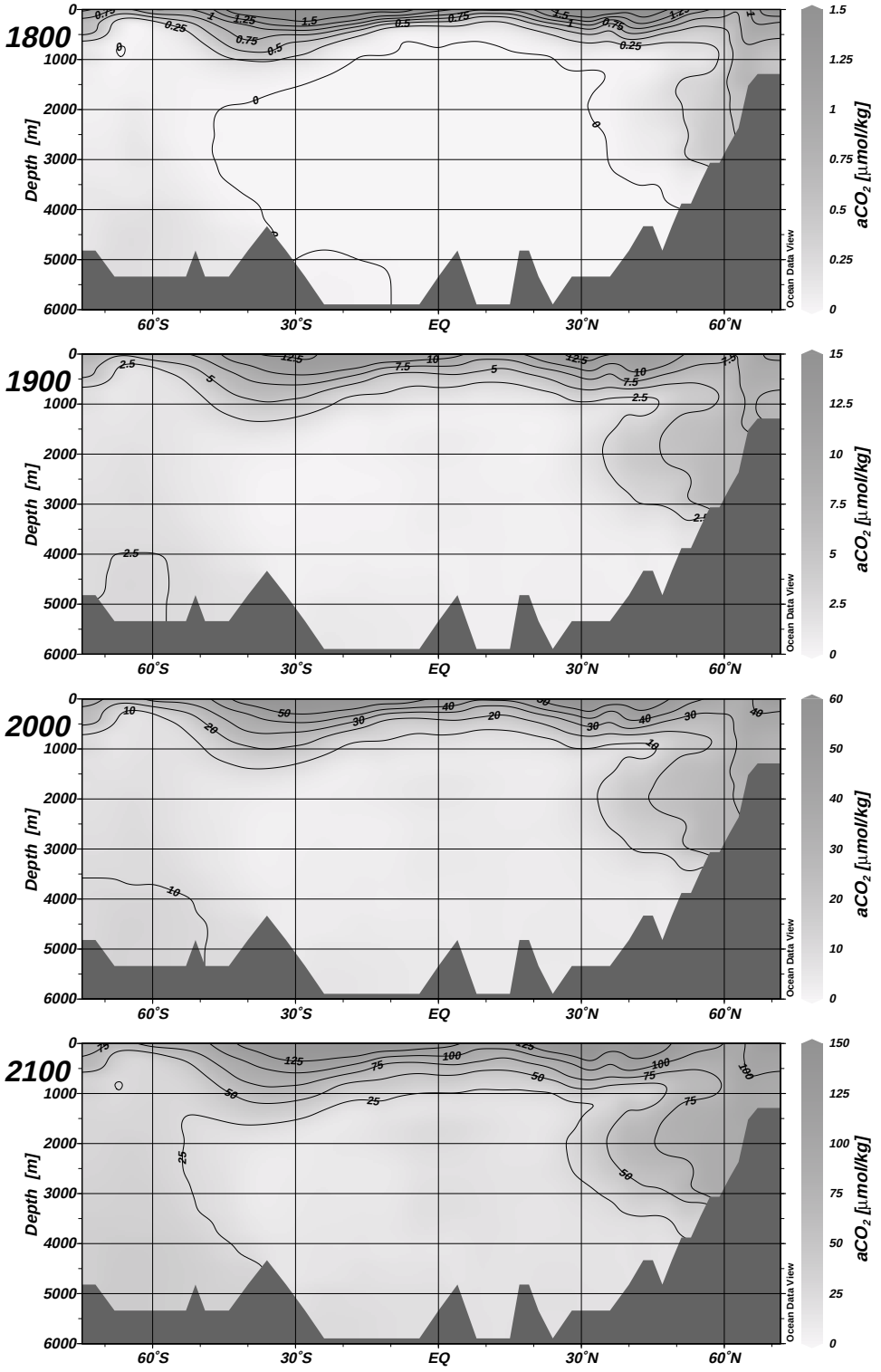

Figure 4.10: Anthropogenic CO_2 concentrations for experiment E for different times (1800, 1900, 2000 and 2100) are displayed on a meridional section along 25^o W in the Atlantic Ocean, showing the patterns of carbon sequestration. Note the different scaling for the plots.

Experiment G

CO_2 dependent element ratios of sinking particles are implemented in experiment G with a C:N ratio at the base of the euphotic zone of 7.1 at the beginning (1770) and 8.1 from the year 2000 until 2200, as shown in Figure 4.5. The C:N depth dependence is implemented as described in the preceding experiments.

The resulting net annual air-sea flux of CO_2 is displayed in Figure 4.8, with a trend following the same patterns as in the previous experiments (E and F), but with absolute values, that are significantly higher. According to this scenario, at the beginning of the simulation the CO_2 flux into the ocean is small and increasing slowly. From the year 1950 on the increase gets steeper, exceeding the fluxes in experiments E and F markedly. In the year 2000 the flux amounts to 3.1 Gt C/yr, and it reaches its maximum in 2080 with 4.2 Gt C/yr. From then on there is a continuously decreasing net air-sea CO_2 flux predicted by the model, with slightly stronger decreasing fluxes as in the experiments E and F.

As a consequence of the elevated air-sea CO_2 flux, the mean DIC inventory increases significantly more than in experiment F, which has the same initial conditions. In Figure 4.9 it is shown that in experiment G in the year 2200 the mean DIC concentration of about 2293 μmol/kg is 6 μmol/kg higher than in experiment F. This corresponds to an increase of the marine carbon inventory of about 100 Gt C.

In experiment G the uptake of anthropogenic CO_2 is caused by both increasing atmospheric CO_2 concentrations and the temporally variable element ratios of sinking particles. To point out the contribution of CO_2 dependent elemental compositions on marine carbon fluxes, the differences in the air-sea CO_2 fluxes between the experiment G and experiment F are calculated and displayed in Figure 4.11. At the beginning of the experiment there is no considerable additional uptake in experiment G until 1900, with differences of air-sea fluxes between experiments F and G are less then 0.1 Gt C/yr. From then on the difference increases exponentially with increasing atmospheric CO_2 to the peak value of 0.56 Gt C/yr in 2000. At this time the C:N ratio of particles at the base of the euphotic zone reaches its maximum value of 8.1, staying constant for the rest of the simulation. Consequently, the difference of the air-sea CO_2 fluxes between experiment F and G starts to decrease from 2000 on and reaches a value of about 0.2 Gt C/yr higher air-sea flux in experiment G at the end of the simulation in the year 2200.

The relative contribution of the additional carbon flux to the total flux rates, which is induced by TEP, is also displayed in Figure 4.11 by the open symbols. It is determined as the difference of air-sea CO_2 flux between experiments F and G divided by the total CO_2 flux of experiment G. Thus, at the beginning of the simulation there is about 8 % of the air-sea CO_2 flux in experiment G attributable to the CO_2 dependent increase of the C:N ratio of sinking particles. This relative contribution increases to its maximum value in the year 2000, when it amounts to 18 %. From then on it decreases and stabilizes on a value of about 7-8 % from the year 2100 on.

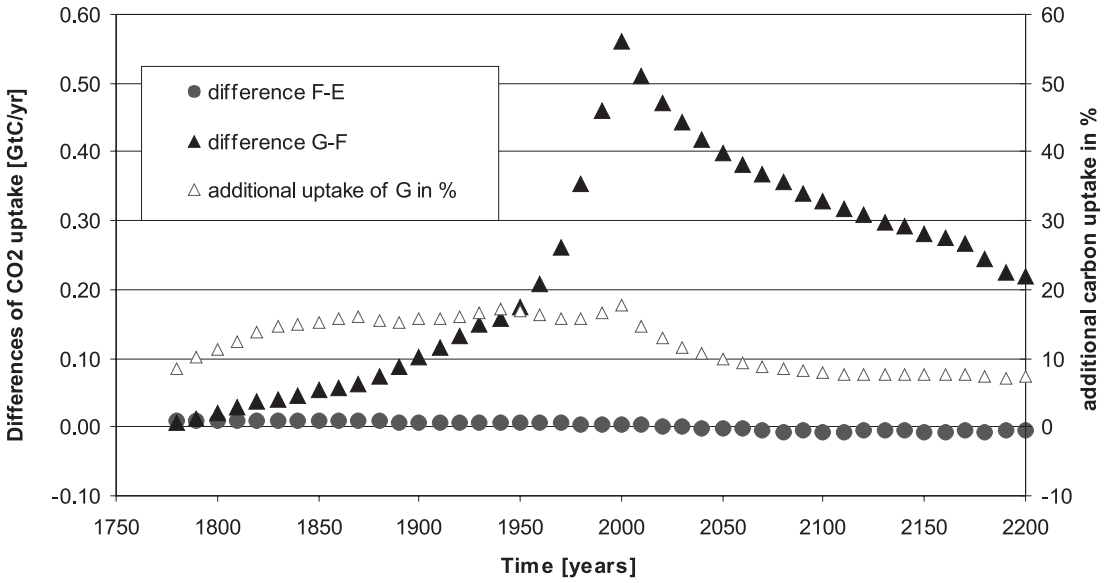

Figure 4.11: Differences of the air-sea fluxes of CO_2 between the experiments E and F (black dots), and experiments F and G (black triangles). The open triangles represent the relative contribution of the CO_2 dependent element ratios to the net air-sea flux of CO_2 in experiment G (right scale).

Figure 4.12 shows spatial and temporal differences in the DIC concentrations between the experiment G and the reference experiment F for the times 1800, 1900, 2000 and 2100 on a meridional section along 25^o W in the Atlantic Ocean. The distribution highlights areas of anthropogenic CO_2 uptake, which are associated with the CO_2 dependent increasing TEP production, simulated in experiment G. The total uptake of anthropogenic CO_2 in experiment G is not shown. It is the sum of the DIC concentrations in Figures 4.10 and 4.12.

Compared to the amount of anthropogenic CO_2 uptake by experiment F, the additional effects of CO_2 dependent element ratios of sinking particles are smaller by a factor of 10. Note the different scaling of individual plots in Figure 4.12. However, there are large areas of significant impact. Some surface ocean areas show a decrease in DIC concentrations while there are generally increasing DIC concentrations in the interior of the ocean. In the lower latitude Atlantic Ocean there is a strong increase of DIC in the subsurface waters from closely beneath the surface until 1000 m depth. This pattern appears already in the year 1800 and strengthens until the end of the simulation pointing out the predominant areas of carbon remineralization.

The accumulation of CO_2 over time in the two different experiments with depth dependent element ratios is shown in Figure 4.13, to determine the ocean's storage capacity of anthropogenic CO_2. For the experiment with temporally constant element ratios of sinking particles (experiment F) the uptake of anthropogenic carbon amounts to 152 Gt C since the beginning of industrialization up to the present (year

2000). This accumulation will rise to 504 Gt C in the year 2100 and furthermore to 844 Gt C in 2200. The cumulative uptake in the experiment with CO_2 dependent element ratios of sinking particles (G) is significantly higher. For present times the model predicts a cumulative uptake of 182 Gt C by the ocean (+30 Gt C) and this enhanced uptake will intensify to 575 Gt C in 2100 (+71 Gt C) and to 942 Gt C in 2200 (+98 Gt C). The relative contribution of the additional carbon uptake due to CO_2 dependent element ratios of sinking POM decreases over time. In the year 2000 the increased carbon uptake, which is associated to TEP, is responsible for as much as 17 % of the accumulated carbon. In the year 2100 this relative contribution is still 12 % and it decreases slightly more until 2200 to a relative amount of 11 %.

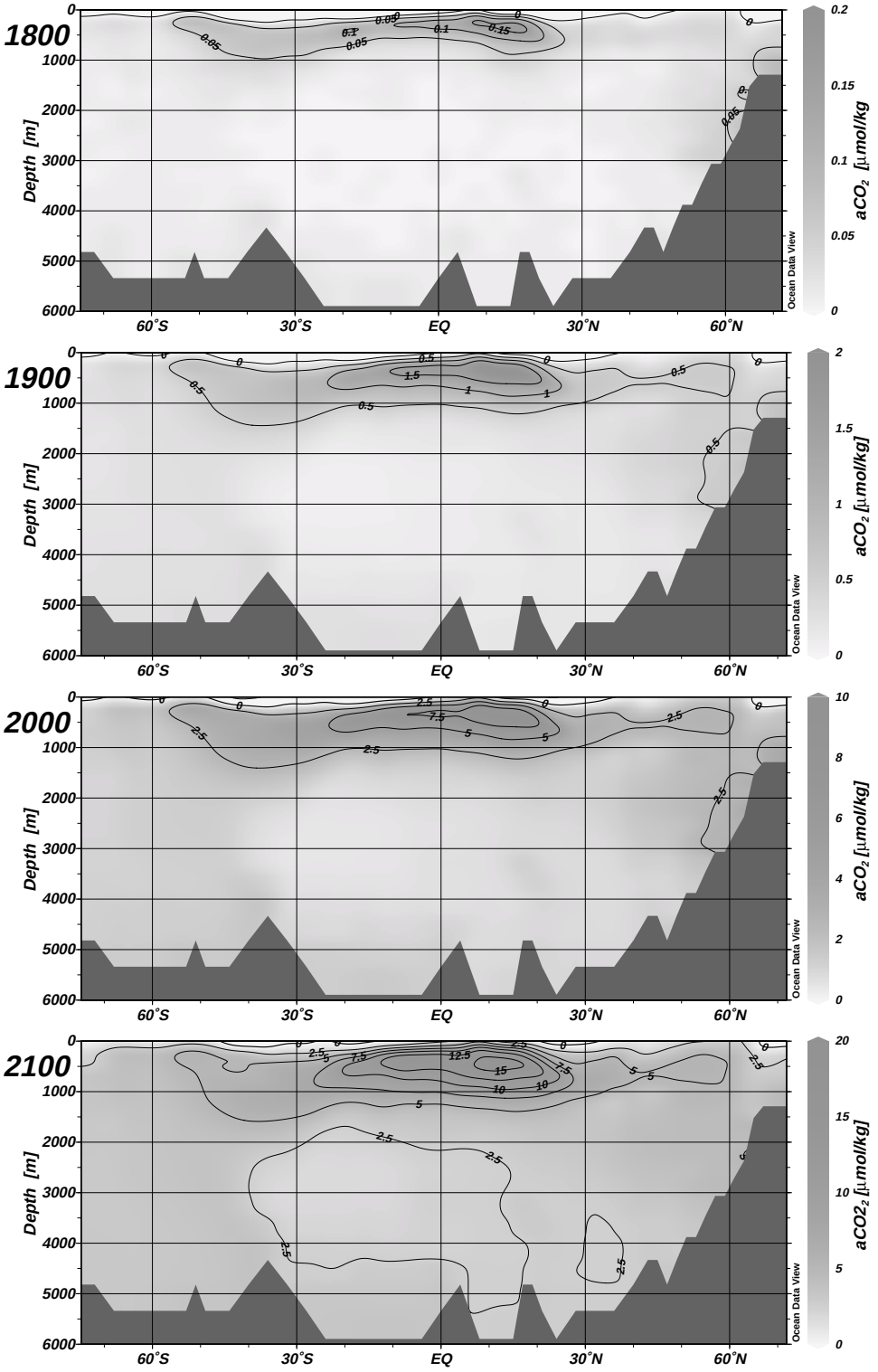

Figure 4.12: Increase of DIC concentrations due to CO_2 dependent particle compositions of the TEP scenario in experiment G in contrast to the results from the reference experiment F on a meridional section along 25^o W in the Atlantic Ocean. Different time steps (1800, 1900, 2000 and 2100) are displayed showing the patterns of carbon sequestration. Note that there is no uniform scaling for DIC increases.

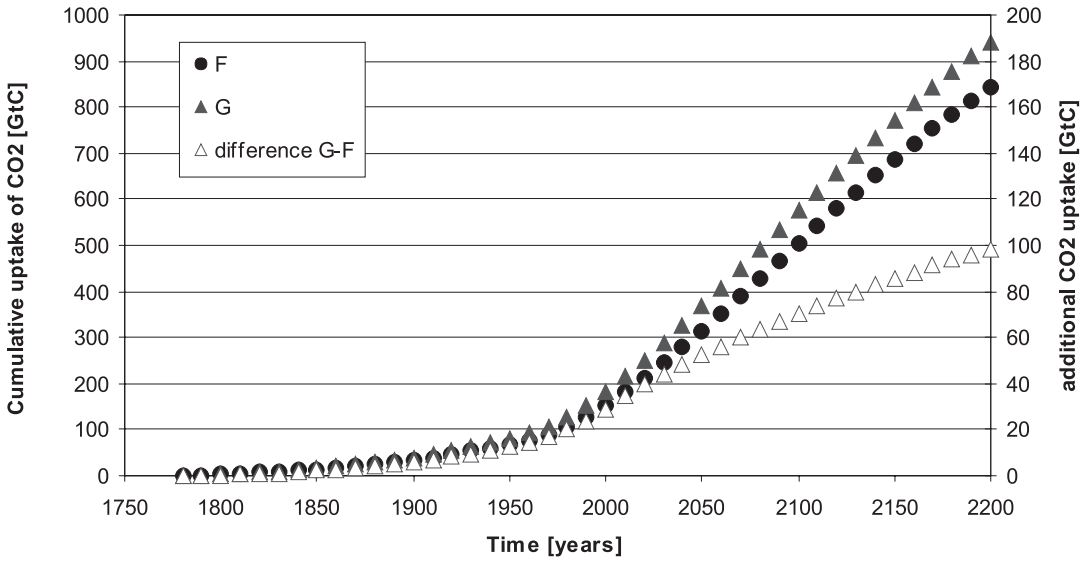

Figure 4.13: Cumulative uptake of CO_2 by the different experiments F (black dots) and G (black triangles) from the beginning of industrialization until the year 2100 (left scale). Open triangles show the additional carbon uptake of experiment G with CO_2 dependent element ratios compared to the accumulation rates obtained by experiment F (right scale).

5 Implications for the Marine Carbon Cycle

5.1 Ocean Carbon Inventory and Uptake of Anthropogenic CO_2

The analysis of data on the elemental composition of POM in the ocean revealed systematic regional, depth dependent [Schneider et al., 2003] and seasonal variations in the C:N ratios with a strong tendency towards above-Redfield C:N ratios. Consequently, calculations of the oceans capacity for carbon sequestration, which often make use of the traditional C:N:P (106:16:1) element ratios of Redfield [1934] and Redfield et al. [1963], may underestimate downward carbon fluxes or overestimate nitrogen and phosphorus fluxes. An underestimation of the carbon flux will occur when models use the phosphorus or nitrogen concentration in the surface water and extrapolate the carbon flux by applying the Redfield factor to the drawdown of phosphorus or nitrogen [Sambrotto et al., 1993]. Vice versa, an overestimation of the nutrient fluxes will be the back calculation of the phosphorus and nitrogen flux from the measured DIC drawdown in the surface water, again using the classical Redfield ratio. Consequently, the coupling of carbon fluxes in the ocean to the abundance of phosphorus and/or nitrogen in the surface water by the application of the classical constant Redfield ratio, most likely, yields incorrect model results.

Originally, the Redfield ratio was considered to describe freshly produced phytoplankton in a bloom during exponential growth [Redfield et al., 1963]. Thus, the Redfield ratio seems to be suitable for the description of living phytoplankton, but the application for a description of the elemental composition of sinking particles is inappropriate. Sinking matter does not consist of pure and fresh marine particles, as it has undergone several stages of decomposition, repackaging and/or aggregation before starting to sink. The results of this study show clearly, that on a global average the material sinking out of the euphotic zone is already carbon enriched (C:N $\approx$ 7.1), predominantly due to preferential remineralization of nitrogen (and phosphorus), but also as a consequence of changes in the element ratio during particle production. Thus, for marine particle export fluxes higher than Redfield and depth dependent carbon to nutrient ratios should be applied in biogeochemical models to achieve a more reliable estimate of particulate carbon fluxes in the ocean.

The comparison of different approaches to determine the elemental composition of particulate organic matter, the analysis of regenerated nutrients and secondly particle measurements, has revealed that it has to be distinguished between several groups of particles and organic matter. There is e.g. living phytoplankton, suspended material, sinking particles and dissolved organic matter (DOM), which are all direct or indirect of products of photosynthesis and will be remineralized more or less later on in the ocean. All these types of organic matter cycle individually in the ocean and thus have different temporal and regional relevance for the marine carbon cycle. Knowing the elemental composition of one of these types can not be transferred

to the others, without leading to miscalculations. Therefore, to determine marine carbon fluxes by sinking particles the element ratios obtained from measurements on sinking particles have to be used, as only those represent the composition of sinking matter, adequately.

The generally higher than Redfield C:N ratios found for sinking particles in this study are explained by both deviations from the Redfield ratio during particle production and preferential remineralization. Carbon overconsumption can also take place during TEP production and nitrogen fixation, leading to higher C:N ratios in the particles in regions of nutrient limitation. Furthermore, the feeding of zooplankton and bacteria on particles changes their original elemental composition, e.g. when particles are consumed and repackaged into fecal pellets by zooplankton. As a matter of fact, the elemental composition of a sinking particle at the base of the euphotic zone is altered in contrast to its initial constitution, which can be explained by above mentioned processes. The further increasing C:N ratios with depth are most probably due to the proceeding preferential nutrient remineralization.

Results from the data analysis in this study (equation 2.3) lead to the conclusion that particle fluxes are more effective in the downward transport of carbon than estimated on the basis of constant elemental ratios according to Redfield's values. The corresponding effects of higher than Redfield and depth dependent C:N ratios of sinking particles on the air to sea CO_2 fluxes and the oceanic carbon inventory are calculated by the implementation into the AWI Adjoined Model for Oceanic Carbon Cycling (AAMOCC) [Schlitzer 1993; 1995; 2000; 2002; de las Heras and Schlitzer,1999]. First of all, the differences between two steady state ocean systems, one with element ratios of sinking particles according to the classical Redfield ratio and a second with element ratios as obtained by the preceding data analysis, are simulated. These experiments show, that the element ratios as determined in this study are likely to increase the global oceanic carbon inventory by about 150 Gt C, and additionally they are leading to stronger DIC gradients towards greater depth (Figure 4.7). The enhanced DIC gradients demonstrate the higher efficiency of carbon transport from the surface into the deep ocean. The amount of increase in the carbon content of the ocean is low compared to the total marine carbon inventory of about $36 \cdot 10^3$ Gt C (model results), but if this carbon is taken from the atmosphere, this effect is likely to reduce the atmospheric CO_2 partial pressure by about 75 μatm.

The results of the data analysis can be separated generally into two features, the elevated C:N ratios at the base of the euphotic zone on one hand and the depth dependence on the other hand. The relative contribution of each individual aspect to the air to sea carbon flux can be estimated from Figure 4.6, by comparing the corresponding air-sea CO_2 fluxes in experiments B and C over 1000 years. It turns out that the integrated carbon uptake by the ocean resulting from elevated C:N ratios of particles at the base of the euphotic zone (100 Gt C) is by a factor of 2.5 larger than the respective effect of preferential remineralization (40 Gt C). There-

fore, approximately 30 % of the total increase of the carbon inventory in experiment D, in which elevated and depth dependent C:N ratios are implemented, is due to the fractionation during remineralization. Consequently, depth dependent C:N ratios of sinking particles in a steady state ocean, as simulated in experiment D, can be responsible for a reduction of the atmospheric CO_2 partial pressure by about 25 μatm, which is in good agreement with results from Shaffer et al. [1999], who determined a reduction of about 20 μatm resulting from depth dependent remineralization rates of sinking particles.

To determine the ocean's response to increasing atmospheric CO_2 concentrations, the two experiments E and F are performed, initialized with the tracer fields (DIC, NO_3, PO_4, O_2, TALK and DOP) of different steady state oceans, each. In experiment E the ocean-atmosphere equilibration of the CO_2 gas exchange is achieved by the application of the traditional constant Redfield ratio for sinking particles, whereas in experiment F the element ratios are set to values according to equation 2.3. A comparison of the air-sea carbon fluxes and the changes in the patterns of DIC enrichment shows that there are no considerable differences between the experiments E and F. Consequently, both, the rates of anthropogenic CO_2 uptake and the pattern of CO_2 sequestration are the same for particle fluxes according to the Redfield ratio (E) and variable element ratios as determined by the data analysis (F). At all times, the total marine carbon inventory of experiment F is 150 Gt higher (9 μmol/kg, see Figure 4.9) than in experiment E with a pattern as shown in Figure 4.7. Consequently, for the ocean uptake of anthropogenic CO_2 it does not matter how the elemental compositions of sinking particles actually were in a preindustrial equilibrium ocean, as long as they are temporally constant, i.e. independent of the atmospheric CO_2 concentration.

Orr et al. [2001] made a comparison of four different three dimensional carbon cycle models responding to the anthropogenic CO_2 emissions according to the S450 scenario [IPCC, 1997]. Their results are comparable to those obtained in the current study. The progression of anthropogenic carbon uptake follows the same pattern as in this study (Figure 4.8), however, in the investigation of Orr et al. [2001] the flux peaks occur earlier and are not as high as in this study. These maxima are reached in the year 2000 with air-sea CO_2 fluxes of about 2-2.8 Gt/yr, which is in good accordance with the air-sea fluxes of 2.6 Gt C/yr in the year 2000, obtained in this study in experiments E and F, which are not the peak values, but further increasing until about the year 2080. The discrepancy in the maxima of air-sea fluxes is due to the fact that different atmospheric CO_2 scenarios have been applied, the S450 scenario by Orr et al. [2001] and the S650 scenario in the current study. Consequently, in the investigations of Orr et al. [2001], the atmosphere stabilizes in the year 2100 at a value of 450 μatm. This saturation is reached 100 years earlier and with 200 μatm less CO_2 than in the S650 scenario, which is applied in the current study. However, up to the present the differences in the atmospheric scenarios are small, and the distributions of anthropogenic CO_2 in the models presented by Orr et al. [2001] are generally very similar to those of the present study.

Comparing the modeled distribution of anthropogenic carbon concentration from the present study (Figure 4.10) with recent measurements shows a good agreement between two approaches in the Atlantic Ocean made by Gruber [1998] and Körtzinger et al. [1999]. Gruber [1998] investigated anthropogenic CO_2 profiles on two North to South transects, in the Eastern and Western Atlantic Ocean. He determined the anthropogenic CO_2 concentration by defining a quasi conservative tracer ΔC^*. A detailed description of the respective method is given by Gruber et al. [1996]. The distribution of anthropogenic CO_2 in the western transect is very close to the results of the current model approach on the Atlantic section along 25^o W. The highest concentrations occur in the tropical and subtropical surface waters with 40-60 μmol/kg of anthropogenic CO_2, whereas the deep water values are slightly higher in the model. While the results of Gruber [1998] show that large parts of the Atlantic deep water body are still unaffected by anthropogenic CO_2, the model results in the current study indicate anthropogenic CO_2 concentrations up to 5 μmol/kg. The higher concentrations in the model of the current study may be explained by the temporal difference between the measurements of Gruber [1998] and the simulated time in this study. The model results are valid for the year 2000, whereas the data in the study of Gruber [1998] are from 1980-1989. At the same time, during this 10-20 year interval, the enrichment of anthropogenic CO_2 in the deep Atlantic will have proceeded, most probably approaching the model results.

Körtzinger et al. [1999] used the back calculation method to investigate anthropogenic CO_2 concentrations in the ocean. A detailed description of the analytical method is given in Körtzinger et al. [1998]. They investigated the concentration of anthropogenic CO_2 for the year 1997 on a more or less zonal transect across the North Atlantic from south of Greenland to southwest of Ireland. For the western part of this transect the model results of this study are very similar to the concentrations obtained by Körtzinger et al. [1999]. The distribution of anthropogenic CO_2 in this section highlights the areas of deep water formation with relatively high concentrations of 60 μmol/kg at the sea surface and 30 μmol/kg between 2000 and 3000 m depth. In the eastern part of the section the model shows significantly lower anthropogenic CO_2 concentrations, and even with respect to a possible error of 10 μmol/kg in the method of Körtzinger et al. [1999], there is only weak correspondence. However, the comparison shows that the results obtained in this study are in reasonable consistence with other results gained from different independent methods, measurements as well as model approaches. Thus, the anthropogenic CO_2 distribution in the present analysis explains the current situation quite well and they provide a reliable basis for further future scenarios.

The effect of an additional carbon sequestration by the ocean due to temporal and CO_2 dependent variations in the elemental composition of sinking particles is simulated in the experiment G, based on the assumption of a CO_2 dependent production of TEP [Engel 2002]. The respective effect on the ocean carbon uptake is determined as the difference between the air-sea carbon fluxes and the pattern of anthropogenic CO_2 uptake in the experiments F and G, as both experiments have the same starting

Table 5.1: Cumulated CO_2 uptake of the ocean in Gt C for the experiments F and G from preindustrial times to 2000 and from 2000 until 2100.

Exp.	1770-2000	2000-2100
F	152 Gt	352 Gt
G	182 Gt (+30)	392 Gt (+40)

conditions, the equilibrium ocean with the element ratio of sinking particles according to equation 2.3. TEP is an explanation for the enhanced carbon uptake during photosynthesis in contrast to nutrients, generally referred to as carbon overconsumption in the recent literature. The model experiment shows significantly enhanced air-sea carbon fluxes in contrast to the experiment F, as displayed in Figure 4.11. There are higher net air-sea carbon fluxes with maximum differences in the year 2000, when the element ratio of particles at the base of the euphotic zone stabilizes, resulting in 0.56 Gt C per year, which is additionally taken up as a consequence of the CO_2 dependent element ratios. This further uptake in the year 2000 accounts for 18 % of the total CO_2 fluxes. The relative contribution of the additional flux to the total CO_2 fluxes increases from 10 % at the beginning to almost 20 % during the interval when the element ratios at the base of the euphotic zone increase over time. From the year 2000 on the relative contribution decreases again to a value of about 7 % in the year 2100, and this is predicted to stay more or less constant over the remaining simulated time until the year 2200. This positive net air-sea CO_2 flux induced by temporally varying C:N ratios indicates, that there is a sustainable effect on marine carbon sequestration on time scales of a few hundred years. Keeping in mind, that actually the *missing sink* amounts to approximately 1.8 Gt C per year [Broecker and Peng, 1993], the additional uptake of currently 0.56 Gt C per year by increased element ratios could explain roughly 30 % of this missing carbon sink. However, as there is a rapid decrease in the absolute additional air-sea CO_2 fluxes after the year 2000 (Figure 4.11), this contribution to the *missing sink* will also decrease in the future.

The cumulative CO_2 uptake by the TEP scenario is also significantly higher (100 Gt C; 1770-2200) than in experiment F, as can be seen in Figure 4.13. Table 5.1 shows the sum of CO_2 uptake in Gt C for the experiments F and G, divided into the time intervals from preindustrial to present (2000) and for the future 100 years (2000-2100), i.e. the time period where the C:N ratio for particles at the base of the euphotic zone increases in experiment G and secondly the 100 year interval, where the element ratios are temporally constant in both experiments. For the first interval, there is a higher net uptake of 30 Gt C in experiment G, compared to experiment F, i.e. the carbon uptake, which is due to the CO_2 dependent increase of the C:N ratios, is strengthened by about 20 %. The amount of additional uptake decreases in the future 100 years as a consequence of the temporally constant C:N ratios of sinking particles after the year 2000. At the same time there is a higher contribution of CO_2 solubility to the total carbon uptake, resulting from the continuously

increasing atmospheric CO_2 concentrations. However, there are still 40 Gt C taken up additionally in the TEP scenario from 2000 until 2100, so that such a process can further enhance the carbon uptake obtained by the scenario with CO_2 independent element ratios (F) by about 10 %.

There are no ocean-atmosphere feedback mechanisms included in the model experiments of this study, and the atmosphere follows the prescribed S650 scenario [IPCC, 1997]. This behavior is not very realistic as the atmospheric CO_2 increase is hypothetical, and secondly because no feedback from ocean carbon sequestration to the atmosphere has been applied. In fact, large scale carbon uptake rates as they occur in all model experiments of this study, should result in a significant lowering of atmospheric pCO_2, which then in turn (as a negative feedback) would lower the CO_2 gas exchange rates. However, this feature has not been applied as there is no dynamic coupling between ocean and atmosphere in the AAMOCC model. An approximation of the effect of the carbon uptake in the ocean on the atmospheric CO_2 concentration is calculated separately. For the TEP experiment (G) it turns out that in the year 2000 the atmospheric pCO_2 should be decreased by about 15 μatm, due to the uptake of CO_2 in the ocean by CO_2 dependent element ratios of sinking particles. Until the end of the next century, this influence again is able to lower the atmospheric CO_2 partial pressure by yet another 20 μatm in the year 2100.

In the current study the TEP scenario can also be seen as a representative for any mechanism leading to a higher CO_2 uptake by the ocean due to variable C:P elemental ratios. Assuming currently no CO_2 dependence of the element ratios of sinking particles does not provide the possibility of additional net carbon uptake as compared to results obtained by experiment F. In an equilibrated ocean, in which the element ratios of sinking particles follow the results of the data analysis in this study (equation 2.3), there is no enhanced carbon uptake in contrast to a steady state ocean with particle compositions according to the classical constant Redfield ratio. Even though in the ocean with non-Redfield particle compositions there is higher gross CO_2 gas exchange, the net fluxes are zero. However, current responses to anthropogenic CO_2 emissions are likely to emerge if there is a CO_2 dependent mechanism involved in the formation of sinking particles. The effects of CO_2 dependent changes on element ratios of sinking particles are highly speculative, but there are some indications for enhanced carbon sequestration following elevated pCO_2, as shown in the TEP experiment. Thus, a moderate rise in the relevance of TEP for global carbon export can lead to a significant increases in the marine carbon sequestration.

The model results show that changes in the elemental composition of POM lead to significant alterations in the ocean carbon uptake and DIC distributions. Models that use the constant Redfield ratio for C:N in sinking particles will either underestimate carbon fluxes or overestimate nutrient fluxes.

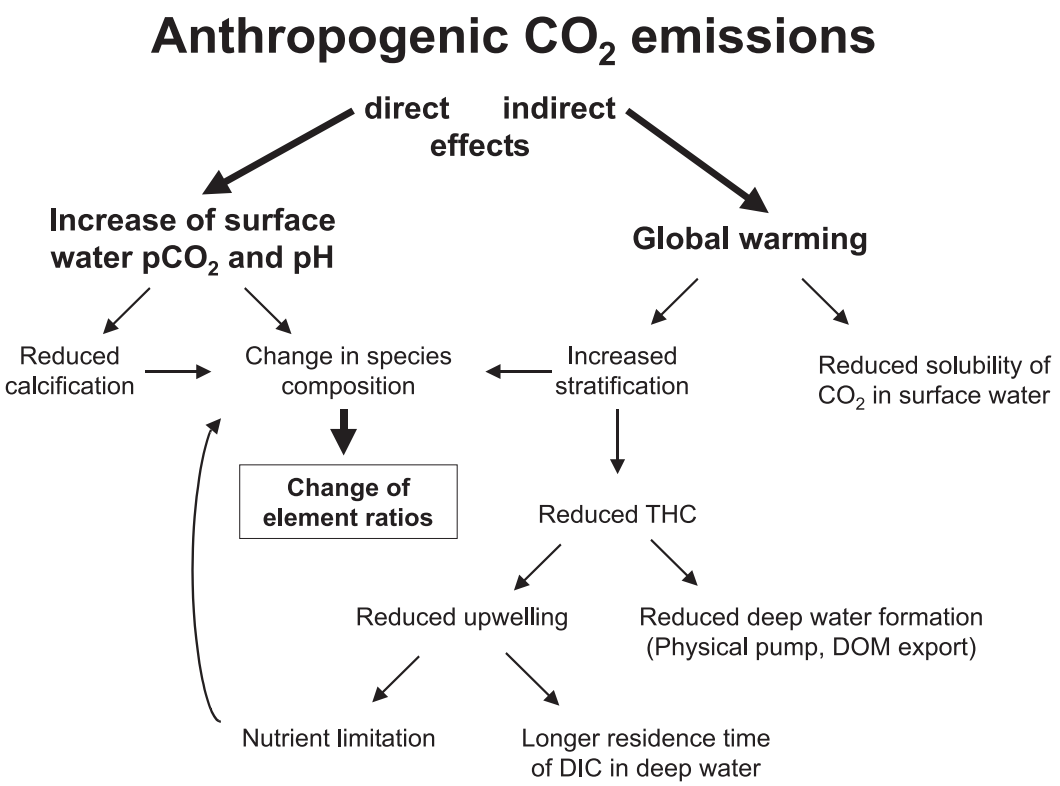

Figure 5.1: Direct and indirect effects of global change on marine physical and biochemical properties. THC: thermohaline circulation; DOM: dissolved organic matter; DIC: dissolved inorganic carbon.

5.2 Variable Element Ratios of POM and Global Change

There are a large number of probable effects of increasing atmospheric CO_2 concentrations on the global oceans discussed in the recent literature, generally referred to as global change. These impacts include direct changes in the surface water biogeochemistry as well as more indirect large scale shifts in surface water stratification, circulation patterns and oceanic overturning due to global warming. Changes in the physical properties of the ocean alter distributions of biochemical tracers which then in turn influence marine biological productivity. Predictions of probable changes in the physical properties of the global ocean often have large uncertainties, as the future development of the atmosphere is not known exactly, and the range of the respective temperature increase differs between 1.5 K and 4.5 K [Houghton et al., 1996]. However, changes in the mass of marine particulate carbon fluxes due to shifting species compositions are expected, but the amount of these shifts (Gt C) are speculative. An overview over the main features of direct and indirect effects projected for global change is displayed in Figure 5.1.

As a direct effect, elevated CO_2 concentrations in the surface water result in large

scale shifts of chemical equilibria and the carbonate system, as e.g. a lowering of surface water pH [Wolf-Gladrow et al., 1999]. This might lead to a general change in species compositions as well as to changes in the elemental composition of single species. Detailed analyses of certain phytoplankton species, however, did not show a general and coinciding trend in their response to higher surface water pCO_2, but rather differing responses by different species [Burkhardt and Riebesell, 1997; Burkhardt et al. 1999]. Thus, under higher CO_2 concentrations some species incorporated more carbon, while others reduced their carbon uptake. Furthermore, the changing surface water pCO_2 and pH evoke shifts in the surface ocean carbonate chemistry. Due to a lower pH, calcification decreases and a weakened carbonate pump in turn increases the CO_2 buffer capacity in the surface water and thereby CO_2 uptake, which can be seen as a positive feedback mechanism helping to mitigate the problem of anthropogenic CO_2 emissions [Riebesell et al., 2000]. But Riebesell et al. [2001] also reported a higher CO_2 sensitivity of calcifying phytoplankton in contrast to non-calcifying phytoplankton with the tendency to increase the contribution of calcifiers to total primary production. This higher sensitivity in contrast to other taxonomic groups is accompanied by a higher organic carbon incorporation within the respective cells, providing the possibility of enhanced carbon drawdown. However, there are two opposing effects, an increase of the relative importance to primary production on one hand, and a decrease in calcification on the other hand. The net effect to the global carbon cycle, however, is yet unknown. Most likely are in general large scale changes in the global phytoplankton species composition which will influence exported elemental ratios, but its potential to affect marine carbon sequestration still has to be determined.

There are a number of investigations estimating probable effects of global change on oceanic carbon uptake through the application of ocean carbon cycle models [Maier-Reimer et al., 1996; Sarmiento and Le Quéré, 1996; Sarmiento et al., 1998; Sarmiento and Hughes, 1999; Matear and Hirst, 1999; Friedlingstein et al., 2001; Bopp et al., 2001]. All these studies agree on the fact that global warming heats the surface ocean and intensifies stratification. Both effects, independently, lead to a decrease in oceanic carbon uptake. Surface heating reduces the CO_2 solubility and an intensified stratification reduces deep water formation and thereby the export of dissolved organic and inorganic carbon. The decreasing uptake rates differ between the different studies, but are of comparable magnitude, depending on the type of ocean circulation model chosen for the respective investigation. Furthermore, the above mentioned authors stated that the ocean's biology will be influenced as well. Decreased overturning leads to weakened upwelling of nutrients, which then again reduces primary and export production at the surface. Thus, next to the decreased solubility pump, a reduced efficiency of the biological pump is predicted as well. In the study of Matear and Hirst [1999] the export production reduces until 2100 by 15 %. For total carbon estimates there are reduced carbon accumulation rates given by the models. Matear and Hirst [1999] predict a lowering of 56 Gt C until 2100, whereas Maier-Reimer et al. [1996] propose 26 Gt C. In the model of Sarmiento

and Le Quéré [1996] there is a distinction between the physical ocean model, where 169 Gt C are taken up less until 2100 and the biological ocean model with a decrease of 58 Gt C. Friedlingstein et al. [2001] calculated for the same time interval a reduced uptake of 35 Gt C for an experiment with a doubling in atmospheric CO_2 and 200 Gt C for a fourfold increase of the atmospheric pCO_2.

The model approach of the current study does not include changes in the physical properties of the ocean due to increased anthropogenic CO_2 emissions. But in contrast to the models above, a positive response of marine biological production to global change is supposed. In the respective experiment (G), there is an additional carbon uptake of 40 Gt C between the years 2000 and 2100. This amount does not compensate the reduced carbon uptake rates as they were calculated in the models above, but it shows that the biological pump has the potential to mitigate the decreases of the physical pump, e.g. by 75 % compared to the results of Matear and Hirst [1999].

Next to model experiments there are measurements of elemental ratios of POM, whose results can be interpreted as probable future developments under global change. Arrigo et al. [1999] found out that the phytoplankton community structure of the Southern Ocean might shift due to increased stratification as a consequence of global warming and increased precipitation. From the Ross Sea they reported a dominance of diatoms in more stratified waters over Phaeocystis which dominate in more deeply mixed water masses. Phaeocystis are able to drawdown and thus export CO_2 from the surface water much more efficiently than diatoms. Even though there was no significant difference in the C:N ratios, both species exhibited higher than Redfield C:N ratios of 9.2 ± 1.7 (diatoms) and 7.8 ± 1.3 (Phaeocystis). The C:P ratio of *Phaeocystis antarctica* with 147 ± 27 molar units, however, was significantly higher than the C:P ratio of the diatoms with 94 ± 20, underlining the higher carbon export potential of phaeocystis. Probable future increases of surface water stratification will lead to a shift in phytoplankton communities towards more diatom dominated populations, and as a consequence, the large sink for anthropogenic CO_2 in the Southern Ocean will diminish.

Changes in elemental composition of DOM over the last decade have been observed by Church et al. [2002] in the subtropical North Pacific Ocean. They reported from the *HOT* time series station that during the last 10 years there was a significant increase in DOC production, rising the C:P ratios of DOM, noticeably. While small and insignificant changes in the DOC:DON and DON:DOP ratios were measured, they found an increase in the DOC:DOP ratio of 17 % from 408 to 478 molar units. Church et al. [2002] explained their findings with a recent reorganization of the plankton community dynamics as a consequence of global change.

The discussion shows that there are a number of indications that the marine carbon cycle is currently not in steady state, and all probable effects described above include the possibility of a change in the elemental composition of marine particle fluxes. However, both direction and amount of these shifts are highly speculative.

Furthermore, elemental compositions provide only relative amounts of carbon and nutrient fluxes. It is also very important to determine changes in the absolute flux rates primarily and secondly the elemental compositions therein. Bopp et al. [2001] investigated the impact of climate change on marine export production with the help of two GCMs (General Circulation Models). They found out, that in general there will be a decrease of marine export production of 6 %, globally. But they also reported regional differences with a stronger decrease of 15 % in the tropics and an increase of 10 % in the Southern Ocean. This increased productivity in the Southern Ocean disagrees with findings from the investigations described above. Bopp et al. [2001] explain their results with a shift of productivity towards higher latitudes, where higher surface water temperatures reduce ice coverage and thus provide a temporal extension of the growing season; favorable conditions for enhanced phytoplankton production. Combining these results with elevated carbon to nutrient ratios at the proceeding particle fluxes, probably results in a further amplification of carbon export fluxes, in addition to the increase in the Southern Ocean predicted by Bopp et al. [2001].

Nevertheless, CO_2 is a strong greenhouse gas, its potential to increase global temperatures is widely accepted and during the last century, a significant increase of global temperatures has also been measured [IPCC, 2001]. The uptake of CO_2 by the ocean and its storage in deep water is largely determined by global deep water formation. Joos et al. [1999] found that with an increase of global mean temperatures exceeding 3 K, there will be a collapse of the thermohaline circulation. If there is less warming, the circulation is predicted be weakened significantly, but with the later stabilization of the atmospheric CO_2 concentrations, the thermohaline circulation is assumed to recover. However, the physical pump only can work as a temporary sink, as the later upwelling of DIC enriched deep water is a source of CO_2 to the atmosphere. Although variations in the elemental composition of marine particle fluxes, as they are found in this study, provide a mechanism for a relative strengthening of marine carbon sequestration, they can not outweigh the decreasing efficiency of the physical pump. Efforts to reduce anthropogenic CO_2 emissions are essential, and to prevent further global warming, it has to be a major goal to reduce future emissions sustainably.

6 Outlook

The elemental composition of particulate organic matter (POM) determines the relative magnitude of the vertical carbon versus phosphorus and nitrogen fluxes caused by the sinking of biogenic material. The Redfield stoichiometry is the most commonly used paradigm therefore. Complex ocean carbon cycle models have been developed to simulate marine biogeochemical processes and to predict future change. However, the most model experiments of particle fluxes are based on spatially and temporally constant element ratios of sinking particles, but the current investigation has shown that changes in the elemental composition of marine particles occur, which have significant effects on the marine carbon cycle. Therefore, to achieve better estimates of marine carbon fluxes and the associated consequences, the elemental composition of sinking particles should be determined with higher precision, including systematic seasonal, regional and depth related variations to feed the models. Whereas the models themselves seem to be well suitable for this particular question.

The current study has shown that there are significant differences in both, the element ratios of sinking particles and the corresponding depth dependencies, between single ocean basins. An improvement of global carbon flux estimates by sinking particles will be achieved if these differences are considered. Therefore, future biogeochemical model experiments should apply regionally variable element ratios for particle export fluxes and depth dependencies, e.g. as they are determined by the current investigation (Table 2.3).

For further improvements of particle flux model results, it is recommended to determine the element composition of sinking particles with higher spatial and temporal resolution. This should be done especially in areas of highest productivity and deepest particle export, as these areas predominantly control marine carbon sequestration on a global scale. Thereby seasonal patterns of both flux rates and element ratios should be observed, to determine those element ratios of sinking particles that are exported primarily. Appropriate regions are e.g. the upwelling areas of eastern boundary currents along the coasts of North and South America and the African continent. Furthermore equatorial upwelling regions, the North Atlantic, the Arabian Sea and high latitude regions like e.g. the Southern Ocean should be investigated, as considerable particle production has also been found in areas associated with strong seasonal signals. For the investigations, sediment trap deployments should be applied, although dissolution of material within the sampling cups of sediment traps has been reported to be a major problem of this sampling method. As it was discussed earlier during this investigation, such processes possibly are leading to shifts in the element ratios measured on particles from the traps [Kähler and Bauerfeind, 2001]. To avoid this sampling bias it will be necessary to record and analyze dissolved organic nutrients from the supernatant of the sediment trap material, and to apply a suitable correction procedure.

Some ocean areas like the North Atlantic and the North Pacific, exhibit the produc-

tion of large amounts of dissolved organic matter (DOM), which is exported into the oceans interior by deep water formation. This mechanism is also part of the biological pump and it should be taken into account by biogeochemical models as well. There are only few investigations on the elemental composition of DOM [Jackson and Williams, 1985; Hansell et al. 1993, 1997; Williams 1995], but in general the C:N ratios seem to lie within the range of 10-20 (mol), and Church et al. [2002] reported C:P ratios higher than 400 (mol). These results indicate that the application of the classical Redfield ratio for DOM production will result in a significant underestimation of the production of dissolved organic carbon (DOC). As there are only few data available, more measurements should be undertaken to determine the element ratios of DOM in the most prominent areas of deep water formation. These are the North Atlantic, especially the area of the Labrador Sea where North Atlantic Deep Water (NADW) is formed, the North Pacific where production of North Pacific Intermediate Water (NPIW) takes place, and the area around the Antarctic, which is the source region of Antarctic Bottom Water (AABW). By this means, parameterizing global particle fluxes with regionally variable particle element ratios and depth dependencies together with the consideration of non-Redfield DOM export, will improve the estimates of present marine carbon fluxes substantially.

Future changes of the biological pump are still subject to speculation. There are probably relative changes in the carbon to phosphorus and nitrogen fluxes due to shifts in the element ratios of sinking particles and absolute changes as consequences of variations in ocean productivity. The TEP scenario of the current investigation (experiment G) has shown a possible relative increase of the carbon content of sinking particles due to higher contributions of TEP to sinking particles, which is one example for a shift in species composition responding to global change. Other probable reactions of species composition and/or mechanisms of carbon acquisition reacting to global change still have to be determined as e.g. described by Riebesell et al. [2001]. A general decrease of ocean productivity as a consequence of wide spread nutrient limitation resulting from global change is predicted by a number of model experiments [Maier-Reimer et al., 1996; Sarmiento and Le Quéré, 1996; Sarmiento et al., 1998; Sarmiento and Hughes, 1999; Matear and Hirst, 1999; Bopp et al., 2001; Friedlingstein et al., 2001]. However, the uncertainties of these predictions are large, as the assumptions for surface water temperature rise following atmospheric CO_2 concentrations diverge by several degrees between single approaches. Therefore, it will be a major issue of future research to determine the current measurable changes associated to global change. These should include changes in surface water temperature, precipitation, thermohaline circulation, biological production and element ratios of sinking particles. Being able to distinguish between natural variability and human impacts is a prerequisite for reliable predictions of future developments.

Acknowledgements

Like many other studies, this work has benefitted from the help of a large number of people, who I cannot name all here. My special thanks I would like to give to:

- PD Dr. Reiner Schlitzer, my supervisor, who introduced me into marine biogeochemistry and ocean carbon cycle modeling, and who inspired me to track this interdisciplinary perspective on the application of one of the classics in the field, the Redfield ratio. With his frankness for all kind of questions, even the seemingly stupid ones, he gave me constant support and constructive criticism in a friendly and agreeable working atmosphere. He also provided the first expert opinion on this thesis.

- Prof. Dr. K. Herterich for his interest in this study and the second expert opinion on this work.

- Prof. Dr. D. Fütterer, who provided me with the research facilities at the Alfred Wegener Institute for Polar and Marine Research, Bremerhaven, allowing efficient research.

- Dr. Gerhard Fischer from the department of geosciences at the University of Bremen, for making a large amount of sediment trap data available to me, and for valuable discussions about the characteristics of sinking matter in the ocean, seen from a geological perspective.

- Dr. Eva-Maria Nöthig from the AWI, who supplied me with a large number of filtration data, some of them unpublished at that time, and who shared her knowledge, helping me to regard things from a biologists point of view.

- Dr. Regina Usbeck, Dr. Marie-France Weirig and Stephanie Ronski, for computing assistance, which contributed to the solution of some of the modeling problems and/or for carefully reading and commenting on earlier versions of this and other manuscripts.

- The members of the Carbon Group at the AWI, especially Dr. Ulf Riebesell and Dr. Anja Engel, who were always very interested in my ideas and findings and who helped to establish some of the main hypotheses of this work. The interdisciplinary constitution of the carbon group provided an excellent basis for many discussions about this very diverse field of research. The always friendly and open atmosphere made this cooperation a great pleasure and support for me.

- The members of the department of geosystems, who created a pleasant and sometimes hilarious working atmosphere.

- Jürgen Schneider, my father, who helped to improve the quality of an important figure.

- Andrea Hackbart, my dearest friend, who strongly supports the Redfield paradigm using the arguments of a social worker, and who convinces me every day that life is wonderful, even beyond the universe of science.

- All those numerous people, who measured the data and made them freely available in the internet, to become an important part of this study.

- The Deutsche Forschungsgemeinschaft (SFB 261), who funded this work.

References

Alldredge, A. and Gotschalk, C. [1989]. Direct observations of the mass flocculation of diatom blooms: characteristics, settling velocities and formation of diatom aggregates. *Deep Sea Research*, 36: 159–171.

Alldredge, A., Passow, U., and Logan, B. [1993]. The abundance and significance of a class of large, transparent organic particles in the ocean. *Deep Sea Research*, 40(6): 1131–1140.

Altabet, M. A. [1988]. Variations in nitrogen isotopic composition between sinking and suspended particles: implications for nitrogen cycling and and particle transformation in the open ocean. *Deep Sea Research*, 35(4): 535–554.

Anadón, R., Alvarez-Marqués, F., Fernández, E., Varela, M., Zapata, M., Gasol, J., and Vaqué, D. [2002]. Vertical biogenic particle flux during austral summer in the Antarctic Peninsula area. *Deep Sea Research*, 49: 883–901.

Anderson, L. and Sarmiento, J. [1994]. Redfield ratios of remineralization determined by nutrient data analysis. *Global Biogeochemical Cycles*, 8(1): 65–80.

Antia, A. N., Koeve, W., Fischer, G., Blanz, T., Schulz-Bull, D., Scholten, J., Neuer, S., Kremling, K., Kuss, J., Peinert, R., Hebbeln, D., Bathmann, U., Conte, M., Fehner, U., and Zeitzschel, B. [2001]. Basin-wide particulate carbon flux in the Atlantic Ocean: Regional export patterns and potential for atmospheric CO_2 sequestration. *Global Biogeochemical Cycles*, 15(4): 845–862.

Armstrong, R. A., Lee, C., Hedges, J. I., Honjo, S., and Wakeham, S. G. [2002]. A new mechanistic model for organic carbon fluxes in the ocean based on the quantitative association of POC with ballast minerals. *Deep Sea Research*, 49: 219–236.

Arrigo, K., Robinson, D., Worthen, D., Dunbar, R., DiTullio, G., VanWoert, M., and Lizotte, M. [1999]. Phytoplankton Community Structure and the Drawdown of Nutrients and CO_2 in the Southern Ocean. *Science*, 283: 365–367.

Barnola, J., Raynaud, D., Lorius, C., and Barkov, N. [1999]. Historical CO_2 record from the Vostok ice core. Trends: A Compendium of Data on Global Change, Carbon Dioxide Information Analysis Center, Oak Ridge National Laboratory.

Behrenfeld, M. and Falkowski, P. [1997]. Photosynthetic rates derived from satellite-based chlorophyll concentration. *Limnology and Oceanography*, 42: 1–20.

Berger, W. H., Smetacek, V. S., and Wefer, G. [1989]. Ocean Productivity and Paleoproductivity – An Overview. In Berger, W. H., Smetacek, V. S., and Wefer, G., editors, *Productivity of the Ocean: Present and Past*, number 44 in Dahlem Workshop Reports, pages 1–34. Wiley & Sons, Chichester.

Bianchi, F., Boldrin, A., Cioce, F., Dieckmann, G., Kuosa, H., Larsson, A.-M., Nöthig, E.-M., Sehlstedt, P.-I., Socal, G., and Syvertsen, E. [1992]. Phytoplankton distribution in relation to sea ice, hydrography and nutrients in the northwestern Weddell Sea in early spring 1988 during EPOS. *Polar Biology*, 12: 225–235.

Bishop, J., Calvert, S., and Soon, M. [1999]. Spatial and temporal variability of POC in the northeast Subarctic Pacific. *Deep Sea Research*, 46: 2699–2733.

Bopp, L., Monfray, P., Aumont, O., Dufresne, J. L., Le Treut, H., Madec, G., Terray, L., and Orr, J. C. [2001]. Potential impact of climate change on marine export production. *Global Biogeochemical Cycles*, 15: 81–99.

Boulahdid, M. and Minster, J. [1989]. Oxygen Consumption and Nutrient Regeneration Ratios along Isopycnal Horizons in the Pacific Ocean. *Marine Chemistry*, 26: 133–153.

Broecker, W. S. [1997]. Will Our Ride into the Greenhouse Future be a Smooth One? *GSA Today*, 7(5): 1–7.

Broecker, W. S. and Peng, T. H. [1993]. Greenhouse puzzles. Technical report, Lamont-Doherty Earth Observatory of Columbia, Palisades, NY 10964.

Broecker, W. S., Takahashi, T., and Takahashi, T. [1985]. Sources and flow patterns of deep-ocean waters as deduced from potential temperature, salinity, and initial phosphate concentration. *Journal of Geophysical Research*, 90(C4): 6925–6939.

Buesseler, K. O., Michaels, A. F., Siegel, D. A., and Knap, A. H. [1994]. A three dimensional time-dependent approach to calibrating sediment trap fluxes. *Global Biogeochemical Cycles*, 8: 179–193.

Burkhardt, S. and Riebesell, U. [1997]. CO_2 availability affects elemental composition (C:N:P) of the marine diatom *skeletonema costatum*. *Marine Ecology Progress Series*, 155: 67–76.

Burkhardt, S., Riebesell, U., and Zondervan, I. [1999]. Effect of CO_2 concentration on C:N:P ratio in marine phytoplankton: A species comparison. *Limnology and Oceanography*, 44(3): 683–690.

Carpenter, E. J. and Romans, K. [1991]. Major role of the cyanobacterium *trichodesmium* in nutrient cycling in the North Atlantic Ocean. *Science*, 254: 1356–1358.

Cauwet, G. [1978]. Organic chemistry of sea water particulates: Concepts and developments. *Oceanologica Acta*, 1(1): 99–105.

CDIAC [2002]. Carbon Dioxide Information Analysis Center. Internet `http://www.whoi.edu/nabe.html`.

Christian, J., Lewis, M., and Karl, D. [1997]. Vertical fluxes of carbon, nitrogen,

and phosphorus in the North Pacific Subtropical Gyre new Hawaii. *Journal of Geophysical Research*, 102(C7): 15667–15677.

Church, M. J., Ducklow, H. W., and Karl, D. M. [2002]. Multiyear increase in dissolved organic matter inventories at Station ALOHA in the North Pacific Subtropical Gyre. *Limnology and Oceanography*, 47(1): 1–10.

Coale, K. H., Fitzwater, S. E., Gordon, R. M., Johnson, K. S., and Barner, R. T. [1996]. Control of community growth and export production by upwelled iron in the equatorial Pacific Ocean. *Nature*, 379: 237–238.

Copin-Montégut, C. and Copin-Montégut, G. [1978]. The chemistry of particulate matter from the south Indian and Antarctic Oceans. *Deep Sea Research*, 25: 922–931.

Copin-Montégut, C. and Copin-Montégut, G. [1983]. Stoichiometry of carbon, nitrogen, and phosphorus in marine particulate matter. *Deep Sea Research*, 30: 31–46.

Cullen, J. J. [1991]. Hypotheses to explain high-nutrient, low chlorophyll conditions in the open sea. *Limnology and Oceanography*, 36: 1578–1599.

de Baar, H. J. W., de Jong, J. T. M., Bakker, D. C. E., Loescher, B. M., Veth, C., Bathmann, U. V., and Smetacek, V. [1995]. Importance of iron for plankton blooms and carbon dioxide drawdown in the southern ocean. *Nature*, 373: 412–415.

de Baar, H. J. W., Farrington, J., and Wakeham, S. [1983]. Vertical flux of fatty acids in the North Atlantic Ocean. *Journal of Marine Research*, 41: 19–41.

de Baar, H. J. W., van Leeuwe, M. A., Scharek, R., Goeyens, L., Bakker, K. M. J., and Fritsche, P. [1997]. Nutrient anomalies in *fragilariopsis kerguelensis* blooms, iron deficiency and the nitrate/phosphate ratio (AC Redfield) of the Antarctic Ocean. *Deep Sea Research*, 44: 229–260.

de las Heras, M. and Schlitzer, R. [1999]. On the Importance of Intermediate Water Flows for the Global Ocean Overturning. *Journal of Geophysical Research*, 104: 15515–15536.

Dietrich, G., Kalle, K., Krauss, W., and Siedler, G. [1975]. *Allgemeine Meereskunde*. Gebrüder Bornträger, Berlin, Stuttgart.

Droop, M. [1973]. Some thoughts on nutrient limitation in algae. *Journal of Phycology*, 9: 264–272.

Druffel, E. R. M., Bauer, J. E., Williams, P. M., Griffin, S., and Wolgast, D. [1996]. Seasonal variability of particulate organic radiocarbon in the northeast Pacific Ocean. *Journal of Geophysical Research*, 101(C9): 20543–20552.

Druffel, E. R. M., Williams, P. M., Bauer, J. E., and Ertel, J. R. [1992]. Cycling

of Dissolved and Particulate Organic Matter in the Open Ocean. *Journal of Geophysical Research*, 97(C10): 15639–15659.

Duce, R. A., Liss, P. S., Merril, J. T., Atlas, E. L., Buat-Menard, P., Hicks, B. B., Miller, J. M., Prospero, J. M., Arimoto, R., Church, T. M., Ellis, W., Galloway, J. N., Hansen, L., Jickells, T. D., Knap, A. H., Reinhardt, K. H., Schneider, B., Soudine, A., Tokos, J. J., Tsunogai, S., Wollast, R., and Zhou, M. [1991]. The atmospheric input of trace species to the world ocean. *Global Biogeochemical Cycles*, 5: 193–259.

Edwards, A. M. [2001]. Adding detritus to a nutrient-phytoplankton-zooplankton model: a dynamical-systems approach. *Journal of Plankton Research*, 23(4): 389–413.

Elfiri, I. and Turpin, D. [1985]. Steady-state luxury consumption and the concept of optimum nutrient ratios: a study with phosphate and nitrate limited *selenastrum minutum* (Chlorophyta). *Journal of Phycology*, 21: 592–602.

Engel, A. [2000]. The role of transparent exopolymer particles (TEP) in the increase in apparent particle stickiness (alpha) during the decline of a diatom bloom. *Journal of Plankton Research*, 22(3): 485–497.

Engel, A. [2002]. Direct relationship between CO_2 uptake and transparent exopolymer particles production in natural phytoplankton. *Journal of Plankton Research*, 24(1): 49–53.

Engel, A., Goldthwait, S., Passow, U., and Alldredge, A. [2002]. Temporal decoupling of carbon and nitrogen dynamics in a mesocosm diatom bloom. *Limnology and Oceanography*, 47(3): 753–761.

Engel, A. and Passow, U. [2001]. Carbon and nitrogen content of transparent exopolymer particles (TEP) in relation to their alcian blue adsorption. *Marine Ecology Progress Series*, 219: 1–10.

Engel, A. and Schartau, M. [1999]. Influence of transparent expolymer particles (TEP) on sinking velocity of *nitzschia closterium* aggregates. *Marine Ecology Progress Series*, 182: 69–76.

Eppley, R. W. and Peterson, B. J. [1979]. Particulate organic matter flux and planktonic new production in the deep ocean. *Nature*, 282: 677–680.

Fischer, G., Donner, B., Ratmeyer, V., Davenport, R., and Wefer, G. [1996a]. Distinct year-to-year particle flux variations off Cape Blanc during 1988-1991: Relation to $\delta^{18}O$-deduced sea-surface temperatures and trade winds. *Journal of Marine Research*, 54: 73–98.

Fischer, G. and Wefer, G. [1996]. Long-term Observation of Particle Fluxes in the Eastern Atlantic: Seasonality, Changes of Flux with Depth and Comparison with the Sediment Record. In Wefer, G., Berger, W. H., Siedler, G., and Webb,

D. J., editors, *The South Atlantic: Present and Past Circulation*, pages 325–344. Springer, Heidelberg.

Friedlingstein, P., Bopp, L., Dufresne, J. L., Fairhead, L., Le Treut, H., Monfray, P., and Orr, J. [2001]. Positive Feedback between future climate change and the carbon cycle. *Geophysical Research Letters*, 28(8): 1543–1546.

Gardner, W., Hinga, K., and Marra, J. [1983]. Observations on the degradation of biogenic material in the deep ocean with implications on accuracy of sediment trap fluxes. *Journal of Marine Research*, 41(2): 195–214.

GEOSECS [1998]. Geochemical Ocean Sections Study. Internet `http://ingrid.ldgo.columbia.edu/SOURCES/.GEOSECS/`.

Gervais, F. and Riebesell, U. [2001]. Effect of phosphorus limitation on elemental composition and stable carbon isotope fractionation in a marine diatom growing under different CO_2 concentrations. *Limnology and Oceanography*, 46(3): 497–504.

Gordon, D. [1971]. Distribution of particulate organic carbon and nitrogen at an oceanic station in the central Pacific. *Deep Sea Research*, 18: 1127–1134.

Gruber, N. [1998]. Anthropogenic CO_2 in the Atlantic Ocean. *Global Biogeochemical Cycles*, 12(1): 165–191.

Gruber, N., Sarmiento, J. L., and Stocker, T. F. [1996]. An improved method for detecting anthropogenic CO_2 in the oceans. *Global Biogeochemical Cycles*, 10(4): 809–837.

Gust, G., Michaels, A. F., Johnson, A., Deuser, W. G., and Bowles, W. [1994]. Mooring line motions and sediment trap hydrodynamics: in situ intercomparison of three common deployment designs. *Deep Sea Research*, 41: 831–857.

Haake, B., Ittekkot, V., Ramaswamy, V., Nair, R., and Curry, W. [1993]. Seasonality and interannual variability of particle fluxes to the deep Arabian Sea. *Deep Sea Research*, 40(7): 1323–1344.

Hansell, D. A. and Waterhouse, T. Y. [1997]. Controls on the distributions of organic carbon and nitrogen in the eastern Pacific Ocean. *Deep Sea Research*, 44: 843–857.

Hansell, D. A., Williams, P. M., and Ward, B. B. [1993]. Measurements of DOC and DON in the Southern California Bight using oxidation by high temperature combustion. *Deep Sea Research*, 40: 219–234.

Hebbeln, D., Marchant, M., and Wefer, G. [2000]. Seasonal variations of the particle flux in the Peru-Chile current at 30^{o}S under 'normal' and El Nino conditions. *Deep Sea Research*, 47: 2101–2128.

Hebel, D. and Karl, D. [2001]. Seasonal, interannual and decadal variations in

particulate matter concentrations and composition in the subtropical North Pacific Ocean. *Deep Sea Research*, 48: 1669–1695.

Hecky, R., Campbell, P., and Hendzel, L. [1993]. The stoichiometry of carbon, nitrogen, and phosphorus in particulate matter of lakes and oceans. *Limnology and Oceanography*, 38(4): 709–724.

Hernes, P., Peterson, M., Murray, J., Wakeham, S., Lee, C., and Hedges, J. [2001]. Particulate carbon and nitrogen fluxes and compositions in the central equatorial Pacific. *Deep Sea Research*, 48: 1999–2023.

Holm-Hansen, O., Strickland, J., and Williams, P. [1966]. A detailed analysis of biologically important substances in a profile off southern California. *Limnology and Oceanography*, 11: 548–569.

Honjo, S. [1980]. Material fluxes and modes of sedimentation in the mesopelagic and bathypelagic zones. *Journal of Marine Research*, 38: 53–97.

Honjo, S. [1982]. Seasonality and Interaction of Biogenic and Lithogenic Particulate Flux at the Panama Basin. *Science*, 218(26): 883–884.

Honjo, S., Dymond, J., Collier, R., and Manganini, S. [1995]. Export production of particles to the interior of the equatorial Pacific Ocean during the 1992 EqPac experiment. *Deep Sea Research*, 42: 831–870.

Honjo, S., Dymond, J., Prell, W., and Ittekkot, V. [1999]. Monsoon-controlled export fluxes to the interior of the Arabian Sea. *Deep Sea Research*, 46: 1859–1902.

Honjo, S., Francois, R., Manganini, S., Dymond, J., and Collier, R. [2000]. Particle fluxes to the interior of the Southern Ocean in the Western pacific sector along 170^o W. *Deep Sea Research*, 47: 3521–3548.

Honjo, S., Manganini, S., and Cole, J. [1982]. Sedimentation of biogenic matter in the deep ocean. *Deep Sea Research*, 29(5A): 609–625.

Hood, R., Bates, N., Capone, D., and Olson, D. [2001]. Modeling the effect of nitrogen fixation on carbon and nitrogen fluxes at BATS. *Deep Sea Research*, 48: 1609–1648.

Houghton, J., Meira Filho, L., Callander, B., Harris, N., Kattenberg, A., and Maskell, K. [1996]. Climate Cange 1995. In Houghton, J., Meira Filho, L., Callander, B., Harris, N., Kattenberg, A., and Maskell, K., editors, *The Science of Climate Change*. Cambridge University Press, New York.

Hupe, A. and Karstensen, J. [2000]. Redfield stoichiometry in the Arabian Sea. *Global Biogeochemical Cycles*, 14(1): 357–372.

IPCC [1997]. Stabilization of Atmospheric Greenhouse Gases: Physical, biological

and socioeconomic implications. Technical report, Intergovernmental Panel on Climate Change.

IPCC [2001]. Summary for Policymakers. Technical report, Intergovernmental Panel on Climate Change.

Ittekkot, V. [1993]. The abiotically driven biological pump in the ocean and short-term fluctuations in atmospheric CO_2 contents. *Global and Planetary Change*, 8: 17–25.

Ittekkot, V. and Laane, R. [1991]. Fate of Riverine Particulate Organic Matter. In Degens, E., Kempe, S., and Richey, J., editors, *Biogeochemistry of Major World Rivers*, SCOPE 42, pages 233–243. Wiley & Sons, Chichester.

Jackson, G. A. and Williams, P. M. [1985]. Importance of dissolved organic nitrogen and phosphorus to biological nutrient cycling. *Deep Sea Research*, 32: 223–235.

JGOFS [2002]. Sampling Protocols. Internet `http://usjgofs.whoi.edu/eqpac-docs/proto-18.html`.

Joos, F., Plattner, G. K., Stocker, T. F., Marchal, O., and Schmittner, A. [1999]. Global Warming and Marine Carbon Cycle Feedbacks on Future Atmospheric CO_2. *Nature*, 284: 464–467.

Kähler, P. and Bauerfeind, E. [2001]. Organic particles in a shallow sediment trap: Substantial loss to the dissolved phase. *Limnology and Oceanography*, 46(3): 719–723.

Karl, D., Knauer, G., and Martin, J. [1988]. Downward flux of particulate organic matter in the ocean: a particle decomposition paradox. *Nature*, 332: 438–441.

Karl, D., Knauer, G., Martin, J., and Ward, B. [1984]. Bacterial chemolithotrophy in the ocean is associated with sinking particles. *Nature*, 309: 54–56.

Keeling, C. and Whorf, T. [2002]. Atmospheric CO_2 records from sites in the SIO air sampling network. Trends: A Compendium of Data on Global Change, Carbon Dioxide Information Analysis Center, Tennessee, USA.

Kjørboe, T., Lundsgaard, C., Olesen, M., and Hansen, J. [1994]. Aggregation and sedimentation processes during a spring phytoplankton bloom: a field experiment to test coagulation theory. *Journal of Marine Research*, 52: 297–323.

Knauer, G. and Martin, J. [1981]. Primary production and carbon-nitrogen fluxes in the upper 1500 m of the northeast Pacific. *Limnology and Oceanography*, 26(1): 181–186.

Knauer, G., Martin, J., and Bruland, K. [1979]. Fluxes of particulate carbon, nitrogen and phosphorus in the upper water column of the northeast Pacific. *Deep Sea Research*, 26: 97–108.

Kononova, M., Nowakowski, T., and Newman, A. [1966]. *Soil organic matter, 2nd Ed.* Pergamon Press, Oxford.

Körtzinger, A., Koeve, W., Kähler, P., and Mintrop, L. [2001]. C:N ratios in the mixed layer during the productive season in the northeast Atlantic Ocean. *Deep Sea Research*, 48: 661–688.

Körtzinger, A., Mintrop, L., and Duinker, J. C. [1998]. On the penetration of anthropogenic CO_2 into the North Atlantic Ocean. *Journal of Geophysical Research*, 103: 18681–18689.

Körtzinger, A., Rhein, M., and Mintrop, L. [1999]. Anthropogenic CO_2 and CFCs in the North Atlantic Ocean - A comparison of man-made tracers. *Geophysical Research Letters*, 26(14): 2065–2068.

Logan, B., Passow, U., Alldredge, A., Grossart, H.-P., and Simon, M. [1995]. Rapid formation and sedimentation of large aggregates is predictable from coagulation rates (half-lives) of transparent exopolymer particles (TEP). *Deep Sea Research*, 42(1): 203–214.

Longhurst, A. [1998]. *Ecological geography of the sea.* Academic Press, San Diego.

Lozan, J. and Kausch, H. [1998]. *Angewandte Statistik für Naturwissenschaftler, 2.Aufl.* Parey, Berlin.

Mahowald, N., Kohfeld, K., Hansson, M., Balkanski, Y., Harrison, S. P., Prentice, I. C., Schulz, M., and Rodhe, H. [1999]. Dust sources and deposition during the last glacial maximum and current climate: A comparison of model results with paleodata from ice cores and marine sediments. *Journal of Geophysical Research*, 104(D13): 15895–15916.

Maier-Reimer, E., Mikolajewicz, U., and Winguth, A. [1996]. Future ocean uptake of CO_2: interaction between ocean circulation and biology. *Climate Dynamics*, 12: 63–90.

Mari, X., Beauvais, S., Lemée, R., and Pedrotti, M. [2001]. Non-redfield C:N ratio of transparent exopolymeric particles in the northwestern Mediterranean Sea. *Limnology and Oceanography*, 46: 1831–1836.

Martin, J. H. [1990]. Glacial-interglacial CO_2 change: the iron hypothesis. *Paleoceanography*, 5(1): 1–13.

Martin, J. H., Fitzwater, S. E., and Gordon, R. M. [1990]. Iron deficiency limits phytoplanton growth in antarctic waters. *Global Biogeochemical Cycles*, 4(1): 5–12.

Martin, J. H., Gordon, R. M., and Fitzwater, S. E. [1991]. The case for iron. *Limnology and Oceanography*, 36(8): 1793–1802.

Martin, J. H., Knauer, G. A., Karl, D. M., and Broenkow, W. W. [1987]. VERTEX: carbon cycling in the northeast Pacific. *Deep Sea Research*, 34: 267–286.

Matear, R. J. and Hirst, A. C. [1999]. Climate Change feedback on the future CO_2 uptake. *Tellus*, 51B: 722–733.

Michaels, A. F., Bates, N. R., Buesseler, K. O., Carlson, C. A., and Knap, A. H. [1994]. Carbon-cycle imbalances in the Sargasso Sea. *Nature*, 372: 537–540.

Minster, J. and Boulahdid, M. [1987]. Redfield ratios along isopycnal surfaces - a complementary study. *Deep Sea Research*, 34(12): 1981–2003.

Moran, S. B., Charette, M. A., Pike, S. M., and Wicklund, C. A. [1999]. Differences in seawater particulate organic carbon concentration in samples collected using small- and large-volume methods: the importance of DOC adsorption to the filter blank. *Marine Chemistry*, 67: 33–42.

Müller, P. J. [1977]. C:N ratios in Pacific deep-sea sediments: effect of inorganic ammonium and organic nitrogen compounds sorbed by clays. *Geochimica et Cosmochimica Acta*, 41: 765–776.

Neftel, A., Friedli, H., Moor, E., Lötscher, H., Oeschger, H., Siegenthaler, U., and Stauffer, B. [1994]. Historical CO_2 record from the Siple Station ice core. Trends: A Compendium of Data on Global Change, Carbon Dioxide Information Analysis Center, Oak Ridge National Laboratory.

Noji, T., Børsheim, K., Rey, F., and Nortvedt, R. [1999]. Dissolved organic carbon associated with sinking particles can be crucial for estimates of vertical carbon flux. *Sarsia*, 84: 129–135.

Nöthig, E.-M. [1987]. Untersuchungen zur Ökologie des Phytoplanktons in der südöstlichen Weddell See im Januar/Februar 1985 (Antarktis III,3). Dissertation, Universität Kiel.

Orcutt, K. M., Lipschutz, F., Gundersen, K., Arimoto, R., Michaels, A. F., Knap, A. H., and Gallon, J. R. [2001]. A seasonal study of the significance of N_2 fixation by *trichodesmium* spp. at the Bermuda Atlantic Time-series Study (BATS) site. *Deep Sea Research*, 48: 1583–1608.

Orr, J. C., Maier-Reimer, E., Mikolajewicz, U., Monfray, P., Sarmiento, J. L., Toggweiler, J. R., Taylor, N. K., Palmer, J., Gruber, N., Sabine, C. L., le Quéré, C., Key, R. M., and Boutin, J. [2001]. Estimates of anthropogenic carbon uptake from four three-dimensional global ocean models. *Global Biogeochemical Cycles*, 15(1): 43–60.

Osterroht, C. and Thomas, H. [2000]. New production enhanced by nutrient supply from non-Redfield remineralisation of freshly produced organic material. *Journal of Marine Systems*, 25: 33–46.

Pahlow, M. and Riebesell, U. [2000]. Temporal Trends in Deep Ocean Redfield Ratios. *Science*, 287: 831–833.

Peng, T. and Broecker, W. [1987]. C/P Ratios in Marine Detritus. *Global Biogeochemical Cycles*, 1(2): 155–161.

Petit, J., Jouzel, J., Raynaud, D., Barkov, N., Barnola, J.-M., Basile, I., Bender, M., Chappellaz, J., Davis, M., Delaygue, G., Delmotte, M., Kotlyakov, V., Legrand, M., Lipenkov, V., Lorius, C., Pépin, L., Ritz, C., Saltzman, E., and Stievenard, M. [1999]. Climate and atmospheric history of the past 420,000 years from the vostok ice core, Antarctica. *Nature*, 399: 429–436.

Rahmstorf, S. [2002]. Ocean circulation and climate during the past 120,000 years. *Nature*, 419: 207–214.

Ratmeyer, V., Fischer, G., and Wefer, G. [1999]. Lithogenic particle fluxes and grain size distributions in the deep ocean off northwest Africa: Implications for seasonal changes of aeolian dust input and downward transport. *Deep Sea Research*, 46: 1289–1337.

Redfield, A. [1934]. On the Proportions of Organic Derivatives in Sea Water and their Relation to the Composition of Plankton. *James Johnstone Memorial Volume*, pages 176–192.

Redfield, A. C., Ketchum, B. C., and Richards, F. A. [1963]. The influence of organisms on the composition of sea water. In Hill, N., editor, *The Sea*, volume 2, pages 26–77. Interscience, New York.

Riebesell, U., Zondervan, I., Rost, B., Tortell, P. D., Zeebe, R. E., and Morel, F. M. M. [2000]. Reduced calcification of marine plankton in response to increased atmospheric CO_2. *Nature*, 407: 364–367.

Riebesell, U., Zondervan, I., Rost, B., and Zeebe, R. E. [2001]. Effects of increasing atmospheric CO_2 on phpytoplankton communities and the biological carbon pump. *Global Change Newsletter*, 47: 12–15.

Roelke, D., Eldrige, P., and Cifuentes, L. [1999]. A Model of Phytoplankton Competition for Limiting and Nonlimiting Nutrients: Implications for Development of Estuarine and Nearshore Management Schemes. *Estuaries*, 22(1): 92–104.

Rutgers van der Loeff, M. M., Friedrich, J., and Bathmann, U. [1997]. Carbon export during the Spring Bloom at the Antarctic Polar Front, determined with the natural tracer ^{234}Th. *Deep Sea Research*, 44: 457–478.

Sachs, L. [1997]. *Angewandte Statistik, 8.Aufl.* Springer, Heidelberg.

Sakshaug, E. and Holm-Hansen, O. [1977]. Chemical composition of *skeletonema costatum* (Grev.) Cleve and *pavlova (monochrysis) lutheri* (Droop) Green as a function of nitrate-, phosphate-, and iron-limited growth. *Journal of Experimental Marine Biology and Ecology*, 29: 1–34.

Sambrotto, R., Savidge, G., Robinson, C., Boyd, P., Takahashi, T., Karl, D., Langdon, C., Chipman, D., Marra, J., and Codispoti, L. [1993]. Elevated consumption of carbon relative to nitrogen in the surface ocean. *Nature*, 363: 248–250.

Sarmiento, J. L. and Hughes, T. M. C. [1999]. Anthropogenic CO_2 uptake in a warming ocean. *Tellus*, 51B: 560–561.

Sarmiento, J. L., Hughes, T. M. C., Stouffer, R. J., and Manabe, S. [1998]. Simulated response of the ocean carbon cycle to anthropogenic climate warming. *Nature*, 393: 245–249.

Sarmiento, J. L. and Le Quéré, C. [1996]. Oceanic Carbon Dioxide Uptake in a Model of Century-Scale Global Warming. *Science*, 274: 1346–1350.

Scharek, R. [1990]. Die Entwicklung des Phytoplanktons im östlichen Weddellmeer (Antarktis) beim Übergang vom Spätwinter zum Frühjahr. Dissertation, Universität Bremen.

Schimel, D., House, J., Hibbard, K., Bousquet, P., Ciais, P., Peylin, P., Braswell, B., Apps, M., Baker, D., Bondeau, A., Canadell, J., Churkina, G., Cramer, W., Denning, A., Field, C., Friedlingstein, P., Goodale, C., Heimann, M., Houghton, R., Melillo, J., Moore III, B., Murdiyarso, D., Noble, I., Pacala, S., Prentice, I., Raupach, M., Rayner, P., Scholes, R., Steffen, W., and Wirth, C. [2001]. Recent patterns and mechanisms of carbon exchange by terrestrial ecosystems. *Nature*, 414: 169–172.

Schlitzer, R. [1993]. Determining the mean, large-scale circulation of the Atlantic with the adjoint method. *J.Phys.Oceanography*, 23: 1935–1952.

Schlitzer, R. [1995]. An adjoint method for the determination of the mean oceanic circulation, air-sea fluxes and mixing coefficients. Reports on Polar Research 156, AWI, Bremerhaven.

Schlitzer, R. [2000]. Applying the Adjoint Method for Global Biogeochemical Modeling. In Kasibhatla, P., Heimann, M., Hartley, D., Mahowald, N., Prinn, R., and Rayner, P., editors, *Inverse Methods in Biogeochemical Cycles*, pages 107–124. AGU, U.S.A.

Schlitzer, R. [2002a]. Carbon export fluxes in the Southern Ocean: Results from inverse modeling and comparison with satellite based estimates. *Deep Sea Research*, 49: 1623–1644.

Schlitzer, R. [2002b]. Ocean Data View by R. Schlitzer. Internet `http://www.awi-bremerhaven.de/GPH/ODV`.

Schlütz, L. and Sebert, M. [1987]. Mineral aerosol and source identification. *Journal of Aerosol Science*, 18: 1–10.

Schneider, B., Schlitzer, R., Fischer, G., and Nöthig, E.-M. in press [2003]. Depth

Dependent Elemental Compositions of Particulate Organic Matter (POM) in the Ocean. *Global Biogeochemical Cycles*.

Scholten, J. C., Fietzke, J., Rutgers van der Loeff, M. M., Mangini, A., Koeve, W., Stoffers, P., Antia, A., Neuer, S., and Waniek, J. [2001]. Trapping Efficiencies of Sediment Traps from the Deep Eastern North Atlantic: The ^{230}Th Calibration. *Deep Sea Research*, 48: 2383–2408.

Shaffer, G., Bendtsen, J., and Ulloa, O. [1999]. Fractionation during remineralization of organic matter in the ocean. *Deep Sea Research*, 46: 185–204.

Siegenthaler, U. and Sarmiento, J. [1993]. Atmospheric carbon dioxide and the ocean. *Nature*, 365: 119–125.

Strom, S., Brainard, M., Holmes, J., and Olson, M. [2001]. Phytoplankton blooms are strongly impacted by microzooplankton grazing in coastal North Pacific waters. *Marine Biology*, 138: 355–368.

Suess, E. [1980]. Particulate organic carbon flux in the ocean–surface productivity and oxygen utilization. *Nature*, 280: 260–263.

Takahashi, T. Wanninkhof, R. H., Feely, R. A., Weiss, R. F., Chipman, D. W., Bates, N. R., Olafsson, J., Sabine, C. L., and Sutherland, S. G. [1999]. In *Proceedings of the Second International CO_2 in the Oceans Meeting*, pages 9–15. Tsukuba, Japan.

Takahashi, T., Broecker, W., and Langer, S. [1985]. Redfield Ratio Based on Chemical Data from Isopycnal Surfaces. *Journal of Geophysical Research*, 90(C4): 6907–6924.

Thomas, H., Ittekkot, V., Osterroht, C., and Schneider, B. [1999]. Preferential recycling of nutrients - the ocean's way to increase new production and to pass nutrient limitation? *Limnology and Oceanography*, 44(8): 1999–2004.

Toggweiler, J. [1993]. Carbon overconsumption. *Nature*, 363: 210–211.

Toggweiler, J. R. [1999]. Oceanography: An ultimate limiting Nutrient. *Nature*, 400: 511–512.

Tomczak, M. and Godfrey, J. S. [1994]. *Regional Oceanography*. Pergamon, London.

Tréguer, P., Gueneley, S., Zeyons, C., Morvan, J., and Buma, A. [1990]. The distribution of biogenic and lithogenic silica and the composition of particulate organic matter in the Scotia Sea and the Drake Passage during autumn 1987. *Deep Sea Research*, 37: 883–851.

Usbeck, R. [1999]. Modeling of marine biogeochemical cycles with an emphasis on vertical particle fluxes. Reports on Polar Research 332, AWI, Bremerhaven.

Usbeck, R., Rutgers van der Loeff, M. M., Hoppema, M., and Schlitzer, R. [2002a].

Shallow remineralization in the Weddell Gyre. *Geochemistry, Geophysics, Geosystems (G^3)*.

Usbeck, R., Schlitzer, R., Fischer, G., and Wefer, G. in review [2002b]. Particle Fluxes in the Ocean: Comparison of sediment trap data with results from inverse modeling. *Journal of Marine Systems*.

Volk, T. and Hoffert, M. I. [1985]. Ocean carbon pumps: analysis of relative strengths and efficiencies in ocean-driven atmospheric CO_2 changes. In Sundquist, E. and Broecker, W. S., editors, *The carbon cycle and atmospheric CO_2: natural variations Archean to Present*, number 32 in Geophysical Monograph, pages 99–110. AGU, Washington D.C.

Wakeham, S., Hedges, J., Lee, C., and Pease, T. [1993]. Effects of poisons and preservatives on the composition of organic matter in a sediment trap experiment. *Journal of Marine Research*, 51(3): 669–696.

Wanninkhof, R. [1992]. Relationship between wind speed and gasexchange over the ocean. *Journal of Geophysical Research*, 97: 7373–7382.

Wefer, G. and Fischer, G. [1993]. Seasonal patterns of vertical particle flux in equatorial and coastal upwelling areas of the eastern Atlantic. *Deep Sea Research*, 40(8): 1613–1645.

Wefer, G., Suess, E., Balzer, W., Liebezeit, G., Müller, P., Ungerer, C., and Zenk, W. [1982]. Fluxes of biogenic components from sediment trap deployment in circumpolar waters of the drake passage. *Nature*, 299: 145–147.

Williams, P. J. l. B. [1995]. Evidence for the seasonal accumulation of carbon-rich dissolved organic material, its scale in comparison with changes in particulate material and the consequential effect on net C:N assimilation ratios. *Marine Chemistry*, 51: 17–29.

WODB [1998]. Ocean Climate Laboratory: Word Ocean Database 1998. Version 2.0. Technical report, Silver Spring, MD.

Wolf-Gladrow, D., Riebesell, U., Burkhardt, S., and Bijma, J. [1999]. Direct effects of CO_2 concentration on growth and isotopic composition of marine plankton. *Tellus*, 51B: 461–476.